

## WORK IN PROGRESS

Esta sección no está terminada. Si puedes echarle un ojo para ver la estructura y cómo encaja con el resto pero no merece la pena revisarla en detalle en el estado actual.

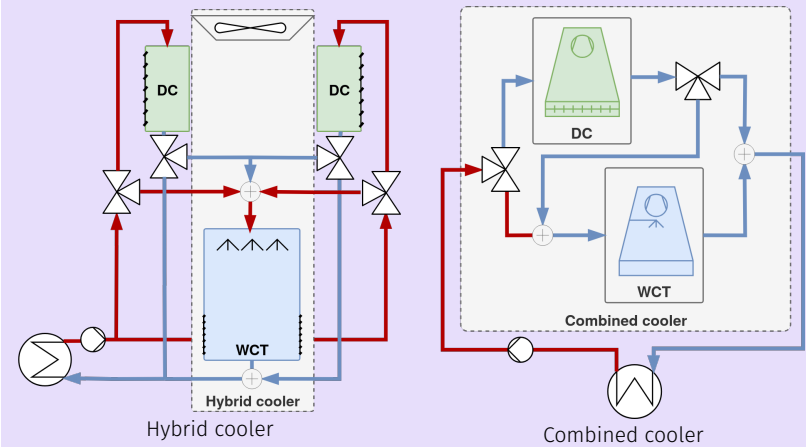
Additional text to add

### Kaobox with custom color

What is thiiis

1. Enumerations
2. should
3. be
4. okay

Even fancy figures™.



Hello, here is some text without a meaning. This text should show what a printed text will look like at this place. If you read this text, you will get no information. Really? Is there no information? Is there a difference between this text and some nonsense like "Huardest gefburn"? Kjift – not at all! A blind text like this gives you information about the selected font, how the letters are written and an impression of the look. This text should contain all letters of the alphabet and it should be written in of the original language. There is no need for special content, but the length of words should match the language. Hello, here is some text without a meaning. This text should show what a printed text will look like at this place. If you read this text, you will get no information. Really? Is there no information? Is there a difference between this text and some nonsense like "Huardest gefburn"? Kjift – not at all! A blind text like this gives you information about the selected font, how the letters are written and an impression of the look. This text should contain all letters of the alphabet and it should be written in of the original language. There is no need for special content, but the length of words should match the language.

### Model 0.1: Test

$T_{cc,out}, C_e, C_w, T_{c,out} = \text{combined cooler model}(q_c, R_p, R_s, \omega_{dc}, \omega_{wct}, T_{amb}, HR_i, T_v, \dot{m}_v)$   
 $T_{cc,in} = T_{c,out}$   
 $T_{dc,in} = T_{cc,in}$   
 $q_{dc} = q_c \cdot (1 - R_p)$   
 $q_{wct,p} = q_c \cdot R_p$   
 $q_{wct,s} = q_{dc} \cdot R_s$   
 $T_{dc,out}, C_{e,dc} = \text{dc model}(q_{dc}, \omega_{dc}, T_{amb}, T_{dc,in})$   
 $q_{wct}, T_{wct,in} = \text{mixer model}(q_{wct,p}, T_{cc,in}, q_{wct,s}, T_{dc,out})$

As can be seen in Model 0.1, the counter is working. As can be seen in Problem .1, the counter is working.

### Problem .1: Test

Hello, here is some text without a meaning. This text should show what a printed text will look like at this place. If you read this text, you will get no information. Really? Is there no information? Is there a difference between this text and some nonsense like "Huardest gefburn"? Kjift – not at all! A blind text like this gives you information about the selected font, how the letters are written and an impression of the look. This text should contain all letters of the alphabet and it should be written in of the original language. There is no need for special content, but the length of words should match the language.

$$\min_{\mathbf{x}, \mathbf{e}; \theta} J = f(\mathbf{x}, \mathbf{e}; \theta) = f(x)$$

with:

- ▶ Model name model

$$out_1, out_2 = f(in_1, in_2, \dots, in_N)$$

- ▶ Decision variables

$$\mathbf{x} = [x_1, x_2]$$

- ▶ Environment variables

$$\mathbf{e} = [e_1, e_2, \dots, e_3]$$

- ▶ Fixed parameters

$$\theta = [\theta_1 = X, \theta_2 = Y]$$

subject to:

- ▶ Box-bounds

- $x_1 \in [x_1, \bar{x}_1]$
- $x_2 \in [\underline{x}_2, \bar{x}_2]$

- ▶ Constraints

- $|out_X - out_Y| \leq \epsilon_1$
- $out_X \leq out_Z - \Delta Z$

Hello, here is some text without a meaning. This text should show what a printed

text will look like at this place. If you read this text, you will get no information. Really? Is there no information? Is there a difference between this text and some nonsense like “Huardest gefburn”? Kjift – not at all! A blind text like this gives you information about the selected font, how the letters are written and an impression of the look. This text should contain all letters of the alphabet and it should be written in of the original language. There is no need for special content, but the length of words should match the language.

### TL;DR

Too Long Didn't Read (TL;DR) boxes are defined with the `tldrbox` command. They are equivalent to abstracts or summaries and are placed at the beginning of sections or chapters.

Hello, here is some text without a meaning. This text should show what a printed text will look like at this place. If you read this text, you will get no information. Really? Is there no information? Is there a difference between this text and some nonsense like “Huardest gefburn”? Kjift – not at all! A blind text like this gives you information about the selected font, how the letters are written and an impression of the look. This text should contain all letters of the alphabet and it should be written in of the original language. There is no need for special content, but the length of words should match the language.

**Definition 0.0.1** Let  $(X, d)$  be a metric space. A subset  $U \subset X$  is an open set if, for any  $x \in U$  there exists  $r > 0$  such that  $B(x, r) \subset U$ . We call the topology associated to  $d$  the set  $\tau_d$  of all the open subsets of  $(X, d)$ .

**Remark 0.0.1** Let  $(X, d)$  be a metric space. A subset  $U \subset X$  is an open set if, for any  $x \in U$  there exists  $r > 0$  such that  $B(x, r) \subset U$ . We call the topology associated to  $d$  the set  $\tau_d$  of all the open subsets of  $(X, d)$ .

### Title of the annotation

Is everything in this life just a wrapped kaobox? What if I told you that a kaobox is just a wrapper of tcolorbox?



The kaobook class

PhD Thesis

**Towards optimal resource management in solar thermal applications:  
CSP and desalination**

Juan Miguel Serrano Rodríguez

September 30, 2025

University of Almería

## The kaobook class

### Disclaimer

You can edit this page to suit your needs. For instance, here we have a no copyright statement, a colophon and some other information. This page is based on the corresponding page of Ken Arroyo Ohori's thesis, with minimal changes.

### No copyright

 This book is released into the public domain using the CC0 code. To the extent possible under law, I waive all copyright and related or neighbouring rights to this work.

To view a copy of the CC0 code, visit:

<http://creativecommons.org/publicdomain/zero/1.0/>

### Colophon

This document was typeset with the help of KOMA-Script and  $\text{\LaTeX}$  using the kaobook class.

The source code of this book is available at:

<https://github.com/fmarotta/kaobook>

(You are welcome to contribute!)

### Publisher

First printed in May 2019 by University of Almería

The harmony of the world is made manifest in Form and Number, and the heart and soul and all the poetry of Natural Philosophy are embodied in the concept of mathematical beauty.

– D'Arcy Wentworth Thompson



## Acknowledgements

Test test test

*Federico Marotta*



## Summary

I am of the opinion that every  $\text{\LaTeX}$  geek, at least once during his life, feels the need to create his or her own class: this is what happened to me and here is the result, which, however, should be seen as a work still in progress. Actually, this class is not completely original, but it is a blend of all the best ideas that I have found in a number of guides, tutorials, blogs and tex.stackexchange.com posts. In particular, the main ideas come from two sources:

- ▶ [Ken Arroyo Ohori's Doctoral Thesis](#), which served, with the author's permission, as a backbone for the implementation of this class;
- ▶ The [Tufte-Latex Class](#), which was a model for the style.

The first chapter of this book is introductory and covers the most essential features of the class. Next, there is a bunch of chapters devoted to all the commands and environments that you may use in writing a book; in particular, it will be explained how to add notes, figures and tables, and references. The second part deals with the page layout and design, as well as additional features like coloured boxes and theorem environments.

I started writing this class as an experiment, and as such it should be regarded. Since it has always been intended for my personal use, it may not be perfect but I find it quite satisfactory for the use I want to make of it. I share this work in the hope that someone might find here the inspiration for writing his or her own class.



# Contents

Acknowledgements	v
Summary	vii
Contents	ix
About the author	1
How to read this document	3
OPTIMAL WATER AND ELECTRICITY MANAGEMENT IN A COMBINED COOLING SYSTEM	
1 Solar thermal energy and water	11
1.1 Concentrated solar thermal . . . . .	11
1.1.1 Concentrated Solar Power (CSP): Concentrated Solar Power . . . . .	12
1.1.2 A brief history of CSP: from the hype to unrealized potential . . . . .	13
1.2 Cooling and water use . . . . .	14
1.2.1 Conventional condenser cooling technologies . . . . .	15
1.2.2 Non-conventional cooling: Combined / hybrid cooling . . . . .	18
1.2.3 Selection of the cooling technology . . . . .	21
2 Combined cooling pilot plant at Plataforma Solar de Almería	23
2.1 Plant description . . . . .	24
2.2 Experimental campaigns . . . . .	25
2.3 Wet cooling tower . . . . .	25
2.3.1 Physical model calibration – Exp 1 . . . . .	25
2.3.2 Data-driven models training – Exp 2 . . . . .	26
2.3.3 Experimental campaign 3 . . . . .	26
2.3.4 Dry cooler, Surface condenser and Combined cooler models . . . . .	26
3 Modelling of a combined cooling system	29
3.1 Wet cooler . . . . .	29
3.1.1 Physical model . . . . .	30
3.1.2 Samples generation for first-principles to data-driven models . . . . .	32
3.1.3 Model interface . . . . .	32
3.2 Dry cooler . . . . .	33
3.2.1 Physical model . . . . .	33
3.2.2 Samples generation for first-principles to data-driven models . . . . .	33
3.2.3 Model interface . . . . .	33
3.3 Other components . . . . .	34
3.3.1 Electrical consumption . . . . .	34
3.3.2 Surface condenser . . . . .	34
3.3.3 Mixers . . . . .	35
3.4 Complete system . . . . .	35
4 Optimization of a combined cooling system	37
4.1 Environment description . . . . .	39
4.2 Static optimization . . . . .	39
4.2.1 Dry cooler . . . . .	40
4.2.2 Wet cooler . . . . .	41
4.2.3 Combined cooler . . . . .	41
4.3 Horizon optimization . . . . .	43
4.3.1 A discussion on solving the optimization problem . . . . .	44
4.3.2 Proposed solution: Decomposition-based multi-objective optimization with trajectory planning	45

<b>5 Validation in the combined cooling pilot plant</b>	<b>49</b>
5.1 Modelling . . . . .	49
5.1.1 Wet cooler model alternatives comparison and validation . . . . .	49
5.1.2 Dry cooler model alternatives comparison and validation . . . . .	50
5.1.3 Main components modelling conclusions . . . . .	53
5.1.4 Condenser model validation . . . . .	55
5.1.5 Complete system model validation . . . . .	56
5.2 Control and optimization results . . . . .	56
5.2.1 Choosing an optimization algorithm . . . . .	57
5.2.2 Comparing the static and horizon optimization strategies . . . . .	58
5.2.3 Validation at pilot plant . . . . .	59
<b>6 Annual analysis: ANDASOL-II CSP plant</b>	<b>63</b>
6.1 Environment definition . . . . .	63
6.1.1 Water context . . . . .	63
6.1.2 Thermal load . . . . .	64
6.1.3 Costs context . . . . .	65
6.2 Implementation results . . . . .	65
6.3 Cooling alternatives comparison . . . . .	67
<b>CONCLUSIONS AND OUTLOOK</b>	<b>69</b>
Conclusions . . . . .	71
Outlook and future work . . . . .	71
Derived scientific contributions . . . . .	72
<b>Bibliography</b>	<b>73</b>
<b>Alphabetical Index</b>	<b>77</b>

## List of Figures

1	Example figure. Try clicking or scanning the QR code to access the interactive version. [1ex]	3
1.1	Two main Concentrated Solar Thermal (CST) technologies . . . . .	11
1.2	Solar tower CSP plant. Source: NREL [6] . . . . .	12
1.3	Levelized Cost of Electricity (LCOE) evolution and capacity predictions . . . . .	13
1.4	Water consumption comparison between CSP and other thermal power generation technologies. . . . .	15
1.5	Source: Aseri et al. [21] . . . . .	15
1.6	Different hybrid/combined coolers configurations . . . . .	16
1.7	Plataforma Solar de Almería (PSA) combined cooling system facility . . . . .	21
2.1	Back view of the Wet Cooling Tower (WCT) . . . . .	23
2.2	Layout of combined cooling systems pilot plant at PSA. . . . .	24
2.3	Control volume in the exchange area of a wet cooling tower arrangement . . . . .	25
3.1	Inputs-outputs block diagram of the main model components . . . . .	31
3.2	Complete model diagram of the combined cooling system . . . . .	35
3.3	Block diagram of the optimization scheme including environment components . . . . .	36
4.1	Diagram of the dry cooler only cooling problem . . . . .	38
4.2	Diagram of the wet cooler only cooling problem . . . . .	40
4.3	Diagram of the combined cooler and condenser problem . . . . .	41
4.4	Pareto fronts in different representative scenarios (top) and detailed power and hydraulic distribution for a specific scenario (bottom) . . . . .	42
4.5	Visualization of a constrained search space for two decision variables . . . . .	43
4.6	Proposed methodology. Decomposition-based multi-objective optimization with trajectory planning	44
4.7	Calibration, tuning, validation and comparison procedure . . . . .	46
5.1	Experimental results for the Me number as a function of $\dot{m}_w/\dot{m}_a$ . . . . .	49
5.2	WCT samples distribution visualization . . . . .	50
5.3	WCT Models performance regression . . . . .	51
5.4	Dry Cooler (DC) samples distribution visualization . . . . .	52
5.5	DC Models performance regression . . . . .	53
5.6	Heat transfer coefficient calibration results . . . . .	54
5.7	Combined cooler model validation . . . . .	55
5.8	Horizon optimization – path selection subproblem. Fitness evolution comparison for four different dates. . . . .	56
5.9	Detailed timeseries simulation results. Combined Cooler (CC)-horizon . . . . .	58
5.10	Implementation of the optimization strategy in the real facility. Hierarchical control . . . . .	59
5.11	Andasol I, II and III . . . . .	60
6.1	Spanish electricity mix on July 12, 2024. The peak in photovoltaic generation is clearly visible at midday, while thermosolar generation is more evenly distributed throughout the day. Peak production is majorly from CSP plants with no storage. Data source: Figure elaborated using data extracted from <a href="https://www.ree.es/es/datos">https://www.ree.es/es/datos</a> . . . . .	63
6.2	Horizon optimization results in three different seasons . . . . .	64
6.3	Annual simulation results for the different studied alternatives optimized with the proposed horizon optimization. Results are resampled every 15 days using their mean values. [1ex] . . . . .	66
6.4	Specific cooling costs comparison . . . . .	67
6.5	Multi-Effect Distillation (MED) plant at PSA specifications and nominal operating conditions . . . . .	68

## List of Tables

1	Multi-Effect Distillation (MED) plant at PSA specifications and nominal operating conditions . . . . .	4
---	--	---

2.1	Characteristics of instrumentation ( <sup>a</sup> value of the temperature in °C, <sup>b</sup> of reading, <sup>c</sup> full scale, <sup>d</sup> mean value) . . . . .	24
2.2	Design of experiments for model comparison (Exp 3) . . . . .	26
2.3	Experimental campaigns performed at the CC pilot plant, where GD- $n_1$ - $n_2$ refers to the spatial grid distribution ( $n_1$ ) around the fan with $n_2$ measurements in each quadrant ( $n_1 \times n_2$ measurements); BB- $n_1$ - $n_2$ denotes a Box-Behnken design with $n_1$ variables and $n_2$ levels; and FF- $n_1$ -...- $n_i$ indicates a full factorial design with $i$ variables, each with $n_i$ levels. . . . .	27
5.1	Bounds and discretization of the model input variables. . . . .	50
5.2	Summary table of the prediction results obtained with the different modelling approaches studied. . . . .	52
5.3	Bounds and discretization of the model input variables. . . . .	53
5.4	Summary table of the prediction results obtained with the different modelling approaches studied. . . . .	54
5.5	Performance metrics obtained with the complete (CC) and component (Cnt) models . . . . .	56
5.6	Static optimization algorithm comparison results . . . . .	57
5.7	Box-bounds for the decision variables. . . . .	60
6.1	ANDASOL-II plant main characteristics . . . . .	63

## List of Listings

## About the author

Un payaso

– Lidia Roca, probablemente

I am currently completing my PhD thesis, with the defense planned for October. My research interests lie primarily in automatic control, optimization, and robotics, especially as applied to solar thermal processes.

I think I am mostly a creative person, but in order to implement those ideas, throughout my work, I've gained experience with a variety of tools and technologies, including Linux, Python, Docker, LaTeX, and the Robot Operating System (ROS). I'm particularly passionate about open science and open source software, and I strive to contribute to communities that value transparency and collaboration.

For my bachelor's thesis, I created a mobile robotics lab in the University of Almería by deploying the [Duckietown project](#). This gave me the opportunity to interact and work with ROS, and since the whole project was deployed using Docker, to learn about containerization technologies. For my master's thesis, work was also software-related, but this time it was about the implementation of a SCADA-like system using Python. During my PhD, I have had four years to really delve into these technologies, so today they are an integral part of my workflow and I am confident to say they've helped me become effective at implementing those (sometimes too) many ideas.



Lidia esto solo lo he copiado  
por tener algo, ya lo mejoraré



# How to read this document

## TL;DR

This preliminary chapter explains how to read this document, mainly the different environment boxes used throughout the manuscript, why the large margins, what is placed in them, and how to use the interactive features of the manuscript. This is an example of a Too Long; Didn't Read (TL;DR) box. It contains an Abstract/Summary of the main point of the chapter and are placed at the beginning of every chapter.

This  $\text{\LaTeX}$  template is designed with large margins, on the one hand this allows to have shorter lines, which makes for an easier reading experience but most interestingly, it also allows to place additional information in the margins, such as side notes, side citations, figures, tables... your imagination is the limit! Or rather  $\text{\LaTeX}$  compilation errors and your patience are. Throughout this manuscript I will add side notes<sup>1</sup> to provide additional information and comments that would otherwise be too distracting and verbose to include in the main text, constantly interrupting the flow of the reading. The side notes are not essential to understand the content of the document, but mostly complementary.

1: Like this one! They are like footnotes, but placed in the margin of the page

## Boxed environments

Both problem definition boxes (e.g. ref) and model definition boxes (e.g. Model 0.2) are countered environments and can (and will) be referenced in the text.

### Problem: Problem definition box example

This is an example of a problem definition box. It is used to formally and concisely define an optimization problem.

$$\min_{\mathbf{x}, \mathbf{e}; \theta} J = f(\mathbf{x}, \mathbf{e}; \theta) = \text{XXXX}$$

with:

$$\begin{aligned} \text{out}_1, \text{out}_2 &= f(\text{in}_1, \text{in}_2, \dots, \text{in}_N) \\ \text{out}_1, \text{out}_2 &= f(\text{in}_1, \text{in}_2, \dots, \text{in}_N) \end{aligned}$$

- ▶ Decision variables

$$\mathbf{x} = [x_1, x_2]$$

- ▶ Environment variables

$$\mathbf{e} = [e_1, e_2, \dots, e_3]$$

- ▶ Fixed parameters

$$\theta = [\theta_1 = X, \theta_2 = Y]$$

subject to:

- ▶ Box-bounds

$$\begin{aligned} \cdot x_1 &\in [\underline{x}_1, \bar{x}_1] \\ \cdot x_2 &\in [\underline{x}_2, \bar{x}_2] \end{aligned}$$

- ▶ Constraints



**Figure 1:** Example figure. Try clicking or scanning the QR code to access the interactive version.



**Table 1:** MED plant at PSA specifications and nominal operating conditions

Parameter	Value
Capacity	72 m <sup>3</sup> /day
Number of effects	14
Feed type	Forward feed
Physical arrangement	Vertically stacked
Heat exchanger configuration	90/10 Cu-Ni HTE
Heat source type	Hot water
Top Brine Temperature (TBT)	70 °C
Condenser temperature	35 °C

2: I believe that this is a good way to make the document more accessible and to encourage readers to explore the content in more depth. However, the interactive features are optional and not necessary to understand the content of the document.



3:

¶: Like hoarding toilet paper

- $|out_X - out_Y| \leq \epsilon_1$
- $out_X \leq out_Z - \Delta Z$

### Model 0.2: Model definition box example

$out_1, out_2 = \text{some cool model}(in_1, in_2, in_3)$

### Other boxes

Other boxes are used to highlight important points, or to provide additional information that is not essential to the main text.

In order to make the book more interactive and link-friendly, I have enabled hyperlinks in the PDF. This means that you can click on the references, citations, and links to external resources, and they will take you to the corresponding location. This is standard latex, however to maintain a consistent experience in the physical version, QR codes are inserted in the margin next to the links. The reader is invited to scan them with a QR code reader to access the corresponding online resource<sup>2</sup>. Some figures also include QR codes that link to an interactive (HTML) version of the figure, see Figure 1 as an example.

The additional material as well as the source code of this document are hosted in a [Zenodo repository](#)<sup>3</sup>. Alternatively, a mirror repository is also available at:

<https://github.com/juan11iguel/my-thesis>

It seems unlikely that both Zenodo and GitHub will go down at a time where this document is still relevant, and if they do, I think there will be more important things to worry about than losing access to the interactive content of this thesis. ¶

*The harmony of the world is made manifest in Form and Number,  
and the heart and soul and all the poetry of Natural Philosophy  
are embodied in the concept of mathematical beauty.*

– D'Arcy Wentworth Thompson



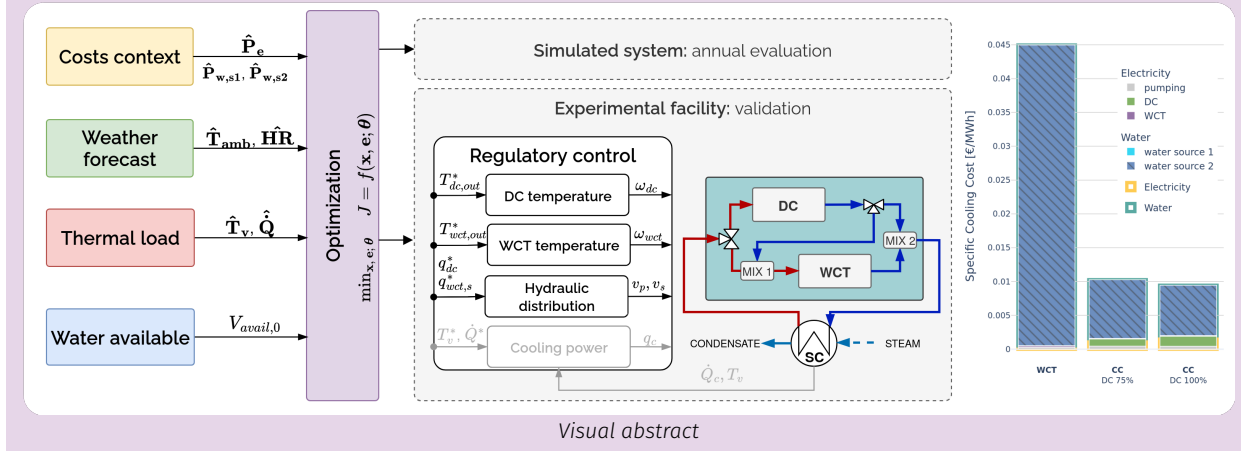
# **OPTIMAL WATER AND ELECTRICITY MANAGEMENT IN A COMBINED COOLING SYSTEM**



## TL;DR

To enhance the applicability and sustainability of solar thermal technologies, this work investigates a novel cooling system for the power block of a CSP plant, combining dry and wet cooling components. A model of the Combined Cooling System (CCS) was developed alongside a two-stage optimization strategy. The methodology was validated using an experimental pilot plant, achieving  $R^2$  values above 0.9 for the main output variables and successfully adapting the plant's operation to changing conditions.

A case study is presented for a commercial 50 MWe CSP plant with 8 hours of storage, Andasol-II, using annual simulations under a water-scarcity scenario where the current wet-only cooling system is replaced with the proposed CCS. Results indicate a potential 80 % reduction in cooling costs and a 48 % reduction in mean annual water use, but more importantly, a 38 % reduction during the driest and hottest months, demonstrating the significant potential of the system when operated optimally.



## Part structure

This part is structured as follows: first in Chapter 1 (Solar thermal energy and water) a context of concentrated solar thermal technologies is provided and their relationship with the water resource, specifically for the case of CSP. Then, the experimental CCS pilot at PSA is presented in Chapter 2. The methodology for modelling and optimizing the operation of the system are described in Chapter 3 and Chapter 4, respectively. Both are validated in the experimental plant as showcased in Chapter 5. Finally, Chapter 6 (Annual analysis: ANDASOL-II CSP plant), describes and analyzes the results of the annual simulations performed for a commercial CSP plant using the proposed cooling system.



# Solar thermal energy and water

## TL;DR

In the pursuit of eliminating reliance on fossil fuels sources for energy generation and replacing them by renewable sources, CSP has proven to be a reliable contributor. In particular, in providing much needed energy storage, dispatchability and ensuring grid stability.

However, water availability emerges not only as a technical constraint but also as a planning and policy issue. CSP deployment in water-stressed regions is strongly dependent on innovative cooling solutions, policy incentives, and careful water resource management to ensure sustainable operation without compromising water security for local communities.

Ideally, negligible raw water would be needed to operate a CSP plant and it should be achieved with no increase in the LCOE. The most water demanding component is the cooling of the power block, and currently this water saving can be achieved with dry cooling and an increase of 7% in the LCOE. A compromise solution can be reached by using hybrid cooling solutions together with water preservation strategies, achieving an 83% decrease in raw water consumption with respect to wet cooling with no reuse and a 5% increase in the LCOE [1].

Further savings can be achieved by optimizing the operation of the combined cooler and take full advantage of its flexibility towards optimal resource management.

<b>1.1 Concentrated solar thermal . . . . .</b>	<b>11</b>
1.1.1 CSP: Concentrated Solar Power . . . . .	12
1.1.2 A brief history of CSP: from the hype to unrealized potential . . . . .	13
<b>1.2 Cooling and water use . . . . .</b>	<b>14</b>
1.2.1 Conventional condenser cooling technologies . . . . .	15
1.2.2 Non-conventional cooling: Combined / hybrid cooling . . . . .	18
1.2.3 Cooling technology selection . . . . .	21

## 1.1 Concentrated solar thermal

CST technologies use heliostats or mirrors to reflect and concentrate solar radiation onto a receiver. There, the radiation is captured as heat, also known as thermal energy. They can be classified in different ways<sup>1</sup>, using temperature, two broad groups can be identified.

The first group includes lower-temperature systems operating below 400 °C. These are typically used for applications such as power generation, district heating, cooling, and desalination. It is worth noting that most industrial heat

1: With some parameters being correlated; for example, higher operating temperatures generally mean higher concentration factors



(a) Parabolic trough pilot plant at PSA



(b) Gemasolar 20MWe-15h central tower CSP plant in Sevilla, Spain. Source: Wikipedia

Figure 1.1: Two main CST technologies. In (a) collector rows positioned facing each other purely for cinematographic purposes

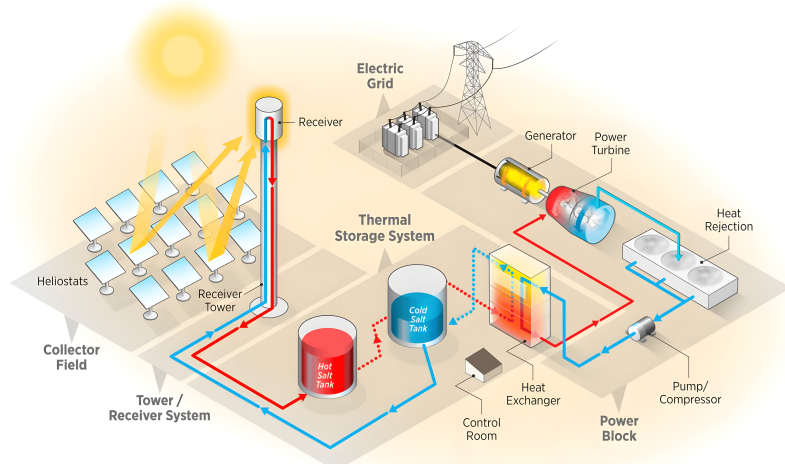


**Figure 1.2:** Solar tower CSP plant. Source: NREL [6]

[2]: Schoeneberger et al. (2020), “Solar for Industrial Process Heat”

2: Flat-plate collectors, though non-concentrating also deserve mention here, as they remain the most widely deployed solar thermal technology [3]

[4]: Thonig et al. (2023), “Concentrating Solar Technology Policy Should Encourage High Temperatures and Modularity to Enable Spillovers”

[5]: Mehos et al. (2020), “Concentrating Solar Power Best Practices Study”

3: In the context of the industrial life-cycle (ILC) [10], the formative phase considers the period in which a technology and its industry and innovation system are still immature and need to grow and develop

[7]: Pfenninger et al. (2014), “Potential for Concentrating Solar Power to Provide Baseload and Dispatchable Power”

[8]: Binz et al. (2017), “Toward Technology-Sensitive Catching-Up Policies”

[9]: Lilliestam et al. (2021), “The Near- to Mid-Term Outlook for Concentrating Solar Power: Mostly Cloudy, Chance of Sun”

[11]: Mir Artigues et al. (2019), *The Economics and Policy of Concentrating Solar Power Generation*

demand lies within this relatively low-temperature range of 100–400 °C [2]. This segment of CST is also the most technically mature. Over the past decades, considerable progress has been made in line-focus technologies such as parabolic troughs (see Figure 1.1 (a)) and linear Fresnel collectors<sup>2</sup>. Although these systems have reached a high level of development, their potential for significant further cost reduction is relatively limited.

The second group comprises high-temperature systems operating above 600 °C. These rely on point-focus technologies, most notably central receiver systems (see Figure 1.1 (b)). Still under development, they show promising potential for higher-value applications, including solar-driven chemical processes (such as aviation fuel production) and the provision of high-grade industrial heat in sectors like cement manufacturing [4]. Central receiver technology, however, remains at an earlier stage of commercial maturity. Fewer plants have been built, and many existing installations employ a mix of technical approaches [5].

### 1.1.1 CSP: Concentrated Solar Power

In a concentrated solar power plant, power is generated with a Rankine-cycle like in a conventional thermal power plant, however, the working fluid is heated up not by combusting/burning a fossil fuel, but as mentioned, by concentrating solar energy as shown in Figure 1.2.

By coupling CSP with thermal storage – Figure 1.2 - *Thermal Storage System* – it can generate electricity after sundown or even days later, for example during adverse weather periods. Because of this ability, CSP is one of the few renewable electricity technologies that can generate fully dispatchable or even fully baseload power at very large scale [7]. Finally, the exhaust steam from the turbine –Figure 1.2 - *Power block* – is directed to a condenser, where its latent heat of vaporization is transferred to the available cooling medium.

CSP is an engineering-heavy, complex technology, with each project being different and tailored to both the environment in which it stands and the requirements of each single offtaker [8]. This means, that despite its relative long history, is still in its formative phase [9]<sup>3</sup>. As CSP is not yet competitive with other new generation, and especially not with operating and depreciated generators, it requires policy support to be economically viable [11]. This is due to its irregular historical development.

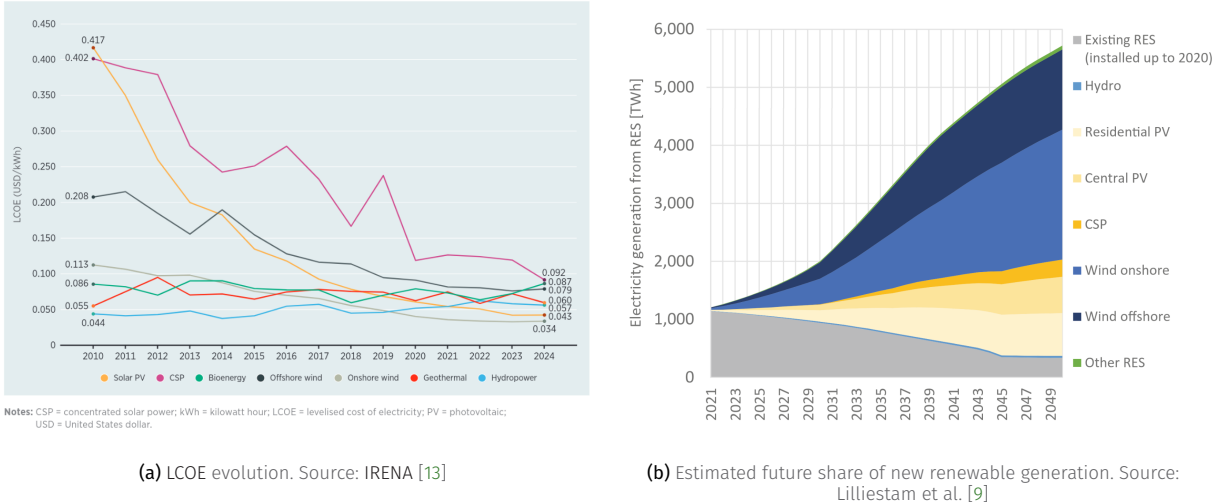


**Figure 1.3:** LCOE evolution and capacity predictions for different renewable technologies. Share is dominated by variable renewable energies and CSP is the fifth largest contributor, serving as a “gap filler” for the system flexibility of the EU electricity system [14]

### 1.1.2 A brief history of CSP: from the hype to unrealized potential

At one point, CSP was seen as the leading alternative for large-scale solar energy. Ambitious visions and bold initiatives—such as the Desertec project—played a key role in generating immediate excitement around the technology [12]. However, the political consequences of raising expectations that were ultimately unmet proved significant. In Europe, this disillusionment contributed to CSP becoming politically sidelined for many years [12]. Additionally, around 2010-2012 the cost crossover with Photovoltaic (PV) occurred and from there the PV cost advantage only increased [13]. Many investments shifted from CSP to the more straightforward and profitable PV technology.

The development of CSP has been marked by alternating periods of rapid expansion and sharp decline, largely shaped by national policy support. In the 1980s, California’s incentives led to the construction of nine CSP plants totaling around 350 MWe, but the withdrawal of support caused the bankruptcy of the main developer of solar thermal electric projects, *Luz*, in 1991, resulting in a 15-year global pause in new projects. A second growth phase began in 2007 with feed-in tariffs in Spain and temporary backing in the US, leading to the construction of about 50 plants, mostly supplied by Spanish and German companies. However, the end of policy support in both countries around 2013 led to a sharp slowdown, with construction activity in 2016 at just one-third the 2012 level, and many firms exiting the sector. CSP remained commercially active mainly through projects in Morocco and South Africa, although costs increased and future prospects dimmed. Momentum returned in 2016 when China introduced a new feed-in tariff aimed at 5 GWe of capacity, sparking renewed global interest. Optimism was further strengthened by major projects launched in Dubai and Morocco in 2018-2019. The near- to mid-term outlook for CSP is very uncertain but there are several positive developments concerning the global value chain and cost development. The market and policy outlook is bleak with the risk of a complete loss in many markets for CSP [9].

Setting realistic targets may ultimately be more effective than raising expectations that cannot be met. CSP remains a valuable technology for the energy transition—though likely at a smaller scale than initially envisioned, and over a longer timeframe. Several studies highlight its potential role in a zero-carbon or near zero power system [15]. For instance, the International Energy Agency

[12]: Schmitt (2018), “(Why) Did Desertec Fail?”

[13]: IRENA (2025), *Renewable Power Generation Costs in 2024*

[9]: Lilliestam et al. (2021), “The Near- to Mid-Term Outlook for Concentrating Solar Power: Mostly Cloudy, Chance of Sun”

[15]: Bonilla et al. (2022), “Feasibility and Practical Limits of Full Decarbonization of the Electricity Market with Renewable Energy”

[16]: IEA (2021), “Net Zero by 2050 - A Roadmap for the Global Energy Sector”

[17]: IRENA (2024), “World Energy Transitions Outlook 2024: 1.5°C Pathway”

[18]: Lilliestam et al. (2023), “Scaling up CSP”

[13]: IRENA (2025), *Renewable Power Generation Costs in 2024*

[19]: Alliance (2024), *Blue Book of China's Concentrating Solar Power Industry 2024*

(IEA)’s Net Zero by 2050 report projects that the global CSP capacity should reach 73 GWe by 2030 and 281 GWe by 2040 [16]. Likewise, IRENA envisions several hundred gigawatts of CSP by 2050, contributing to grid stability alongside a projected 8500 GWe of solar PV and 6000 GWe of wind capacity [17]. These projections suggest that CSP can play a complementary role to PV and wind by providing dispatchable, on-demand renewable electricity—further enabling intermittent renewable alternatives. However, even at these more modest levels, CSP deployment would need to accelerate rapidly (see Figure 1.3 (b)). To meet the IEA’s 2030 target, the global CSP fleet—standing at just 6 GWe in 2021—would need to expand more than tenfold in under a decade [18]. So far this is not happening, CSP technology remains niche with only 7 plants coming online in the 2020–2023 period [13] and is unlikely to become a globally important contributor to power system balancing in the next decade [18]. However the winds might be changing: 4 new plants came online in 2024, the costs of new CSP stations have decreased rapidly in the last years, 77% from 2010 to 2024, including a 46% reduction from 2023 to 2024 (see Figure 1.3 (a)). In terms of LCOE, it means that CSP has improved from 0.402 \$<sub>2024</sub>/kWh to below 10 cents (0.092 \$<sub>2024</sub>/kWh) making it competitive with new fossil fuel power stations [13] and the Chinese CSP project pipeline includes 37 future and ongoing projects, with a total capacity of 4.8 GWe [19].

## 1.2 Cooling and water use

The successful deployment of CSP plants depends on several key factors: high annual direct normal irradiance, adequate land availability, and sufficient water resources. However, while the first two are typically found in arid regions as shown in Figure 1.4, the availability of water is often limited. In such locations, the source of raw water is usually restricted to groundwater or limited surface water bodies such as rivers, lakes, wells, or artificial reservoirs.

A CSP plant consumes water for various purposes, with the most significant demand coming from the cooling of the power block<sup>4</sup>. The power output and efficiency of a thermal power plant are strongly influenced by the operating temperature and pressure conditions at the condenser, which are directly linked to the turbine backpressure, and in turn to the cooling system.

In addition to cooling, water is also required for other plant operations, including [1]:

- ▶ Mirror cleaning (1.3% of total water consumption)
- ▶ Boiler blowdown (1.4%)
- ▶ Miscellaneous uses, such as air-cooled condenser (Air-Cooled Condenser (ACC)) bundle cleaning, auxiliary equipment cooling, and general infrastructure and staff needs.

In wet-cooled CSP plants, cooling water accounts for over 95% of the total water consumption, which can be further broken down into evaporation: 77.8% and blowdown and drift: 19.1% [1].

4: When wet cooling is used, further explained in the following

[1]: Rohani et al. (2021), “Optimization of Water Management Plans for CSP Plants through Simulation of Water Consumption and Cost of Treatment Based on Operational Data”

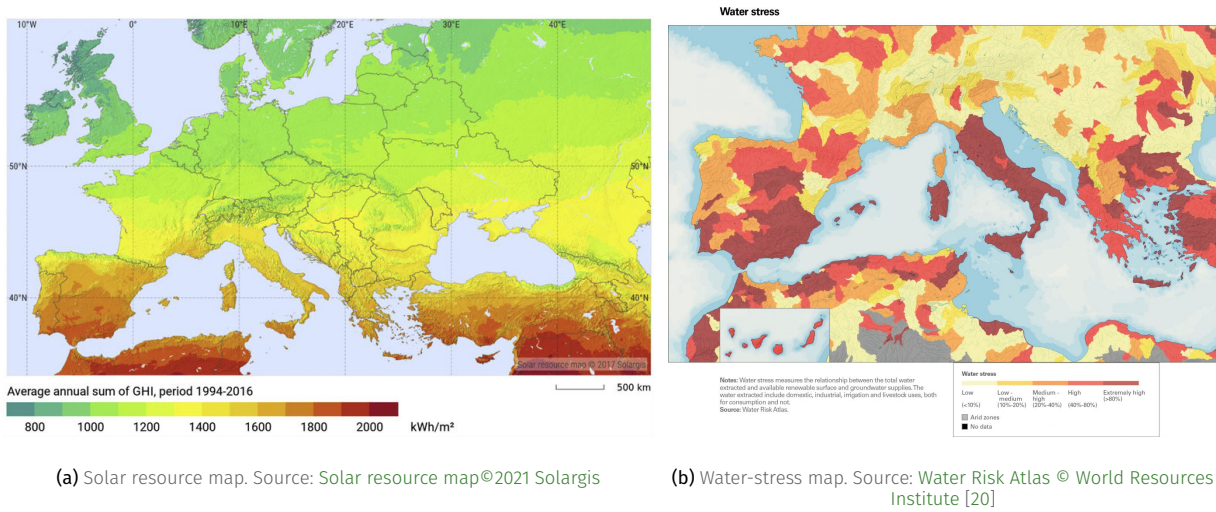


**Figure 1.4:** Greater potential for solar-powered processes takes place in water-scarce regions

Although CSP plants share a similar power cycle with other thermal power technologies, their water consumption patterns differ (see Figure 1.5). This is due to their unique capacity factor, operating schedule, and particularly their strong dependency on weather conditions, which contrasts with the more stable operation of fossil-fired plants. In contrast, conventional thermal power plants (e.g. coal, gas, or nuclear) are often sited near reliable freshwater sources, such as rivers or lakes, allowing them to utilize wet cooling without severe resource constraints. These plants are not tied to solar availability and can prioritize water access in their location decisions. CSP plants, however, must prioritize solar access and land availability — and thus have less flexibility in selecting sites with abundant water.

### 1.2.1 Conventional condenser cooling technologies

To date, the conventional systems used to remove excess heat from CSP plants are either wet (water-cooled) or dry (air-cooled), each with distinct characteristics and trade-offs regarding water usage, thermal performance, and cost.

#### Reminder: Cooling thermodynamic concepts

- ▶ The *cooling range* refers to the temperature drop experienced by the cooling water as it circulates through the condenser. The greater the better.
- ▶ The *approach* of the cooling tower is the temperature difference between the circulating water at the condenser inlet (or cooling tower outlet) and the lowest attainable cooling medium temperature, which varies depending on the cooling technology used.
- ▶ The *Initial Temperature Difference (ITD)* is the temperature difference between the hot fluid entering the cooler and the reference sink (e.g., dry-bulb temperature) at the cooler inlet.
- ▶ *Terminal Temperature Difference (TTD)* represents the difference between the outlet temperatures of the cooling and the cooled fluids.

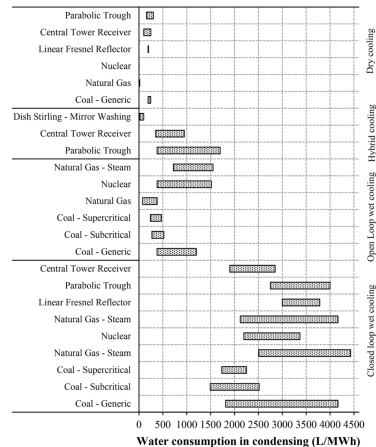


**Figure 1.5:** Water consumption comparison between CSP and other thermal power generation technologies. Source: Aseri et al. [21]



Figure 1.6: Conventional cooling technologies

### Wet cooling

Water has traditionally been used as the cooling medium in wet cooling technology due to its high heat capacity and the possibility of reuse. In power plants, the steam exiting the turbine is condensed in a surface condenser, where cooling water circulates through tubes and absorbs the latent heat of the steam. The warmed cooling water is then returned to the cooling system for heat rejection, in closed-loop systems, or returned to the body of water in open-loop (*i.e.* once-through) systems. In CSP plants, closed-loop systems are predominantly used, as they require significantly less water.

Wet cooling towers function as heat rejection devices by bringing warm water from the condenser into direct contact with air. As part of the water evaporates, it absorbs heat from the remaining liquid, thereby lowering its temperature. The cooled water is then recirculated back to the condenser, completing the loop. This process is highly efficient, but it also leads to water losses from evaporation, drift, and blowdown.

Wet cooling technology requires a substantial amount of water (1.8–4 l/kWh) for condenser cooling, particularly in closed-loop systems that employ wet cooling towers to reject heat from the condenser water to the atmosphere through evaporative cooling [22]. While a small share of heat is removed through sensible air-to-water heat transfer, 80–90% of the cooling is achieved through the latent heat of vaporization [23].

Land availability for cooling systems is often constrained, particularly in central receiver plants where the solar field surrounds the receiver and requires unobstructed space for heliostat placement. For this reason, compact wet cooling designs using forced-draft towers are predominantly employed, such as the example shown in Figure 1.6 (a).

#### CSP plants next to the sea, why not?

Building CSP plants near the sea is generally not recommended. Although seawater could serve as an unlimited resource for once-through steam condensation, solar radiation is typically lower in coastal areas, land prices are higher, and the salty environment accelerates corrosion, which significantly reduces optical efficiency

[22]: Meldrum et al. (2013), "Life Cycle Water Use for Electricity Generation"

[23]: Colmenar-Santos et al. (2014), "Water Consumption in Solar Parabolic Trough Plants"

#### Wet cooling main characteristics

- ▶ Water consumption: 1.8–4 l/kWh [22]
- ▶ Parasitic load:  $\approx 0.0165 \text{ kW/KWh}$  or 0.165 % average annual consumption [24].
- ▶ Wet cooling consumes similar power along the year but increases its water consumption in the hotter months [25].

- ▶ CSP plants with wet cooling towers consume as much as  $1.7 \times 10^6 \text{ m}^3$  per year of operation [1].
- ▶ Greater available approach, since the lowest attainable temperature is the wet-bulb temperature.
- ▶ 55 % of CSP plants worldwide make use of wet cooling technology for condenser cooling [26, 27]

## Dry cooling

In dry cooling, heat is rejected to the surroundings by convection via extended or finned surfaces or tubes arranged in a row, and each row consists of numerous cells [28]. In this type of cooling, the warm water and the ambient air do not have direct contact with each other (as in wet cooling). But because air is a poor heat transfer medium, the condenser must operate at a higher temperature and pressure to drive heat out efficiently. This sensitivity to ambient air temperature leads to elevated turbine backpressure, specially during hot weather, reducing thermal efficiency and power output compared to wet cooling systems. Dry cooling systems can be broadly categorized as direct or indirect [29].

In direct systems, turbine exhaust steam is delivered straight to an ACC (see Figure 1.6 (b)), where heat rejection to the environment occurs in a single step. The steam is condensed inside finned tubes by ambient air blown across the exterior finned surfaces arranged in A-frame (forced draft) or delta (induced draft) configuration. This process relies on latent heat transfer and can employ either mechanical or natural draft designs. ACCs have been used for nearly 70 years, and were pioneered in regions as diverse as Western Europe, South Africa and the Middle East. The largest ACC units in operation is in South Africa (Medupi) with six fossil-fuel driven 800-MWe units on ACCs [30].

In indirect systems, steam first condenses in a separate condenser, which may be either a conventional shell-and-tube surface condenser or a barometric condenser (direct-contact type), where steam meets a spray of cooling water. The resulting warm cooling water is then circulated to an ACHE (see Figure 1.6 (c)) for final heat rejection to the atmosphere. This arrangement introduces an additional heat exchange stage, so the ACHE handles only sensible heat transfer, requiring greater heat exchange surface area but being less sensitive to fluctuations in ambient temperature.

A prominent example of an indirect dry cooling configuration is the Heller system, named after its inventor Prof. H. Heller in Hungary in the 1940's [31, 32]. In the direct-contact Heller system, steam from the turbine condenses in a barometric condenser, and the resulting warm cooling water is cooled in an ACHE before recirculation. Thermal performance is generally comparable to that of an ACC, but mechanically driven Heller systems tend to have higher specific electrical consumption because, in addition to fan power, extra pumping power is required to overcome the jet condenser's added pressure drop [33].

If an indirect-contact surface condenser is used instead of a barometric condenser, the setup is generally less efficient than both ACCs and the direct-contact Heller configuration because it introduces a TTD (TTD  $\approx 3\text{--}4^\circ\text{C}$  versus  $\approx 0.3^\circ\text{C}$  for direct-contact), resulting in lower overall cycle efficiency.

Natural draft dry cooling towers—commonly associated with barometric condenser systems—can only be used in parabolic trough plants. In central receiver systems, their significant size (about 135 m tall) would obstruct the heliostat field. A possible alternative is fan-assisted natural draft systems, which reduce tower height to around 50–70 m while retaining some benefits of natural draft operation [34]. According to Andras et al., Heller systems require approximately the same capital costs but are much cheaper to operate since they do not need

[28]: Turchi (2010), *Parabolic Trough Reference Plant for Cost Modeling with the Solar Advisor Model (SAM)*

[29]: Maulbetsch (2004), *Comparison of Alternate Cooling Technologies for U.S. Power Plants: Economic, Environmental, and Other Tradeoffs*

[30]: Maulbetsch (2012), *Economic Evaluation of Alternative Cooling Technologies*

[31]: Jászay (1958), “Indudustrial Review-Aus Der Industrie. The Air-Cooled Condensing Equipment” System Heller” a Comprehensive Survey”

[32]: Balogh et al. (2006), “Heller’s Indirect Approach Widens Applicability of Dry Cooling”

[33]: Mil’man et al. (2020), “Air-Cooled Condensing Units in Thermal Engineering (Review)”

[34]: Andras et al. (2005), “Advanced Heller System Technical Characteristics”

to be mechanically driven. They have been operating for decades in 17 power plants including the largest indirect dry cooled combined cycle power plant with 3x777 MWe dry towers at Gebze-Adapazari combined cycle (Turkey).

Unlike wet cooled plants, the dry cooled plants require minimal waterside infrastructure and other related components. None dedicated to the cooling such as water supply network evaporation ponds, storage ponds, treatment plants for condenser cooling water. As a consequence, for the dry-cooled plants, capital and operation and maintenance costs of these components are negligible [30].

[21]: Aseri et al. (2022), "Condenser Cooling Technologies for Concentrating Solar Power Plants"

[29]: Maulbetsch (2004), *Comparison of Alternate Cooling Technologies for U.S. Power Plants: Economic, Environmental, and Other Tradeoffs*

However, a recent review on condenser cooling technologies [21] shows that a dry-cooled Parabolic Trough (PT) based plant would deliver 3–10% less annual electricity output and would cost 4% to 10% more than a wet-cooled plant resulting in 2% to 19% increase in LCOE. It was also observed that due to large differences in operating temperature of power cycle (560 °C for Solar Tower (ST) based plants and 391 °C for PT based plants), the reduction in net electricity output for ST based plants is less as compared to PT based plants (Sau et al., 2016). It should be noted that many of these analysis were made for first generation CSP with no thermal storage, which is an outdated technology. The inclusion of thermal energy storage in the dry or hybrid cooling plant (six hours of storage capacity) can reduce the overall penalty of LCOE considerably: 8.1% to 6.3% for dry-cooled as compared to wet-cooled plants [21]. According to Maulbetsch et al. [29], the *breakeven* water cost at which wet and dry cooling have the same annual costs (for situations in which the rest of the base case values and assumptions apply) is between 2.00 and 3.00 USD<sub>2002</sub>/kgal.

#### Dry cooling main characteristics

- ▶ Capital cost ratio ranges from 4.5 times at a hot, arid site to about 3.5 times at more moderate sites [29].
- ▶ Electrical consumption: 1.5 to 5 times wet cooling, 0.05–0.06 kWe/kWh
- ▶ Penalty up to 25% during the hottest hour of the year [29] and 5–6% average annual parasitic consumption [21, 35, 36].
- ▶ Limited approach, constrained by the dry-bulb temperature, worsened if an indirect contact surface condenser is used.
- ▶ 24% of commercial plants make use of this technology [26, 27].
- ▶ Most new plants expected to be built in the next years will make use of dry cooling [19].

[37]: Hu (1976), *Engineering and Economic Evaluation of Wet/Dry Cooling Towers for Water Conservation*

[38]: Zaloudek et al. (1976), *Study of the Comparative Costs of Five Wet/Dry Cooling Tower Concepts*

[39]: Loscutoff (1975), *Preliminary Evaluation of Wet/Dry Cooling Concepts for Power Plants*

[40]: Wiles et al. (1978), *Description and Cost Analysis of a Deluge Dry/Wet Cooling System*.

#### 1.2.2 Non-conventional cooling: Combined / hybrid cooling

While energy efficiency has long been a priority, water conservation only began receiving significant attention in recent years. This is reflected in the large number of wet-cooled CSP plants built in the past. Today, some of these plants face growing scrutiny and competition for water resources, as many regions of the world experience prolonged periods of water stress. In response, a third alternative is gaining traction: hybrid or combined cooling technologies, which integrate the advantages of different cooling methods (wet and dry) into a single, innovative system. The concept has been explored since the 1970s [37–40] and regained momentum in the following decades [29, 30], although early studies primarily focused on fossil-fuel and nuclear thermal power plants. Over the past decade, interest sparked in evaluating hybrid cooling solutions specifically for concentrated solar power systems.

### Terminology: Combined vs Hybrid Cooling

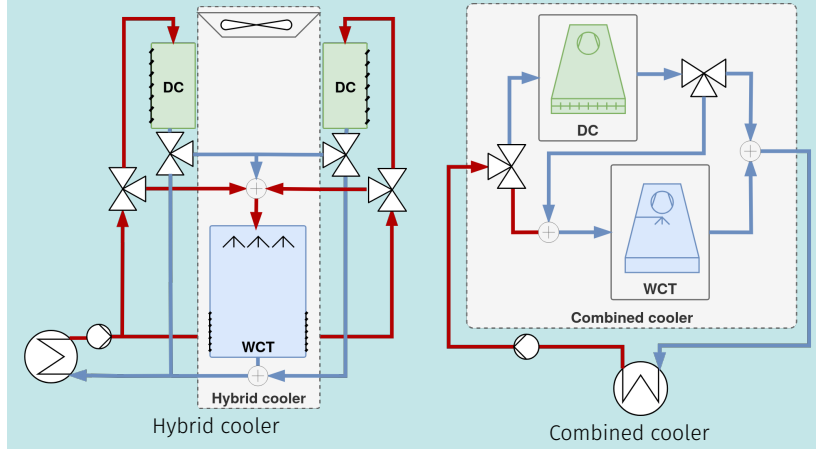
In the literature, two terms are commonly used to describe cooling systems that integrate both wet and dry components: *hybrid* and *combined*.

**Hybrid systems** refer to configurations where the dry and wet cooling components are integrated into a single physical unit. An example is a cooling tower with two sections—an upper dry section followed by a wet section that can be activated as needed.

**Combined systems** by contrast, consist of separate, independent dry and wet units connected by a hydraulic circuit. Each component is physically distinct and operates independently.

From a thermodynamic perspective, hybrid and combined systems are functionally equivalent. However, hybrid systems tend to be more compact due to their integrated design, while combined systems offer greater flexibility in component layout and maintenance. Additionally, combined systems are often easier to implement in practice, as the individual dry and wet components are commercially available off the shelf—unlike hybrid units, which may require custom design and manufacturing.

These differences are not all that important, so the two terms can be used interchangeably.



Many heterogeneous hybrid/combined coolers can be found comprising different components with different arrangements:

1. Water-enhanced dry cooling. A dry cooler (usually ACC) switchable to wet (deluge condenser cell). In the deluged condenser configuration, dry-cooling is prioritized until a certain backpressure is reached. When this happens water is sprayed wetting the exchanging surfaces, which now act equivalently to the packing bed in a wet cooling tower [1, 38–41]. The overall heat transfer rates are improved since now the transfer mechanism is air to the water film that evaporates, but air-metal contact is lost, effectively disabling the dry-cooling mechanism. In this configuration is either one or the other. Still, because the nominal cooling capacity of such systems is usually achieved by assembling multiple smaller cells, it is possible to operate them in parallel. In practice, this means that some cells can remain in dry mode (or even be designed exclusively for dry operation), while others can be switchable to wet mode when needed. See Figure 1.7 (a) for an example of such system.
2. Dry cooler (usually ACC) + WCT in parallel [30, 42, 43]. In this configuration

[1]: Rohani et al. (2021), “Optimization of Water Management Plans for CSP Plants through Simulation of Water Consumption and Cost of Treatment Based on Operational Data”

[38]: Zaloudek et al. (1976), *Study of the Comparative Costs of Five Wet/Dry Cooling Tower Concepts*

[39]: Loscutoff (1975), *Preliminary Evaluation of Wet/Dry Cooling Concepts for Power Plants*

[40]: Wiles et al. (1978), *Description and Cost Analysis of a Deluge Dry/Wet Cooling System*.

[41]: Golkar et al. (2019), “Determination of Optimum Hybrid Cooling Wet/Dry Parameters and Control System in off Design Condition”

[30]: Maulbetsch (2012), *Economic Evaluation of Alternative Cooling Technologies*

[42]: Barigozzi et al. (2011), “Wet and Dry Cooling Systems Optimization Applied to a Modern Waste-to-Energy Cogeneration Heat and Power Plant”

[43]: Barigozzi et al. (2014), “Performance Prediction and Optimization of a Waste-to-Energy Cogeneration Plant with Combined Wet and Dry Cooling System”

[44]: Palenzuela et al. (2022), "Experimental Assessment of a Pilot Scale Hybrid Cooling System for Water Consumption Reduction in CSP Plants"

[45]: Asvapoositkul et al. (2014), "Comparative Evaluation of Hybrid (Dry/Wet) Cooling Tower Performance"

[46]: Hu et al. (2018), "Thermodynamic Characteristics of Thermal Power Plant with Hybrid (Dry/Wet) Cooling System"

5: Specially in the combined cooler case, in the hybrid alternative it might not be as straightforward

part of the vapor is directed to an ACC while the rest goes to a surface condenser cooled by a wet cooling tower. Each cooler can be sized independently. A commercial example of such system can be seen in Figure 1.7 (b).

3. Surface Condenser (SC) + ACHE + WCT in series.
4. SC + (ACHE+WCT) in series-parallel [44–46]. The series-parallel configuration is interesting since it offers the greatest degree of flexibility, at the cost of adding two heat transfer processes in series at a minimum (SC→ACHE) and three if in series configuration: SC→ACHE→WCT, though this last one is intended and not so problematic since the wet cooling has a higher ITD (difference between outlet temperature from dry cooler and wet bulb temperature). Flexibility is provided by the almost continuous flexible hydraulic configuration: only series, only parallel, any configuration in between or only one of the systems. But also in the design, each cooler can be sized independently<sup>5</sup>. This allows to optimize the system adhoc for each particular deployment by running simulations with the expected operation conditions and prioritizing more the wet or the dry component. An example of such system is shown in Figure 1.7 (c).

From a literature review a few conclusions can be drawn:

- ▶ Air flow rates are very different between dry and wet systems, so any design needs to allow independent regulation of each. In the combined configuration (separate coolers) this is easily achieved since they have independent fans. On the other hand for hybrid systems with a single shared fan louvers can be used to regulate the air flow through each section [45].
- ▶ Corrosion might be a problem in the deluged condenser, if so, plastic exchange surfaces might have to be used, further decreasing already low heat transfer coefficients.
- ▶ If dry and wet systems share the condenser *i.e.* the hydraulic circuit. A direct contact jet-condenser type cannot be used, since the power cycle requires high-quality water and large amounts would need to be constantly replenished because of the wet cooler evaporation.
- ▶ If the dry cooler is going to be the main cooling source throughout the year, options that combine an ACHE with a surface condenser, are going to penalize the dry cooling component compared to alternatives like the ACC or Heller system -both with or without delugement or a parallel only configuration.
- ▶ On the contrary, during operation systems that allow combinations of series-parallel configurations provide the greatest potential to adapt the cooling system to the changing operation and ambient conditions. The series configuration is a water conservative configuration while still being able to maintain the required backpressure despite adverse conditions. The parallel configuration maximizes cooling capacity but is more water intensive.

Hybrid/combined cooling technology generally requires larger infrastructure as it comprises of components of both wet and dry cooling technologies, though much smaller water side infrastructure [1]. Also, the potential for water reuse for a hybrid system according to Rohani et al. [1] can amount to 23% of the total raw water consumption. An important part of this water can be treated and reused without significantly increasing the production costs: up to 14% reduction with the same production cost or even slightly reduced.

These systems are a compromise between full-wet and full-dry systems. Due to their heterogeneity depending on the prioritized objective their costs and consumptions can be closer to one or the other. Such systems can be sized for a range of desired water savings. The systems are normally considered for annual water use targets of from 15 % to 85 % of that used by a wet cooling

[1]: Rohani et al. (2021), "Optimization of Water Management Plans for CSP Plants through Simulation of Water Consumption and Cost of Treatment Based on Operational Data"



(a) Schematic depicting the integration of a deluge condenser (wet) cell together with an ACC cell  
Source: ENEXIO Management GmbH

(b) A parallel ACC-WCT.  
Source: Maulbetsch et al. [29]

(c) Combined cooling system at PSA

**Figure 1.7:** Different hybrid/combined coolers configurations

system. Outside that range, they are normally not economically attractive. When even less water than this is available, water-enhanced dry systems might be the better option [29]. For some configurations (when using indirect dry cooling) they can get more expensive than the standalone ACC alternative [30]. Finally, the inclusion of thermal energy storage in the hybrid cooled plant (six hours of storage capacity) can reduce the overall penalty of LCOE from 6.4 % to 3.2 compared to wet-cooled plants [21].

[21]: Aseri et al. (2022), "Condenser Cooling Technologies for Concentrating Solar Power Plants"

#### Hybrid cooling main characteristics

1. Capital cost: 2–3.5x [30]
2. Penalty: 1–3 %, 2–8 % in LCOE [21],
3. Just one commercial CSP plant makes use of this technology [47]

**NOTE:** Due to the novelty and heterogeneity of these systems, values can change significantly.

### 1.2.3 Selection of the cooling technology

Selection of condenser cooling technology can affect the financial as well as technical viability of concentrating solar power (CSP) plants. These differences between technologies are dependent on the environmental conditions (local water cost, local temperature, etc). Except for extreme cases: no water availability making a dry cooler the only choice or plenty water availability throughout the year leading to the obvious decision of a wet cooler, this is not a trivial decision. Dry cooling is increasingly used in CSP projects, even though they typically come with higher capital costs and reduced thermodynamic performance, particularly in hot weather for the dry only alternative. These systems trade water savings for lower efficiency, making the choice of cooling technology a critical design decision that balances technical, economic, and environmental considerations.

Selecting the cooling technology is not trivial, specially if a hybrid cooler is chosen. The relative capability of the wet and dry systems is the primary determinant of the system cost. This, in turn, depends on: the amount of water available for cooling and the value of plant output during the hottest hours of the year compared to the average value over the entire year. As a general rule, the more water available for cooling, the cheaper and more efficient is the cooling system. If the amount of water available is between 15% and 85%

of that required for an all-wet system, the capital cost of a hybrid system will be intermediate between the costs of an all-wet and an all-dry system [29]. Also, environment context and costs structures are strongly dependent on the particular location and affect decision-making. Annual simulations of the different cooling alternatives should be performed using weather data for the particular location, local water availability throughout the year, and performing a techno-economical analysis in order to make an informed decision.

6: the remaining 21% is unknown, but likely to be either of the conventional technologies

7: and probably in many dry only ones too

[47]: SPX (2012), *SPX Awarded Contract to Supply Parallel Condensing System For Crescent Dunes Solar Energy Project near Tonopah, Nevada*

[48]: GmbH (2020), *Blog #29 – Full Scale Testing in Stellenbosch, South Africa | MinwaterCSP*

So far most systems make use of either wet cooling (55% worldwide) or dry (24%) [26]<sup>6</sup>, but it is likely that some hybrid cooling configuration would be the optimal choice in most situations where a wet only alternative is used<sup>7</sup> due to their adaptive nature and flexible operation. Currently, few commercial plants make use of hybrid cooling technologies. An example of a series, integrated, hybrid system providing significant water conservation exists at the San Juan Generating Station in Farmington, New Mexico. It consists of a conventional, shell-and-tube steam condenser coupled to a hybrid tower with an air-cooled dry section on top which discharges into a wet cooling tower beneath. For CSP, the only known plant to make use of this technology is the Crescent Dunes Solar Energy Project, a 110 MWe concentrated solar power station equipped with 1.1 GWh of molten-salt thermal energy storage. This plant makes use of the described parallel configuration [47]. Also, within the *MinWaterCSP* project, a full scale pilot hybrid plant consisting of an air cooled deluged condenser was successfully built and tested in Stellenbosch, South Africa [48].

# Combined cooling pilot plant at Plataforma Solar de Almería

## 2

### TL;DR

In this chapter a detailed description of the combined cooling pilot plant at PSA is provided including a Piping and Instrumentation Diagram (P&ID) diagram and the methodology followed to perform the experimentation and data-processing. Several experimental campaigns have been performed to characterize the different components of the pilot plant and the complete system, at a wide range of operating conditions. Combined, 198 tests are processed most of which are openly available in public repositories.

2.1	Plant description . . . . .	24
2.2	Experimental campaigns . . . . .	25
2.3	Wet cooling tower . . . . .	25
2.3.1	Exp 1 . . . . .	25
2.3.2	Exp 2 . . . . .	26
2.3.3	Exp 3 . . . . .	26
2.3.4	Dry cooler, Surface condenser and Combined cooler models	26

### Introduction

The combined cooling pilot plant at Plataforma Solar de Almería is a unique facility that integrates a wet cooling tower and a dry cooler in a flexible hydraulic configuration. It allows for the study and validation of different cooling configurations, models, and control and optimization strategies.

Historia de la planta

This chapter describes the plant in Section 2.1 (Plant description) and the experimental campaigns carried out in Section 2.2 (Experimental campaigns).

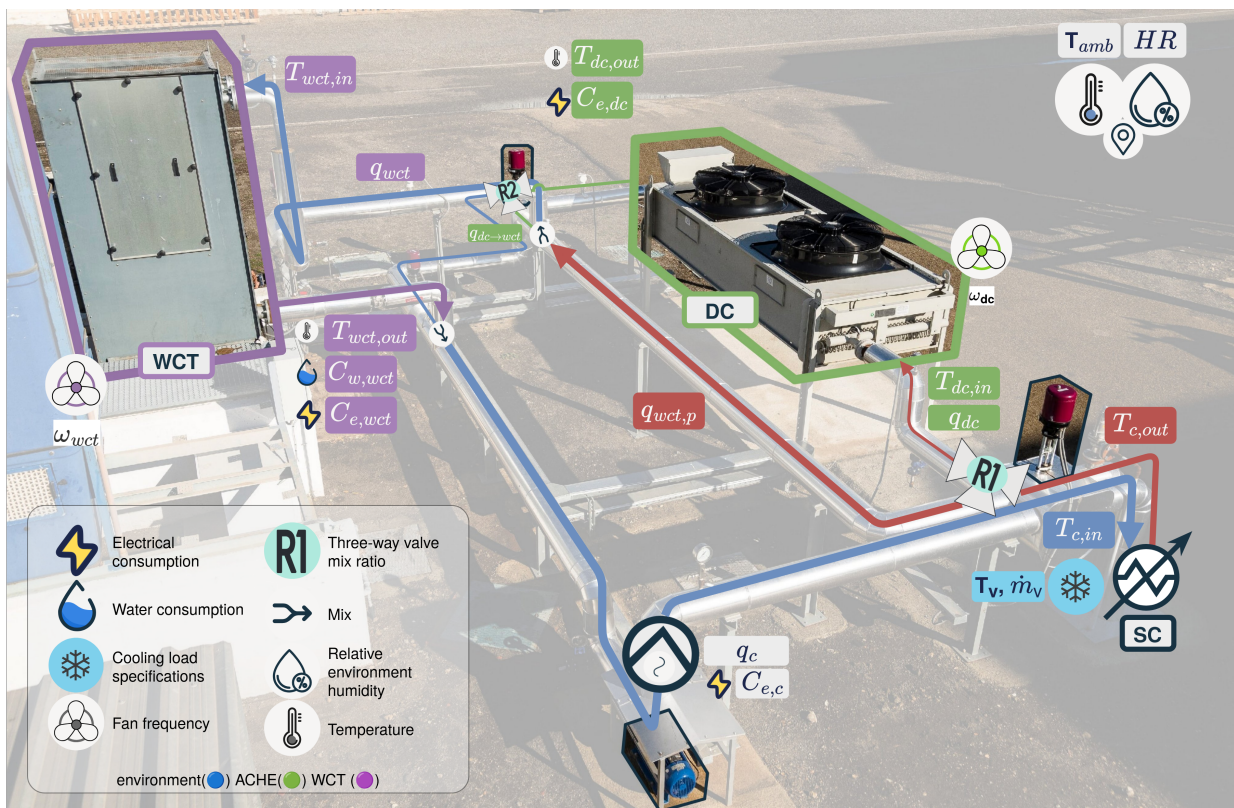


Figure 2.1: PSA combined cooling system facility

## 2.1 Plant description

The pilot plant of combined cooling systems located at PSA (see the layout in Figure 2.3) consists of three circuits: cooling, exchange and heating. In the cooling circuit (see a picture in Figure 2.2), water circulating inside the tube bundle of a Surface Condenser (SC) can be cooled through a Wet Cooling Tower and/or a Dry Cooling Tower (type Air Cooled Heat Exchanger, ACHE), both with a designed thermal power of 204 kW<sub>th</sub>. In the exchange circuit, a saturated steam generator of 80 kW<sub>th</sub> (on the design point), generates steam at different pressures (in the range between 82 mbar and 200 mbar), which is in turn condensed in the surface condenser. In this way, the steam transfers its latent heat of condensation to the refrigeration water, that is heated. Finally, in the heating circuit, a solar field with a thermal power of 300 kW<sub>th</sub> at the design point, provides the energy required by the steam generator, in the form of hot water. It is a unique, very flexible, fully instrumented and versatile facility, able to operate in different operation modes: series and parallel mode, conventional dry-only mode (all water flow is cooled through the dry cooling tower) and wet-only mode (all water flow is cooled through the wet cooling tower). The instrumentation related to the WCT is described in Table 2.1.

Note that sensors measuring the air velocity, temperature and relative humidity at the outlet area of the wet cooling tower are not permanently installed in the plant. Portable sensors were used instead in some experiments to characterize them. They were measured at the outlet area of the cooling tower<sup>1</sup>. The outlet area was divided into 9 quadrants and the above mentioned magnitudes were registered at the center of each quadrant. The obtained values were averaged to determine the mean velocity, temperature and relative humidity used in the air mass flow rate calculation.

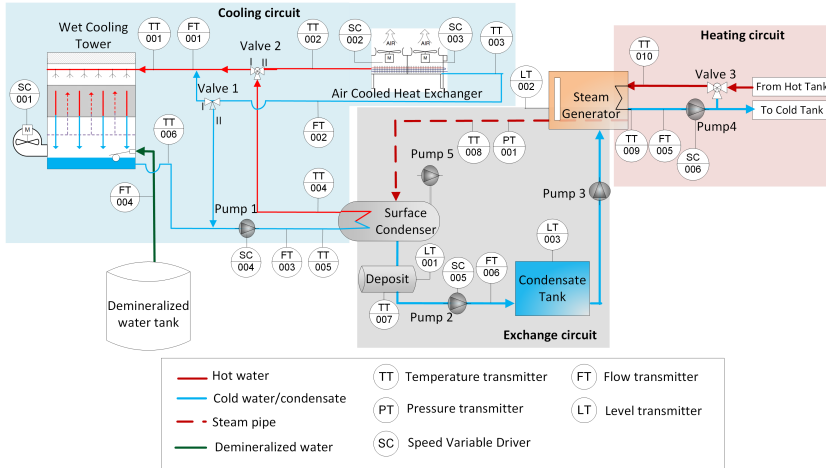


Figure 2.2: Back view of the WCT

In regards to operational aspects of the system, note that the cooling water and air flow rates at the experimental facility ( $\dot{m}_w$ , and air,  $\dot{m}_a$ , respectively), are modified with the *Pump 1* and the fan frequency percentage SC-001, respectively (see Figure 2.3).

**Table 2.1:** Characteristics of instrumentation (<sup>a</sup> value of the temperature in °C, <sup>b</sup> of reading, <sup>c</sup> full scale, <sup>d</sup> mean value).

Measured variable	Instrument	Range	Measurement uncertainty
Water temperature (TT-001... TT-007)	Pt100	0 - 100 °C	0.03 + 0.005·T <sup>a</sup>
Cooling water flow rate (FT-001...FT-003)	Vortex flow meter	9.8 - 25 m <sup>3</sup> /h	± 0.65 % o.r. <sup>b</sup>
Water flow rate (FT-004)	Paddle wheel flow meter	0.05 - 2 m <sup>3</sup> /h	± 0.5 % of F.S <sup>c</sup> + 2.5 % o.r
Condensate water flow rate (FT-006)	Coriolis flow meter	0.1 - 0.3 m <sup>3</sup> /h	< 0.1 % +
Ambient temperature	Pt1000	-40 - 60 °C	± 0.4 @20 °C
Relative humidity	Capacitive sensor	0 - 98%	± 3 % o.r @20 °C
Air velocity	Impeller anemometer	0.1-15 m s <sup>-1</sup>	± 0.1 m s <sup>-1</sup> + 1.5 % o.r
Outlet air temperature	Pt100	-20-70°C	±0.5°C
Outlet air humidity	Capacitive sensor	0-100%	± 2%



**Figure 2.3:** Layout of combined cooling systems pilot plant at PSA.

## 2.2 Experimental campaigns

With the aim of characterizing and developing models for this novel facility, over the years several experimental campaigns have been carried out.

The normative framework followed to carry out the experiments, in order to ensure stable conditions, has been the standards UNE 13741 [49] and the Spanish CTI [50]. These standards specify the test duration and the allowed variations of the most representative ambient and operating magnitudes (water flow rate, heat load, cooling tower range, wet-bulb and dry-bulb temperatures and wind velocity) during the tests. Although the duration of the test should not be less than one hour according to the standards, due to the low capacity of the WCT in the PSA pilot plant and the operational experience, the duration of the tests has been reduced to up to 30 minutes. Once stable conditions are maintained during the defined interval time, the average and deviations values of each measurement are calculated in order to check that they are within the allowable limits of the norm, which finally lead to a valid steady-state operating point.

[49]: UNE (2004), *Thermal Performance Acceptance Testing of Mechanical Draught Series Wet Cooling Towers*

[50]: CTI (2000), *Code Tower, Standard Specifications. Acceptance Test Code for Water Cooling Towers*

## 2.3 Wet cooling tower

A total of 132 steady-state experimental points have been obtained. These data cover a large variety of ambient conditions (different seasons, days and nights) and thermal loads (from 27 to 207 kW). The objective of the experimental campaigns is to develop and validate two modelling strategies for the performance evaluation of the WCT<sup>2</sup>.

The data from the different experimental campaigns is available at [51, 52].

2: See Section 3.1 (Wet cooler)

[51]: Palenzuela et al. (2024), *Steady-State Operation Dataset of an Experimental Wet Cooling Tower Pilot Plant Located at Plataforma Solar de Almería*

[52]: Serrano et al. (2024), “Wet Cooling Tower Performance Prediction in CSP Plants”

### 2.3.1 Physical model calibration – Exp 1

The experimental campaign was designed to calibrate the physical model by focusing on the Merkel number, which depends on the water-to-air mass flow ratio. A total of 19 tests were carried out at the PSA combined cooling pilot plant, covering a wide range of water and air flow conditions. Water flow rates varied from 8 to 22 m<sup>3</sup>/h (2.17–6.15 kg/s), while air flow rates ranged from 1.16 to 4.32 kg/s by adjusting the fan frequency between 25 % and 100 %. Air velocity, temperature, and humidity maps were measured at eight fan levels<sup>3</sup>. Tests were performed

3: This enables the calculation of the air mass flow rate at the outlet of the cooling tower,  $\dot{m}_a$ , using the permanent sensors installed in the facility

under consistent summer conditions, with high ambient temperatures (32–41 °C) and low relative humidities (13–40 %).

### 2.3.2 Data-driven models training – Exp 2

The data required for data-driven models depends on several factors such as the complexity of the model and the error allowed or the diversity of the inputs. With the aim of obtaining a reliable model for the WCT, data collected over several years of operation of the combined cooling system have been used for tuning. They are a set of 115 stationary data covering the following operating ranges: ambient temperature,  $T_{\infty}$ , [9–39] °C, ambient humidity,  $\phi_{\infty}$ , [10–87] %, inlet water temperature,  $T_{w,i}$  [33–41] °C, cooling water flow rate,  $q_w$ , [6–23] m<sup>3</sup>/h and fan frequency percentage,  $f_{fan}$  [21–94] %. The thermal load in these tests varies in the range of [27–178] kW<sub>th</sub>. The number of steady-state data obtained is a reasonable value when compared to other similar data-driven models of counter-flow cooling towers, as in the case of [54], where 81 experimental points were collected for training and testing.

### 2.3.3 Validation – Exp 3

**Table 2.2:** Design of experiments for model comparison (Exp 3)

Variable	Low level	High level
$T_b$ (°C)	≤ 10	≥ 15
$T_{w,i}$ (°C)	≤ 37	≥ 39
$\dot{m}_w$ (kg/s)	≤ 3.3	≥ 5
$T_{w,i} - T_{w,o}$ (°C)	≤ 7	≥ 8

With the aim of validating and comparing different modelling approaches, a dataset of 17 tests (different from the ones taken for experimental campaigns 1 and 2) has been compiled. This experimental campaign was designed using a design of experiments based on full factorial design with 4 factors and 2 levels (low and high), whose values are shown in Table 2.2.

### 2.3.4 Dry cooler, Surface condenser and Combined cooler models

Table 2.3 summarizes the experimental campaigns, describing the Design of Experiments (DoE) employed and indicating the number of tests conducted under steady-state conditions. The ranges of the variables involved in the experiments are also indicated, with those used to define the DoE for each test campaign shown in bold.

#### Dry cooler model – DC-f, DC-cal, DC-val

An experimental campaign (Table 2.3 – DC-cal) was designed and performed to calibrate the Nusselt number correlation as described in Section ???. This campaign comprises 27 tests.

As air mass flow rate measurements are a specific requirement for the DC model, the  $\dot{m}_{air}$ - $w_{dc}$  relationship was derived during an experimental campaign (Table 2.3 – DC-f). Air velocity and temperature were measured at 10 different fan speed levels, ranging from 11 % to 100 % in 10 % increments. The ACHE fan area was divided into eight quadrants, and measurements were taken at the center of each quadrant. The recorded values were then averaged to obtain the mean air velocity and temperature, which were used to calculate the air mass flow rate.

campaña para modelo basado en datos??

#### Surface condenser model – SC-cal, SC-val

An experimental campaign (Table 2.3 – SC-cal) was designed and performed to calibrate the global heat transfer coefficient,  $U_c$ , as a function of inlet water temperature,  $T_{c,in}$  and water flow rate,  $q_c$ . This campaign comprises 15 tests.

Features	Component calibration			Component validation		System validation CC-val
	DC-f	DC-cal	SC-cal	DC-val	SC-val	
DoE	GD-8-10	BB-4-3	BB-3-3	BB-4-3	BB-3-3	FF-2-2-2-3
NumTests	80	27	15	27	15	24
$T_{amb}$ (°C)	26	<b>12 - 29</b>	-	<b>13 - 32</b>	-	<b>12 - 37</b>
HR (%)	-	-	-	-	-	14 - 63
$\dot{m}_v$ (kg/h)	-	-	118 - 328	-	133 - 287	200 - 310
$Q_c$ (kW)	-	-	78 - 216	-	88 - 187	132 - 202
$q_c$ (m³/h)	-	-	10 - 24	-	10 - 24	18 - 24
$q_{dc}$ (m³/h)	-	<b>5 - 25</b>	-	<b>5 - 24</b>	-	<b>5 - 24</b>
$q_{wct}$ (m³/h)	-	-	-	-	-	<b>6 - 24</b>
$T_{dc,in}$ (°C)	-	<b>35 - 41</b>	-	<b>31 - 42</b>	-	33 - 54
$T_{dc,in} - T_{dc,out}$ (°C)	-	<b>2 - 7</b>	-	<b>2 - 9</b>	-	1 - 11
$T_v$ (°C)	-	-	<b>36 - 56</b>	-	<b>36 - 56</b>	<b>36 - 57</b>
$T_{wct,in}$ (°C)	-	-	-	-	-	33 - 54
$\omega_{dc}$ (%)	11 - 100	<b>11 - 76</b>	-	<b>11 - 98</b>	-	11 - 100
$\omega_{wct}$ (%)	-	-	-	-	-	21 - 87

### Complete system validation – CC-val

An additional experimental campaign (Table 2.3 – CC-val) was designed and performed to validate the complete model of the CC system. This campaign comprises 24 tests.

**Table 2.3:** Experimental campaigns performed at the CC pilot plant, where GD- $n_1$ - $n_2$  refers to the spatial grid distribution ( $n_i$ ) around the fan with  $n_2$  measurements in each quadrant ( $n_1 \times n_2$  measurements); BB- $n_1$ - $n_2$  denotes a Box-Behnken design with  $n_1$  variables and  $n_2$  levels; and FF- $n_1$ -...- $n_i$  indicates a full factorial design with  $i$  variables, each with  $n_i$  levels.



# 3

## Modelling of a combined cooling system

### TL;DR

This chapter describes the steady-state modelling of the different components of a combined cooling system, mainly a WCT and a DC. Different alternatives are presented: from physical models to data-driven approaches, including the generation of samples for data-driven models trained using data from a physical model. Models are also developed for the other components of the system and finally it is shown how they are integrated into a complete system model. The complete system model interface is defined at Model ?? and a block diagram is presented in Figure 3.3 including all relevant variables.

### Introduction

In order to study the potential advantages of making use of a combined cooling system, it is first necessary to develop the modelling of its components. Since the objective is performance prediction, this chapter focuses on the steady state modelling of the combined cooler main components, *i.e.* the WCT and the DC. More specifically, the aim is to compare two modelling strategies: that based on physical equations (Section ??) and that based on black box models (Section ??) such as Artificial Neural Networks (ANNs), in order to see which one is more suitable for its integration in the optimization of the complete process.

This chapter presents a comparison between the two modelling approaches, at steady state and with a focus on optimization applications, in terms of predictive capabilities, experimental and instrumentation requirements, execution time, implementation and scalability. A sensitivity analysis is performed to further analyze and compare each case study. It also presents and evaluates all relevant aspects of interest in the development of such models, specifically for ANNs, model configuration, architecture and topology are discussed. Other system components are also described in Section 3.3 (Other components) and finally their integration is discussed in Section 3.4 (Complete system).

### 3.1 Wet cooler

In the case of the models based on physical equations, the analysis of wet cooling towers has its origin in [55], in which the theory for their performance evaluation was developed. Merkel proposed a model based on several assumptions to simplify the heat and mass transfer equations to a simple hand calculation. However, these assumptions mean that Merkel's method does not reliably represent the physics of the heat and mass transfer process in a cooling tower. This was already stated by Bourillot [56] who concluded that the Merkel method is simple to use and can correctly predict cold water temperature when an appropriate value of the coefficient of evaporation is used. However, it is insufficient for the estimation of the characteristics of the warm air leaving the fill and for the calculation of changes in the water flow rate due to evaporation. Jaber and Webb [57] developed the equations necessary to apply the effectiveness-NTU<sup>1</sup> method directly to counterflow or crossflow cooling towers. This approach is particularly useful in the latter case and simpler compared to a more conventional numerical procedure. Notice that the effectiveness-NTU

3.1	Wet cooler . . . . .	29
3.1.1	Physical model . . . . .	30
3.1.2	Samples generation for first-principles to data-driven models . . . . .	32
3.1.3	Model interface . . . . .	32
3.2	Dry cooler . . . . .	33
3.2.1	Physical model . . . . .	33
3.2.2	Samples generation for first-principles to data-driven models . . . . .	33
3.2.3	Model interface . . . . .	33
3.3	Other components . . . . .	34
3.3.1	Electrical consumption . . . . .	34
3.3.2	Surface condenser . . . . .	34
3.3.3	Mixers . . . . .	35
3.4	Complete system . . . . .	35

Ahora mismo esta introducción es demasiado parecida al TL;DR, hay que distinguirla

Pendiente adaptar (reducir) y que no sea copiado tal cual del artículo

[55]: Merkel (1925), "Verdunstungskühlung"

[56]: Bourillot (1983), "Hypotheses of Calculation of the Water Flow Rate Evaporated in a Wet Cooling Tower"

[57]: Jaber et al. (1989), "Design of Cooling Towers by the Effectiveness-NTU Method"

1: The effectiveness-NTU method estimates how well a heat exchanger transfers heat by comparing the actual heat transfer to the maximum possible, using a parameter, Number of Transfer Units (NTU), that reflects its size and flow characteristics.

[58]: Poppe et al. (1991), "Berechnung von Rückkühlwerken"

[59]: Kloppers et al. (2005), "A Critical Investigation into the Heat and Mass Transfer Analysis of Counterflow Wet-Cooling Towers"

[60]: Cutillas et al. (2021), "Energetic, Exergetic and Environmental (3E) Analyses of Different Cooling Technologies (Wet, Dry and Hybrid) in a CSP Thermal Power Plant"

[54]: Hosoz et al. (2007), "Performance Prediction of a Cooling Tower Using Artificial Neural Network"

2: The notation  $n_1 \dots n_l$  represents the architecture of the ANN model, where  $l$  is the number of layers and  $n_i$  are the nodes in each one of the layers.

[61]: Gao et al. (2013), "Artificial Neural Network Model Research on Effects of Cross-Wind to Performance Parameters of Wet Cooling Tower Based on Level Froude Number"

[62]: Song et al. (2021), "A Novel Approach for Energy Efficiency Prediction of Various Natural Draft Wet Cooling Towers Using ANN"

3: ANN uses as input  $f_{fan}$  whereas Poppe's model uses  $\dot{m}_a$ .

Pendiente adaptar (reducir) y que no sea copiado tal cual del artículo

[63]: Navarro et al. (2022), "Critical Evaluation of the Thermal Performance Analysis of a New Cooling Tower Prototype"

method is based on the same simplifying assumptions as the Merkel method. On the other hand, Poppe and Rögner [58] developed the Poppe method. They derived the governing equations for heat and mass transfer in a wet cooling tower and did not make any simplifying assumptions as in the Merkel theory, which makes it a very precise model. As a matter of fact, predictions from the Poppe formulation have resulted in values of evaporated water flow rate that are in good agreement with full scale cooling tower test results [59]. This model has already been used for the evaluation of the thermal performance of solar power plants using different condensation systems (wet, dry and hybrid system), as can be found in Cutillas et al. [60].

In the case of black box models, numerous authors in the literature have designed ANN models for WCT with different objectives, such as performance prediction, simulation and optimization. One of the first works in this area is the one described in [54] where an ANN model was developed to predict the performance of a forced-counter flow cooling tower at lab scale. In this case, the input variables were the dry bulb temperature, the relative humidity of the air stream entering the tower, the temperature of the water entering the tower, the air volume flow rate and the cooling water mass flow rate. The outputs of this model were the heat rejection rate at the tower, the mass flow rate of water evaporated, the temperature of the cooling water at the tower outlet, the dry bulb temperature and the relative humidity of the air at the outlet of the tower. The results obtained with a 5-5-5<sup>2</sup> ANN demonstrated that wet cooling towers at lab-scale can be modelled using ANNs with a high degree of accuracy. There are also ANN models for Natural Draft Counter-flow Wet Cooling Towers (NDWCT) at lab-scale, such as the one proposed by [61]. In this case, the authors used a 4-8-6 ANN structure and considered some additional variables, such as air gravity, wind velocity, heat transfer coefficients and efficiency as outputs. All these works can be useful to validate the model development methodology but may fail predicting the performance of WCT at larger scale. In this sense, special attention deserves the study carried out by [62] where an 8-14-2 ANN model was proposed to predict the performance (the cooling number and the evaporative loss proportion) of NDWCTs at commercial scale. The model is based on 638 sets of field experimental data collected from 36 diverse NDWCTs used in power plants. It is a very challenging work since it covers samples from a wide range of tower sizes and capacities being the Mean Relative Error (MRE) below 5 %.

From the literature review, it can be stated that there are works based on Poppe and ANN models that evaluate the main output variables of WCTs. Nevertheless, to the author knowledge, there are no studies focused on the comparison between both modelling strategies. Also lacking is a comprehensive analysis of the different aspects that affect the models development and performance.

The static models presented in this section have been developed to predict two main outputs, the water temperature at the outlet of the WCT,  $T_{w,or}$  and the water consumed due to evaporation losses,  $\dot{m}_{w,lost}$ . The inputs variables required by both modelling approaches, Poppe model and ANN models, are: the cooling water flow rate ( $\dot{m}_w$ ), the water temperature at the inlet of the WCT ( $T_{w,i}$ ), the ambient temperature ( $T_\infty$ ), the ambient relative humidity ( $\phi_\infty$ ) and the frequency percentage of the fan ( $f_{fan}$ ) (or its equivalence in air mass flow rate<sup>3</sup>,  $\dot{m}_a$ ).

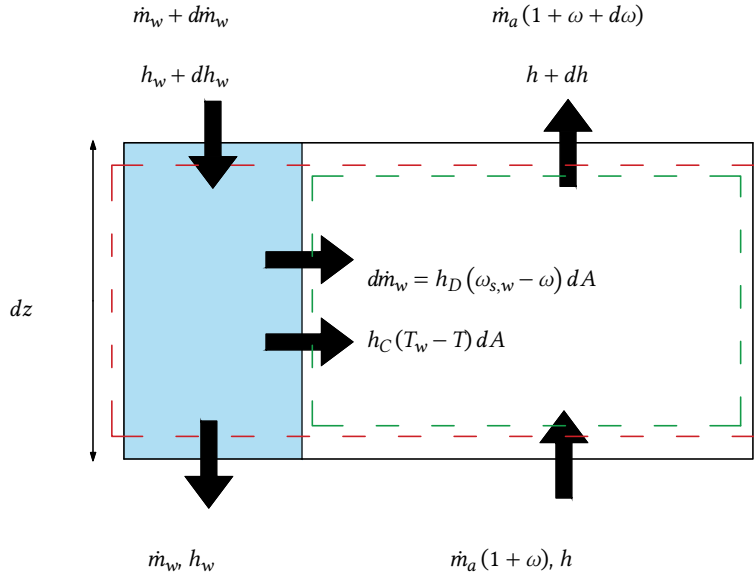
### 3.1.1 Physical model

The well-known Merkel number is accepted as the performance coefficient of a wet cooling tower [63]. This dimensionless number is defined in Equation 3.1, and it measures the degree of difficulty of the mass transfer processes occurring in the exchange area of a wet cooling tower.

$$Me = \frac{h_D a_V V}{\dot{m}_w}, \quad (3.1)$$

where  $h_D$  is the mass transfer coefficient,  $a_V$  is the surface area of exchange per unit of volume and  $V$  is the volume of the transfer region.

The Merkel number can be calculated using the Merkel and Poppe theories for the performance evaluation of cooling towers. On the one hand, the Merkel theory [55] relies on several critical assumptions, such as the Lewis factor ( $Le$ ) being equal to 1, the air exiting the tower being saturated with water vapour and it neglects the reduction of water flow rate by evaporation in the energy balance. On the other hand, the Poppe theory [58], which is the one used in this work, do not consider simplifying assumptions, thus being the one most usually preferred. In this theory, the authors derived the governing equations for heat and mass transfer in the transfer region of the wet cooling tower (control volume shown in Figure 3.1) assuming a one dimensional problem. In this figure, the red and green dashed lines indicate the fill and air-side control volumes, respectively.



[55]: Merkel (1925), "Verdunstungskühlung"

[58]: Poppe et al. (1991), "Berechnung von Rückkühlwerken"

**Figure 3.1:** Control volume in the exchange area of a wet cooling tower arrangement.

Following the detailed derivation process and simplification of the previously-mentioned governing equations described in [63], the major following equations for the heat and mass transfer obtained, according to the Poppe theory, are:

$$\frac{d\omega}{dT_w} = \frac{c_{p_w} \frac{\dot{m}_w}{\dot{m}_a} (\omega_{s,w} - \omega)}{(h_{s,w} - h) + (Le - 1) [(h_{s,w} - h) - (\omega_{s,w} - \omega) h_v] - (\omega_{s,w} - \omega) h_w} \quad (3.2)$$

$$\frac{dh}{dT_w} = c_{p_w} \frac{\dot{m}_w}{\dot{m}_a} \left[ 1 + \frac{(\omega_{s,w} - \omega) c_{p_w} T_w}{(h_{s,w} - h) + (Le - 1) [(h_{s,w} - h) - (\omega_{s,w} - \omega) h_v] - (\omega_{s,w} - \omega) h_w} \right] \quad (3.3)$$

$$\frac{dMe}{dT_w} = \frac{c_{p_w}}{(h_{s,w} - h) + (Le - 1) [(h_{s,w} - h) - (\omega_{s,w} - \omega) h_v] - (\omega_{s,w} - \omega) h_w}, \quad (3.4)$$

where the quantity referred to as  $Me$  in Eq. 3.4, is the Merkel number calculated according to the Poppe theory. The above described governing equations can be solved by the fourth order Runge-Kutta method to provide the evolution of

[63]: Navarro et al. (2022), "Critical Evaluation of the Thermal Performance Analysis of a New Cooling Tower Prototype"

[53]: Ashrae (2004), "HVAC Systems and Equipment"

the air humidity ratio, air enthalpy and Merkel number inside the transfer area of the cooling tower (fill). Once these profiles are known, the amount of water lost due evaporation can be calculated as per Eq. Equation 3.6. Refer to [63] for additional information concerning the calculation procedure.

$$Me = \frac{h_D a_v V}{\dot{m}_w}, \quad (3.5)$$

$$\dot{m}_{w,lost} = \dot{m}_a (\omega_{a,o} - \omega_{a,i}) \quad (3.6)$$

It is important to mention that the Merkel number varies with the operation conditions and its value can be obtained using a correlation with the water-to-air mass flow ratio as an independent variable. One of the proposed correlations in ASHRAE [53] is:

$$Me = c (\dot{m}_w / \dot{m}_a)^{-n} \quad (3.7)$$

4: See Section 5.1.1 (Wet cooler model alternatives comparison and validation)

where the constants  $c$  and  $n$  can be obtained from the fitting of experimental data<sup>4</sup>.

### 3.1.2 Samples generation for first-principles to data-driven models

The first pair of input variables for the WCT sample generation are the wet bulb temperature ( $T_{wb}$ ) and the difference between this temperature and the system inlet temperature ( $\Delta T_{wb-in}$ ). The wet bulb temperature is used instead of the ambient temperature or the relative humidity, because as it can be derived from the physical model, it is the most relevant thermodynamic variable for the wet cooling tower performance. Using both the ambient temperature and the relative humidity would lead to a larger than necessary input space with many duplicate samples, as the wet bulb temperature is a function of both variables. The second pair of input variables are the cooling water flow rate ( $q_{wct}$ ) and, following the reasoning from the physical model, the air to water mass flow ratio ( $\dot{m}_a / \dot{m}_{wct}$ ), since it is a key parameter in defining the operating conditions of the tower. From the resulting 2D grid, valid combinations are obtained by calculating the air mass flow rate and finding if a valid fan speed can be obtained using an air mass flow rate to fan speed empirical correlation.

Finally, all valid thermodynamic and operational combinations are merged into a comprehensive sample set, enabling detailed system evaluations across a realistic and constrained input space.

### 3.1.3 Model interface

Model 3.1: Wet cooling tower
$T_{wct,out}, C_{w,wct} = \text{wct model}(q_{wct}, \omega_{wct}, T_{amb}, HR, T_{wct,in})$

### Model 3.2: Wet cooling system model

$T_{wct,out}, C_e, C_w, T_{c,in}, T_{c,out} = \text{wcs model}(q_{wct}, \omega_{wct}, T_{amb}, HR, T_{wct,in})$   
 $T_{c,in}, T_{c,out} = \text{condenser model}(q_c, \dot{m}_v, T_v)$   
 $T_{wct,out}, C_{w,wct} = \text{wct model}(q_{wct}, \omega_{wct}, T_{amb}, HR, T_{c,out})$   
 $C_{e,c} = \text{electrical consumption}(q_c)$   
 $C_{e,wct} = \text{electrical consumption}(\omega_{wct})$   
 $C_e = C_{e,wct} + C_{e,c}$   
 $C_w = C_{w,wct}$

## 3.2 Dry cooler

### 3.2.1 Physical model

### 3.2.2 Samples generation for first-principles to data-driven models

Pendiente adaptar (reducir) y que no sea copiado tal cual del artículo

Similar to the wet cooling tower case, setting absolute values for both the inlet temperature and the environment temperature will lead to many unfeasible combinations ( $T_{dc,in} \leq T_{db}$ ). So instead, values are generated for the temperature difference, therefore, a 2D grid is constructed using combinations of ambient/dry-bulb temperature ( $T_{amb}$ ) and the difference between inlet and ambient temperature ( $(\Delta T_{amb-in})$ ). For each valid temperature pair ( $T_{amb}, T_{dc,in}$ ), additional independent variables ( $q_{dc}, \omega_{dc}$ ) are combined via a Cartesian product, resulting in a full multidimensional grid of plausible operating points. This systematic procedure ensures a dense and uniform sampling across all relevant input dimensions. Finally, infeasible combinations are filtered based on physical constraints.

### 3.2.3 Model interface

#### Model 3.3: Dry cooler

$T_{dc,out} = \text{dc model}(q_{dc}, \omega_{dc}, T_{amb}, T_{dc,in})$

#### Model 3.4: Dry cooling system model

$T_{dc,out}, C_e, T_{c,in}, T_{c,out} = \text{dcs model}(q_{dc}, \omega_{dc}, T_{amb}, T_{dc,in})$   
 $T_{c,in}, T_{c,out} = \text{condenser model}(q_c, \dot{m}_v, T_v)$   
 $T_{dc,out} = \text{dc model}(q_{dc}, \omega_{dc}, T_{amb}, T_{c,out})$   
 $C_{e,c} = \text{electrical consumption}(q_c)$   
 $C_{e,dc} = \text{electrical consumption}(\omega_{dc})$   
 $C_e = C_{e,dc} + C_{e,c}$

### 3.3 Other components

#### 3.3.1 Electrical consumption

Electrical consumption is modelled with polynomial regressions of order 3 from experimental data:

##### Model 3.5: Electrical consumption

$$C_e = \text{electrical consumption model}(x)$$

$$C_e = p_1 \cdot x^3 + p_2 \cdot x^2 + p_3 \cdot x + p_4$$

where  $C_e$  represents the electrical consumption, and  $x$  is the input variable (e.g., the recirculated cooling water flow rate, particular cooler fan speed, etc.). The coefficients  $p_i$  correspond to a polynomial regression and must be calibrated individually for each component.

#### 3.3.2 Surface condenser

The surface condenser is a heat exchanger that condenses steam into water, assuming that all the vapor that enters the condenser (at saturated conditions), leaves it as saturated liquid, it can be modelled by applying the first law of thermodynamics, which states that the heat lost by the steam (*released*) is equal to the heat gained by the cooling water (*absorbed*), and equal to the heat transferred by the condenser heat transfer surfaces (*transferred*).

##### Model 3.6: Surface condenser

$$T_{c,in}, T_{c,out} = \text{condenser model}(\dot{m}_c, T_v, \dot{m}_v)$$

$$LMTD = \frac{T_{c,out} - T_{c,in}}{\ln\left(\frac{T_v - T_{c,in}}{T_v - T_{c,out}}\right)}$$

$$\dot{Q}_{released} = \dot{m}_v \cdot (h_{sat,vap} - h_{sat.liq})$$

$$\dot{Q}_{absorbed} = \dot{m}_c \cdot c_p (T_{c,out} - T_{c,in})$$

$$\dot{Q}_{transferred} = U \cdot A \cdot LMTD$$

$$U = \dots$$

The condenser area ( $A$ ) is a constant parameter

where  $T_{c,in}$  and  $T_{c,out}$  are the cooling water inlet and outlet temperatures, respectively,  $\dot{m}_c$  the cooling water mass flow rate,  $T_v$  vapour temperature and  $\dot{m}_v$  its mass flow rate and  $h_{sat,vap}$  and  $h_{sat.liq}$  are the specific enthalpies of the steam at the inlet and outlet of the condenser, respectively.  $\dot{Q}$  represents the heat transfer rate *i.e.* the thermal power.

### 3.3.3 Mixers

The mixers outlet flow ( $q_{mix,out,i}$ ) and temperature ( $T_{mix,out,i}$ ) can be determined with a simple mass and energy balances from its inlets streams ( $q_{mix,in}$ ,  $T_{mix,in}$ ):

#### Model 3.7: Mixer model

$$q_{mix,out}, T_{mix,out} = \text{mixer model}(q_{mix,in,1}, T_{mix,in,1}, q_{mix,in,2}, T_{mix,in,2}) \quad (3.8)$$

$$q_{mix,out} = q_{mix,in,1} + q_{mix,in,2} \quad (3.9)$$

$$\begin{aligned} T_{mix,out} &= T_{mix,in,1} \cdot \frac{c_p(T_{mix,in,1})}{c_p(T_{out,i})} \frac{q_{mix,in,1}}{q_{mix,out,i}} + \\ &T_{mix,in,2} \cdot \frac{c_p(T_{mix,in,2})}{c_p(T_{out,i})} \frac{q_{mix,in,2}}{q_{mix,out,i}} \end{aligned} \quad (3.10)$$

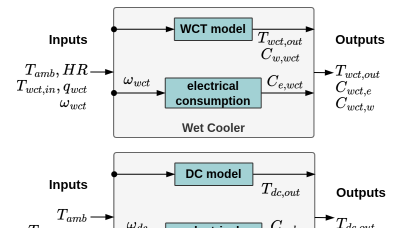
where  $c_p(\cdot)$  is the specific heat, which can be assumed to be the same for the mixing temperature differences of this type of system.

## 3.4 Complete system

The complete model of the combined cooling system integrates the models of the WCT and DC, along with the surface condenser and the mixers, as defined in Model 3.8 (Complete system)<sup>5</sup>. The full diagram, including all variables, is shown in Figure 3.3.

5: Although the electrical consumption for cooling water recirculation is attributed to the condenser in this model, other components—particularly the hydraulic circuit and the dry cooler—also contribute significantly to circulation resistance

To solve the system, the condenser model is evaluated first, providing the inlet temperature for the dry cooler. Once the dry cooler is solved, the resulting temperatures allow for solving the wet cooling tower. Finally, the mixers are evaluated to determine the final outlet temperature of the combined cooler, which should match the condenser's inlet temperature.



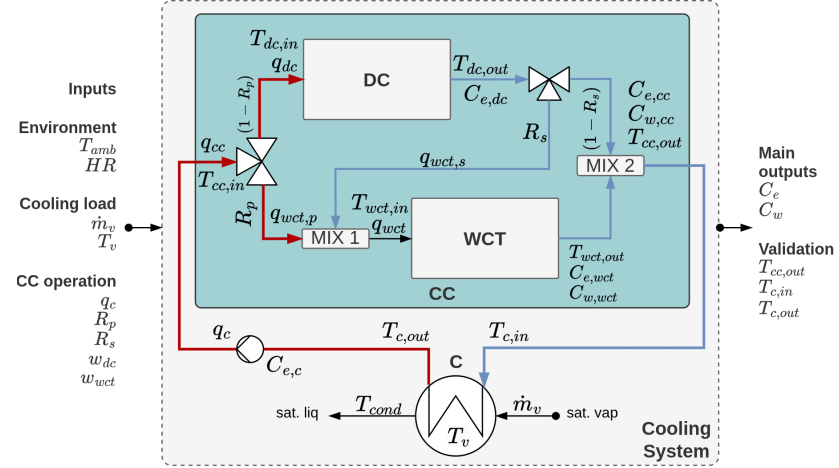


**Figure 3.3:** Complete model diagram of the combined cooling system

#### Model 3.8: Combined cooling system

$T_{cc,out}, C_e, C_w, T_{c,in}, T_{c,out} = \text{ccs\_model}(q_c, R_p, R_s, \omega_{dc}, \omega_{wct}, T_{amb}, HR_i, T_v, \dot{m}_v)$   
 $T_{cc,in} = T_{c,out}$   
 $T_{dc,in} = T_{cc,in}$   
 $q_{dc} = q_c \cdot (1 - R_p)$   
 $q_{wct,p} = q_c \cdot R_p$   
 $q_{wct,s} = q_{dc} \cdot R_s$   
 $T_{dc,out}, C_{e,dc} = \text{dc model}(q_{dc}, \omega_{dc}, T_{amb}, T_{dc,in})$   
 $q_{wct}, T_{wct,in} = \text{mixer model}(q_{wct,p}, T_{cc,in}, q_{wct,s}, T_{dc,out})$   
 $T_{wct,out}, C_{e,wct}, C_{w,wct} = \text{wct model}(q_{wct}, \omega_{wct}, T_{amb}, HR, T_{wct,in})$   
 $T_{c,in}, T_{c,out} = \text{condenser model}(q_c, \dot{m}_v, T_v)$   
 $q_{cc}, T_{cc,out} = \text{mixer model}(q_{wct}, T_{wct,out}, q_{dc}, T_{dc,out})$   
 $C_{e,c} = \text{electrical consumption}(q_c)$   
 $C_{e,dc} = \text{electrical consumption}(\omega_{dc})$   
 $C_{e,wct} = \text{electrical consumption}(\omega_{wct})$   
 $C_e = C_{e,dc} + C_{e,wct} + C_{e,c}$   
 $C_w = C_{w,wct}$

# Optimization of a combined cooling system

## TL;DR

This chapter describes optimization problems for a combined cooling system, a DC and a WCT as well as different optimization strategies propositions to solve them. The objective is to minimize the daily cost of operation made up by the electricity and water costs, while ensuring the cooling demand is met. The key challenge is to manage the available water resource, since there is a limited amount of cheap rainwater available and any excess water required must be purchased at a significantly higher cost. From the alternatives, this can only be effectively achieved by the shrinking horizon optimization strategy applied to the combined cooler for which an implementation methodology is proposed.

## Introduction

Over the years, various studies have compared wet and dry cooling systems for CSP plants. Most of these works are limited to studying the effect of some operating parameters via a sensitivity analysis [43, 45, 46, 64–66]. Nonetheless, several have focused on improving cooling system performance through optimization of the individual component operation. Among them, the works from Martín et al. stand out. In [25] they were the first to optimize the year-round operation of a CSP system not only considering the cooling side but also integrating the power block. The problem was formulated as a multiperiod Non-Linear Programming (NLP) problem with air flow rate and outlet temperature as decision variables for the cooling system. They showed that the obtained complex problem can feasibly be solved and an average water consumption of 2.1 l/kWh was obtained with the least efficient month amounting to 2.5 l/kWh. In [35] the same strategy was applied this time for a dry cooling alternative (ACC) and formulating the optimization as a multiperiod Mixed Integer Non-Linear Programming (MINLP) problem. This integer extension to the problem was done to account for the addition of a new decision variable: the discrete number of units and fans that make up the ACC *i.e.* their active state. The problem was solved via relaxation of the integer variables and after evaluating the annual operation they found the optimized dry cooler consumed around 5% of the total generated power compared to 3.44% of the wet alternative, and increasing a cent the LCOE (0.16 vs 0.15 €/kWh, respectively). A limitation of both studies is the use of monthly average values, which masks the significant daily temperature variations—often exceeding 10°C—that coincide with peak power production and can have a substantial impact on cooling system performance.

Two distinct configurations can be found in the literature where a discussion is made about its operation strategy: water-enhanced dry cooling and parallel configuration. Rohani et al. [1] and Golkar et al [41]. In the latter, Rohani et al. implement a thorough model of water streams in a CSP plant that was experimentally validated. Different scenarios and cooling alternatives were analyzed and each of them was simulated for a year of operation. In the hybrid configuration the operation strategy consisted on always prioritizing the dry sections up until a set value in the condenser pressure was reached, in which case the wet units activated. This strategy offers a simple and robust solution but leaves a lot of performance on the table. Water will be left unused despite potentially being available to prioritize the more expensive dry cooler operation. While Golkar et al [41] delved more in the design and sizing of the hybrid cooler

4.1 Environment description . . . . .	39
4.2 Static optimization . . . . .	39
4.2.1 Dry cooler . . . . .	40
4.2.2 Wet cooler . . . . .	41
4.2.3 Combined cooler . . . . .	41
4.3 Horizon optimization . . . . .	43
4.3.1 Problem discussion . . . . .	44
4.3.2 Proposed solution . . . . .	45

[43]: Barigozzi et al. (2014), “Performance Prediction and Optimization of a Waste-to-Energy Cogeneration Plant with Combined Wet and Dry Cooling System”

[45]: Asvapoositkul et al. (2014), “Comparative Evaluation of Hybrid (Dry/Wet) Cooling Tower Performance”

[46]: Hu et al. (2018), “Thermodynamic Characteristics of Thermal Power Plant with Hybrid (Dry/Wet) Cooling System”

[64]: Asfand et al. (2020), “Thermodynamic Performance and Water Consumption of Hybrid Cooling System Configurations for Concentrated Solar Power Plants”

[65]: Mdallal et al. (2024), “Modelling and Optimization of Concentrated Solar Power Using Response Surface Methodology”

[66]: Tang et al. (2013), “Study on Operating Characteristics of Power Plant with Dry and Wet Cooling Systems”

[25]: Martín et al. (2013), “Optimal Year-Round Operation of a Concentrated Solar Energy Plant in the South of Europe”

[35]: Martín (2015), “Optimal Annual Operation of the Dry Cooling System of a Concentrated Solar Energy Plant in the South of Spain”

Realmente lo que proponen no es nada nuevo, exactamente esa operación ya se propuso por ejemplo en wiles\_description\_1978 y zaloudek\_study\_1976

[1]: Rohani et al. (2021), “Optimization of Water Management Plans for CSP Plants through Simulation of Water Consumption and Cost of Treatment Based on Operational Data”

by application of a genetic algorithm, it then applied a very similar operation strategy.

In Maulbetsch et al. [30], a parallel combined system is analyzed, where the operation strategy is set as follows: At some temperature, the condensing pressure achieved will raise above a desired limit. For ambient temperatures above that level, both systems are operated at full design fan power. When the condensing pressure is below that limit, the capacity of the wet section is reduced to maintain it while the dry section is operated at full capacity. At lower temperature where the dry section can maintain the condensing pressure by itself, the wet system is no longer operated. Finally, at even lower temperatures, the fan power is gradually reduced on the dry section.

One inherent limitation that no optimization strategy can fully overcome is the seasonal mismatch between temperature and water availability. In many locations, ambient temperatures are lowest—favoring dry cooling—during times of the year when water is most abundant—favoring wet cooling. The opposite occurs during hot, dry summer periods, when cooling demand is highest but water becomes a scarce resource. Many studies report annual water savings figures, but this does not offer a complete picture and can be misleading, as it may mask poor performance during critical periods. Reducing water use during times of abundance, while failing to achieve significant savings during water-scarce periods, does not represent an optimal solution—even if total annual water consumption appears lower. Significant cost savings can be achieved with increasing water availability, either from the specification of a smaller condenser or by lowering operating turbine exhaust pressures (increasing the wet ratio). In conclusion, there remains significant potential for improved water management through optimized system operation, particularly when resource availability is explicitly considered in the decision-making process:

- ▶ Humidity is higher at night where ambient temperatures are lower, partially alleviating the limitations of the dry system and making it less unfavorable.
- ▶ Take full advantage of the cheaper and more efficient wet cooling when water is plentiful.
- ▶ Consider the availability of alternative water sources and their dynamic costs.
- ▶ When using a combined cooling system its operation is not trivial but inherently becomes more complex; thus requiring an operation strategy to, at a minimum, robustly satisfy the cooling demand, but preferably also minimize the cost of operation.

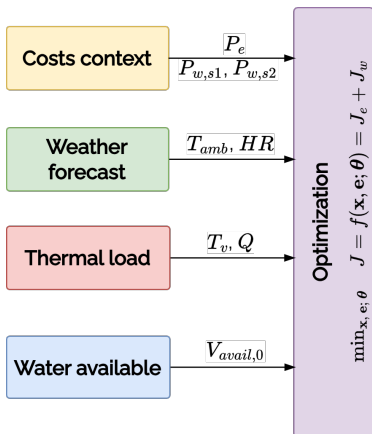


**Figure 4.1:** Block diagram of the optimization scheme including environment components

This chapter analyzes the optimization of different cooling system configurations, focusing on their two primary resource consumptions: electricity and water. The optimization problems are formulated to minimize the total cost of cooling a thermal load, with cost defined as the combined use of these two resources. The thermal load is treated as an external requirement and is therefore excluded from the decision space. This work addresses existing limitations in the literature and presents, for the first time, an actual optimization of the operation of a combined cooling system in the context of CSP applications.<sup>1</sup>

The chapter is structured as follows: first, the environment definition is presented in Section 4.1 (Environment description), which includes a description of the variables taking part in the costs context, weather forecast, thermal load, and water resource availability. Next the two optimization strategies are presented, first a static optimization in Section 4.2 (Static optimization) where the dry cooler, wet cooler and combined cooler static problems are defined; followed by a shrinking horizon optimization approach in Section 4.3 (Horizon optimization) where the combined cooler is optimized over a prediction horizon. This last section includes a discussion on the problem nature and then presents the proposed methodology to solve it.

1: Although the proposed methodology is applicable to any system requiring thermal load cooling, particular emphasis is placed on water resource availability, given its critical importance in solar thermal applications. See Section 1.2 (Cooling and water use)

## 4.1 Environment description

The environment for the optimization problems described in this section includes the following components and is visualized in Figure 4.1:

1. **Costs context** The cooling system has mainly two associated operational costs: electricity ( $J_e$ ) and water use ( $J_w$ ). For the electricity the sale price of electricity ( $P_e$ ) is used since whatever is consumed by the cooling system, it is electricity that cannot be sold to the market in the case of a system that produces electricity like a CSP plant, and it is electricity that needs to be purchased at market price in the case of any other system.  
As for the water, two sources are considered, water price from source 1 is referred as  $P_{w,s1}$  and  $P_{w,s2}$  for source 2. Source 1 is cheaper than source 2.
2. **Weather forecast** The only two weather variables that have an impact on the cooling system are the ambient temperature ( $T_{amb}$ ) and the relative humidity ( $HR$ ) since they set the dry and wet bulb temperatures.
3. **Thermal load** The thermal load is defined either by a vapor flow rate ( $\dot{m}_v$ ) or a thermal power ( $\dot{Q}$ ), which enters the condenser at a temperature  $T_v$ <sup>2</sup>
4. **Water resource availability** Two sources of water are available, one of them, the cheaper one coming from a dam is limited in volume ( $V_{avail}$ ). The cheaper source ( $s_1$ ) is prioritized until it is depleted, then the alternative source ( $s_2$ ) is used:

$$C_{w,s1,i} = \frac{\min(V_{avail,i}, C_{w,i} \cdot T_s)}{T_s} \quad (4.1)$$

$$C_{w,s2,i} = C_{w,i} - C_{w,s1,i} \quad (4.2)$$

$$V_{avail,i} = V_{avail,i-1} - C_{w,s1,i} \cdot T_s \quad (4.3)$$

2: Vapor can also be referred as steam, usually steam is used when the vapor performs work, like in a turbine.

where  $i$  represents the step, at every step the amount used from each source is estimated and the source 1 availability is updated accordingly.  $C_w$  represents the flow rate of water consumed and  $T_s$  is the sample time at which steps are computed.

## 4.2 Static optimization

Static optimization problems are defined in a particular time, given an environment, and decisions do not take into account prior states or decisions, neither consider the effect on future state.

From a process perspective this also characterizes the cooling process, except for the water resource availability, being the only variable that depends on the previous state, *i.e.* is not static. Each time a static problem is evaluated, it begins with a specific initial water volume ( $V_{avail,0}$ ) for that step. After solving the problem, this volume must be updated before proceeding to the next step. As a result, evaluating multiple consecutive steps requires a sequential approach.

### Reminder: Optimization problem definition

The general optimization function is defined as:<sup>a</sup>

$$\min_{\mathbf{x}, \mathbf{e}; \theta} J = f(\mathbf{x}, \mathbf{e}; \theta) \quad \text{s.t.} \quad g_i(\mathbf{x}) \leq 0, \quad i = 1, \dots, m$$

where  $\mathbf{x}$  is the decision vector,  $\mathbf{e}$  represents the environment, and  $\theta$  contains the fixed parameters.

<sup>a</sup> See Section ?? (??)

In order to streamline the problem formulation, a general combined cooling system model is used for every scenario. This unified model incorporates both the dry and wet coolers, as well as the shared surface condenser. For cases where only one cooler is used, the other can be effectively disabled by setting its associated variables to zero and configuring the hydraulic circuit to prevent water circulation through it.

#### 4.2.1 Dry cooler

3: Achieved by setting  $R_p = 0$  and  $R_s = 0$

In the first case study, the optimization focuses exclusively on the dry cooler. Consequently, all variables and terms associated with the wet cooler, as well as water resource management, are omitted from the formulation, making the problem completely static<sup>3</sup>. This configuration is illustrated in Figure 4.2 and the problem is defined as follows:

##### Problem: DC - static

See Section ?? (??) for a detailed description of the dry cooler and Section 3.3.2 (Surface condenser) for the condenser model.

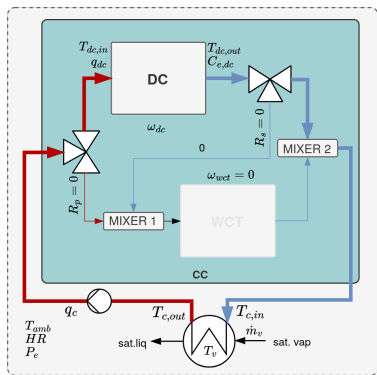


Figure 4.2: Diagram of the dry cooler only cooling problem

4: In order to better comprehend why mismatches between cooler and condenser can exist, the reader is referred to Section 3.4 (Complete system)

$$\min_{\mathbf{x}, \mathbf{e}; \theta} J = f(\mathbf{x}, \mathbf{e}; \theta) = C_e \cdot P_e$$

with:

$$T_{dc,out}, C_e, T_{c,in}, T_{c,out} = dcs \text{ model}(q_c, \omega_{dc}, T_{amb}, T_v, \dot{m}_v)$$

► Decision variables

$$\mathbf{x} = [q_c, \omega_{dc}]$$

► Environment variables

$$\mathbf{e} = [T_{amb}, P_e, T_v, \dot{m}_v]$$

► Fixed parameters

$$\theta = [R_p = 0, R_s = 0, \omega_{wct} = 0]$$

subject to:

► Box-bounds

- $\omega_{dc} \in [\underline{\omega}_{dc}, \bar{\omega}_{dc}]$
- $q_c \in [\underline{q}_c, \bar{q}_c]$

► Constraints

- $|T_{dc,out} - T_{c,in}| \leq \epsilon_1$
- $T_{c,out} \leq T_v - \Delta T_{c-v,min}$
- $|Q_{dc} - Q_{c,released}| \leq \epsilon_2$

The cost of cooling ( $J$ ) is equivalent to the cost of electricity ( $J_e$ ), which in turn is the product of the electricity price ( $P_e$ ) and the electricity consumption ( $C_e$ ). Only two decision variables are defined, the cooling water recirculation flow rate ( $q_c$ ) and the dry cooler fan speed ( $\omega_{dc}$ ). Any two pair of values for these variables that satisfy the bounds do not necessarily yield a feasible solution, that is why three constraints are introduced, the first one ensures that the outlet cooler temperature matches the inlet condenser temperature (since they are directly connected, they must be the same), the second one ensures that the condenser outlet temperature respects the minimum temperature difference with the vapor temperature, and the last one ensures that the cooling duty of the dry cooler matches the one of the condenser<sup>4</sup>.

#### 4.2.2 Wet cooler

Conversely to the dry cooler, the wet cooler optimization problem is configured by setting  $R_p = 1$ , effectively disabling the dry cooler. In this case, water associated variables are included in the problem formulation:<sup>5</sup>

## Problem: WCT – static

$$\min_{\mathbf{x}, \mathbf{e}; \theta} J = f(\mathbf{x}, \mathbf{e}; \theta) = J_e + J_w$$

**with:**

$$J_e = C_e \cdot P_e$$

$$J_w = C_{w,s1} \cdot P_{w,s1} + C_{w,s2} \cdot P_{w,s2}$$

$$C_{w,s1} = \min((V_{avail}, C_w \cdot T_s)/T_s)$$

$$C_{w,s2} = C_w - C_{w,s1}$$

$T_{wct,out}, C_e, C_w, T_{c,in}, T_{c,out} = \text{wcs model}(q_c, \omega_{wct}, T_{amb}, HR, T_v, \dot{m}_v)$

- ## ► Decision variables

$$x = [q_c, \omega_{\text{wct}}]$$

- ## ► Environment variables

$$e = [T_{\text{amb}}, HR, P_e, P_{w,s1}, P_{w,s2}, V_{\text{avail}}, T_v, \dot{m}_v]$$

- #### ► Fixed parameters

$$\theta = [R_p = 1, R_s = 0, \omega_{\text{DC}} = 0]$$

subject to:

- #### ► Box-bounds

- $w_{wct} \in [\underline{w}_{wct}, \bar{w}_{wct}]$
  - $q_c \in [q_c, \bar{q}_c]$

- ## ► Constraints

- $|T_{\text{wct,out}} - T_{c,\text{in}}| \leq \epsilon_1$
  - $T_{c,\text{out}} \leq T_v - \Delta T_{c-v,\text{min}}$
  - $|Q_{\text{wct}} - Q_{c,\text{released}}| \leq \epsilon_2$

In this version of the problem, the decision vector is composed by the recirculation flow rate, but now the fan speed of the wet cooler ( $\omega_{wet}$ ) is included. The cost of cooling now includes the cost of water ( $J_w$ ) and its availability is updated using the water consumption ( $C_w$ ) as described in Equations (4.1)–(4.3). The environment now includes the air relative humidity and water prices.

### 4.2.3 Combined cooler

The last static optimization problem is the combined cooler, which incorporates both the dry and wet coolers, as well as the condenser. Here the hydraulic distribution is not fixed but is part of the decision variables, allowing the optimization to determine the optimal distribution between the two coolers. The problem is defined as follows:<sup>6</sup>

5: See Section 3.1 (Wet cooler) for a detailed description of the wet cooler and condenser model.

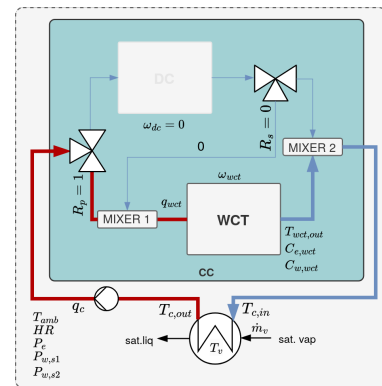


**Figure 4.3:** Diagram of the wet cooler only cooling problem

6: See Section 3.4 (Complete system) for a detailed description of the combined cooler and condenser model.

**Problem: CC - static**

$$\min_{\mathbf{x}, \mathbf{e}; \theta} J = f(\mathbf{x}, \mathbf{e}; \theta) = J_e + J_w$$

with:

$$J_e = C_e \cdot P_e$$

$$J_w = C_{w,s1} \cdot P_{w,s1} + C_{w,s2} \cdot P_{w,s2}$$

$$C_{w,s1} = \frac{\min(V_{avail}, C_w \cdot T_s)}{T_s}$$

$$C_{w,s2} = C_w - C_{w,s1}$$

$$T_{cc,out}, C_e, C_w, T_{c,in}, T_{c,out} = \text{ccs model}(q_c, R_p, R_s, \omega_{dc}, \omega_{wct}, T_{amb}, HR, T_v, \dot{m}_v)$$

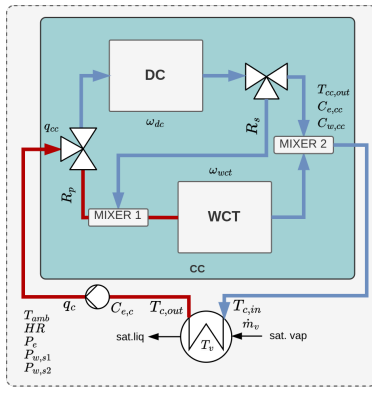


**Figure 4.4:** Diagram of the combined cooler and condenser problem

7: Particularly for the pilot plant described in Chapter 2

**subject to:**

## ► Box-bounds

- $\omega_{dc} \in [\underline{\omega}_{dc}, \bar{\omega}_{dc}]$
- $\omega_{wct} \in [\underline{\omega}_{wct}, \bar{\omega}_{wct}]$
- $q_c \in [q_c, \bar{q}_c]$
- $R_p \in [0, 1]$
- $R_s \in [0, 1]$

## ► Constraints

- $|T_{cc,out} - T_{c,in}| \leq \epsilon_1$
- $T_{c,out} \leq T_v - \Delta T_{c-v, \min}$
- $|Q_{cc} - Q_{c,released}| \leq \epsilon_2$

Figure 4.5 illustrates the various ways a combined cooler<sup>7</sup> can meet a specific cooling load under four diverse scenarios: two different environment conditions and cooling loads. The optimal operating points are evaluated in terms of the two consumptions: electricity ( $C_e$ ) and water ( $C_w$ ) and form the Pareto front.

In **Case I**, which presents the highest water and electricity consumptions, it can be observed that the water consumption is always above zero. This indicates that the use of the WCT is essential, as the DC alone is not capable of cooling the nominal thermal load at 42 °C, during summer conditions. If the system operated only with the DC, the vapor temperature (*i.e.* turbine back-pressure) would rise, negatively impacting the power cycle performance of a CSP plant. Maintaining the same ambient conditions, when the thermal power is reduced (**Case II**), it becomes feasible to operate using only the DC, although with a high parasitic load (74 kW<sub>e</sub>). By combining the DC with the WCT, electricity consumption can be reduced by half, with water consumption remaining below 50 l/h. Under more favorable winter conditions (**Cases III and IV**), the DC alone becomes more efficient as demonstrated by the significant reduction in electricity demand. Still, when coupled with the WCT, electricity consumption can decrease by about 35 % at full thermal load, with a limited water consumption of 50 l/h. At reduced thermal load the additional benefit of the WCT becomes negligible, making this the only case where operating with DC alone is more favorable.

The figure also details the optimal cooling power and hydraulic distribution for **Case III**. The background color represents the distribution of cooling power: green indicates a greater contribution from the dry cooler, while purple indicates a greater contribution from the wet cooler. To avoid water consumption, steam

**Reminder: Pareto front**

When dealing with multiple objectives where no single solution is optimal, but improvements in one objective lead to trade-offs in others, a set of points is obtained that represents the best trade-offs between the objectives—known as a Pareto front<sup>a</sup>.

<sup>a</sup> See Section ?? (??)

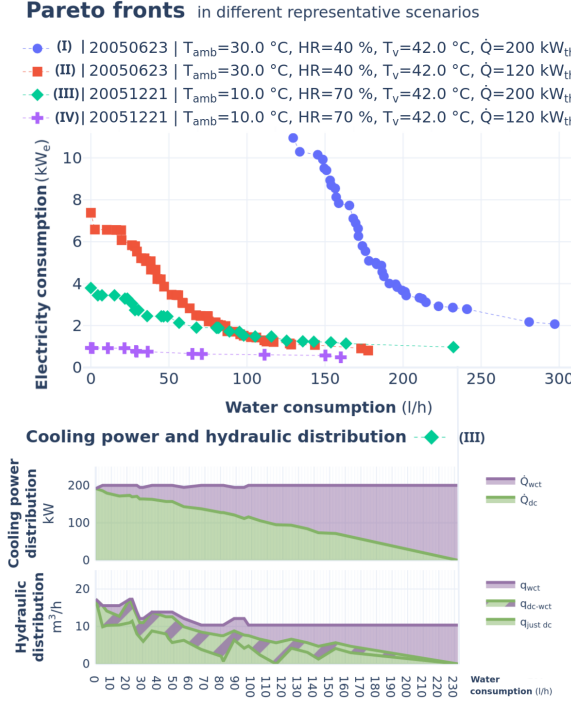


**Figure 4.5:** Pareto fronts in different representative scenarios (top) and detailed power and hydraulic distribution for a specific scenario (bottom)

must be cooled exclusively using the DC. At the other extreme, to minimize electricity consumption, only the WCT should be used. At intermediate optimal points, both systems are combined. This is achieved by series configurations at prioritized dry cooling and progressively increasing parallel configurations for predominantly WCT use. As expected, the cooling water flow rate (Figure 4.5 - *Hydraulic distribution*) is higher ( $17 \text{ m}^3 / \text{h}$ ) for a drier operation, since the reduced temperature component of the cooling driving force is limited and therefore needs to be compensated with a higher flow. Higher compared to the wet operation and its inherently higher temperature difference available, allowing for a better (lower) flow of  $10 \text{ m}^3/\text{h}$ . In Figure 4.5 - *Cooling power distribution* it is also interesting to highlight how the series-parallel flexibility of the system enables it to achieve almost a continuous division of the cooling power from full dry to full wet, at least for this particular case.

### 4.3 Horizon optimization

The problem structure is very similar to the static alternative, the main difference is that now the decision and environment vectors are composed not from the expected value for the optimization step, but an array of values from the current optimization step ( $i$ ) until the end of the prediction horizon ( $n_{steps}$ )<sup>8</sup>:

Problem: CC - horizon

$$\min_{\mathbf{x}, \mathbf{e}; \theta} J = f(\mathbf{x}, \mathbf{e}; \theta) = \sum_{i=1}^{n_{steps}} (J_{e,i} + J_{w,i}) \cdot T_s$$

8: Bold notation is used to indicate that the variable is an array and not a single value, e.g.  $\mathbf{x}$

$\forall i = 1 \dots n_{steps}$  is a notation to indicate that a condition must be held at every step  $i$  in the optimization horizon ( $n_{steps}$ )

with:

$$\begin{aligned}
 & \text{for } i = 1 \dots n_{\text{steps}} : \\
 & \quad J_{e,i} = C_{e,i} \cdot P_{e,i} \\
 & \quad J_{w,i} = C_{w,s1,i} \cdot P_{w,s1,i} + C_{w,s2,i} \cdot P_{w,s2,i} \\
 & \quad C_{w,s1,i} = \frac{\min(V_{\text{avail},i}, C_{w,i} \cdot T_s)}{T_s} \\
 & \quad C_{w,s2,i} = C_{w,i} - C_{w,s1,i} \\
 & \quad V_{\text{avail},i} = V_{\text{avail},i-1} - C_{w,s1,i} \cdot T_s \\
 & \quad T_{cc,out,i}, C_{e,i}, C_{w,i}, T_{c,out,i} = f(q_{c,i}, R_{p,i}, R_{s,i}, \omega_{dc,i}, \omega_{wct,i}, T_{amb,i}, HR_i, T_{v,i}, \dot{m}_{v,i})
 \end{aligned}$$

► Decision variables

$$\mathbf{x} = [\mathbf{q}_c, \mathbf{R}_p, \mathbf{R}_s, \omega_{dc}, \omega_{wct}]$$

$$\text{where } x = [x_{1,1}, \dots, x_{1,n_{\text{steps}}}, \dots, x_{n_x,n_{\text{steps}}}]$$

► Environment variables

$$\mathbf{e} = [\mathbf{T}_{\text{amb}}, \mathbf{HR}, \mathbf{P}_e, \mathbf{P}_{w,s1}, \mathbf{P}_{w,s2}, \mathbf{V}_{\text{avail},0}, \mathbf{T}_v, \mathbf{m}_v]$$

$$\text{where } e = [e_{1,1}, \dots, e_{1,n_{\text{steps}}}, \dots, e_{n_e,n_{\text{steps}}}]$$

subject to:

► Box-bounds

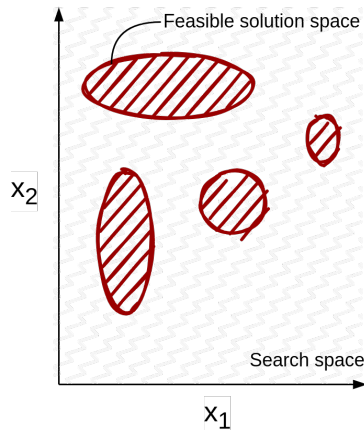
- $\mathbf{w}_{dc} \in [\underline{w}_{dc}, \bar{w}_{dc}]$
- $\mathbf{w}_{wct} \in [\underline{w}_{wct}, \bar{w}_{wct}]$
- $\mathbf{q}_c \in [q_c, \bar{q}_c]$
- $\mathbf{R}_p \in [0, 1]$
- $\mathbf{R}_s \in [0, 1]$

► Constraints,  $\forall i = 1 \dots n_{\text{steps}}$ :

- $|T_{cc,out,i} - T_{c,in,i}| \leq \epsilon_1$
- $T_{c,out,i} \leq T_{v,i} - \Delta T_{c-v,\min}$
- $|Q_{cc,i} - Q_{c,released,i}| \leq \epsilon_2$

This formulation allows for an arbitrary long prediction horizon, however, since forecasts for each variable in the environment are needed, it will be limited to a number of steps where reliable predictions can be obtained. On this work water availability is allocated daily, so the prediction horizon is established until the end of the operation day and it starts from the current time when the optimization is launched.

### 4.3.1 A discussion on solving the optimization problem



As defined, the CCS problem decision vector is composed by five variables that are direct inputs on the process<sup>9</sup>. But as mentioned, not any five values for these variables will yield a feasible solution, in the real system this translates to the fact that a stable operation *i.e.* steady-state would never be reached for that set of inputs. To check for feasible operation the three mentioned constraints are introduced, however, this increases the complexity of the solution space significantly, since the solution space will not be continuous, but as seen in Figure 4.6, it will be formed by islands of feasible solution space regions separated by infeasible regions. This means that finding a feasible solution is not trivial, and the optimization algorithm will need to explore the solution space-a global search algorithm-in an attempt to find the global minimum.

**Figure 4.6:** Visualization of a constrained search space for two decision variables

For one single step, most global search algorithms with multiple runs<sup>10</sup> were able to consistently find the global optima, this was not the case for local gradient-based algorithms, which were very sensible to the initial conditions and often converged to local minima, even when coupled with other techniques, such as Generalized Monotonic Basin Hopping [67], they struggled to consistently escape these local optima.

The problem becomes significantly more complex when the prediction horizon is extended, the decision vector grows five-fold for each additional step in the prediction horizon, and the optimization algorithm is tasked with finding a feasible solution for this much larger decision vector, in a very complex solution space, at once for all steps. The chances of finding a feasible solution decrease significantly, and this was reflected in the failure to find a single feasible solution. Even when providing an initial guess composed by the static problem solutions for each step in a 24 steps horizon, the returned solution was that same initial guess.

### 4.3.2 Proposed solution: Decomposition-based multi-objective optimization with trajectory planning

A two-level optimization strategy is proposed to solve a multi-step decision problem<sup>11</sup>. At each step of the prediction horizon, a multi-objective optimization problem is independently solved, yielding a Pareto front. A global optimization problem is then formulated to select a path through the sequence of Pareto fronts, minimizing a cumulative objective (*i.e.*, cost), akin to a pathfinding or Traveling Salesman Problem (TSP)-like over Pareto-optimal points.

The methodology is illustrated in Figure 4.7 and its components are described in the following sections.

#### Solving the multi-objective optimization problems

To limit the complexity of the problem, the decision space can be reduced by one variable by analyzing how the complete model is solved and described in Section 3.4 (Complete system); firstly, the condenser can be solved just by using the recirculation flow rate ( $q_c$ ), it follows the dry cooler by adding the first valve ratio ( $R_p$ ) and dry cooler fan speed ( $\omega_{dc}$ ). The only remaining component to solve is the wet cooler. The wet cooler inlet conditions ( $q_{wct}, T_{wet,in}$ ) can be determined by using the second valve ratio ( $R_s$ ). As for the outlet conditions, from the condenser evaluation, its inlet temperature is known and it sets the value of the combined cooler outlet temperature ( $T_{cc,out}$ ), which in turn is the result of the mixing from the DC and WCT outlet temperatures ( $T_{dc,out}$  and  $T_{wct,out}$ , respectively).

The result of this analysis is that the wet cooler fan speed is not a decision variable anymore, but an output of the model, which can be computed by inverting the wet cooler model, where an outlet temperature is provided as input, and the fan speed is computed as an output. Summarizing, the decision vector can be reduced from five to four variables:<sup>12</sup>

$$\mathbf{x} = [q_c, R_p, R_s, \omega_{dc}]$$

More importantly, now the optimization algorithm does not need to find a set of five inputs that produce a feasible solution in a complex solution space, but only four values from which a feasible wet cooling tower fan speed exists<sup>13</sup>, thus greatly simplifying the problem.

10: Tried algorithms include: Algoritmos probados de pygmo y Poner Gaussian también

[67]: Wales et al. (1997), "Global Optimization by Basin-Hopping and the Lowest Energy Structures of Lennard-Jones Clusters Containing up to 110 Atoms"

11: Alternative wording: Pareto front chaining, multi-step Pareto optimization, path planning on Pareto surfaces.

12: This reasoning works only for a system with this particular configuration, a different combined cooler layout would require a different analysis.

13: *i.e.* within its bounds  $\omega_{wct} \in [\underline{\omega}_{wct}, \bar{\omega}_{wct}]$  and producing a balanced system

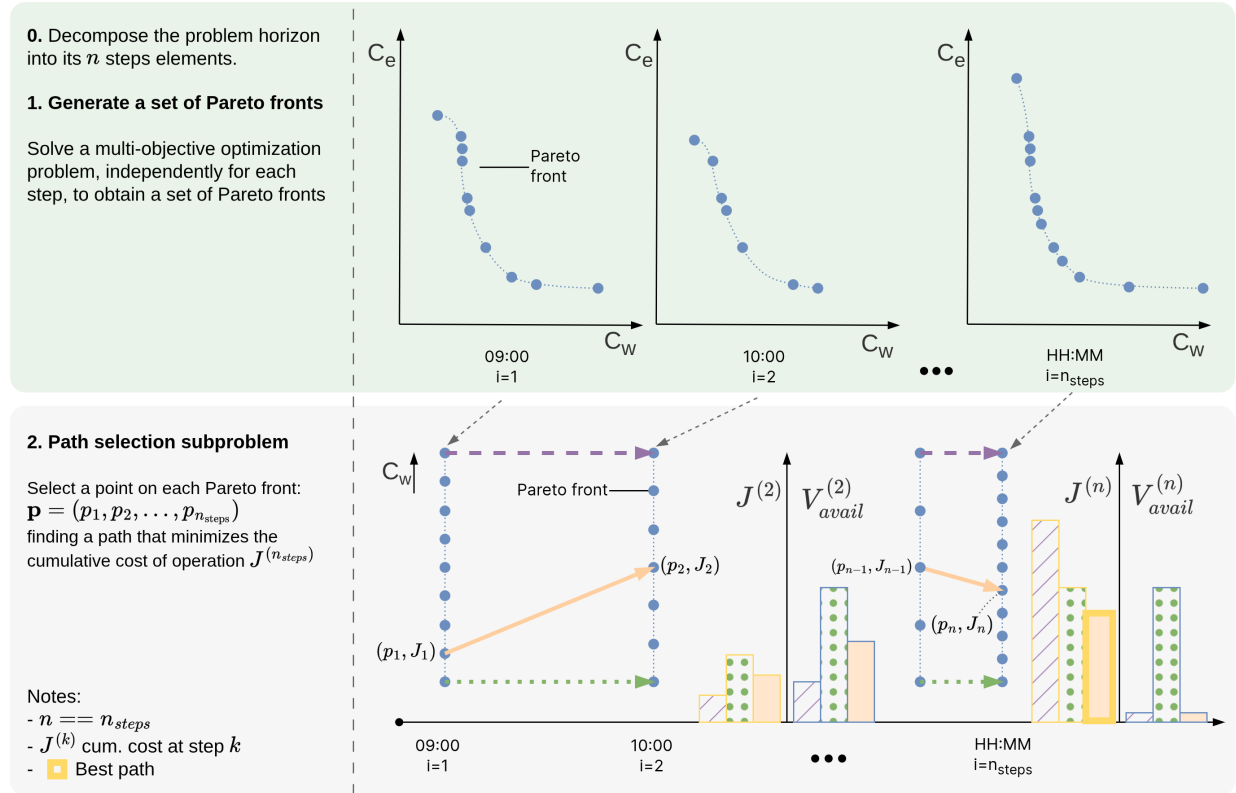


**Figure 4.7:** Proposed methodology. Decomposition-based multi-objective optimization with trajectory planning. Blue-dots (•) represent points on the Pareto front. In step 2, three paths are illustrated: a water-greedy dash-purple (—) path, a water-conservative green-dotted (..) path and a compromise-approach solid-orange path (—).

A straightforward approach to solve the multi-objective optimization is to do a grid-search over the decision space, evaluating the model for every combination of decision variables, and then storing only the points for which a feasible  $\omega_{wct}$  exists. This approach is not recommended for large decision spaces, but for the four-dimensional decision space and with a model that can be evaluated in fractions of a second, it is feasible.

Next, the Pareto front is computed from the feasible points, which are evaluated in terms of the two consumptions: electricity ( $C_e$ ) and water ( $C_w$ ). By definition, the Pareto front is the set of points that cannot be improved in one objective without worsening the other, and it is computed by checking for each point if there is another point that is better in both objectives, and if so, it is removed from the set of feasible points. The remaining points form the Pareto front. This process is repeated for each step in the horizon, resulting in a set of Pareto fronts as visualized in Figure 4.7-1.

### Path selection subproblem

The path selection subproblem is a combinatorial optimization problem over a layered weighted directed graph, where each layer corresponds to a time step in the prediction horizon, and each node in a layer represents a point on the corresponding Pareto front. The objective is to find a path  $\mathbf{p} = (p_1, p_2, \dots, p_{n_{\text{steps}}})$ , where  $p_i$  is the selected node at time step  $i$ , that minimizes the total cumulative cost along the path ( $J$ ). The problem can be formulated as:

$$\min_{\mathbf{p}} \quad J = \sum_{i=1}^{n_{\text{steps}}-1} C_{\text{transition}}(p_i, p_{i+1})$$

Each transition cost  $C_{\text{transition}}(p_i, p_{i+1})$  depends on both consumptions (i.e. electricity and water consumption) of the nodes  $p_i$  and  $p_{i+1}$ , as well as a dynamic price function that depends on the path history. Specifically, the transition cost is correlated to the current resource availability ( $V_{\text{avail},i}$ )<sup>14</sup> and will depend on the current state of the system, which is a function of the previous decisions. This is a very simple calculation that can be computed almost instantly, and it is the only information needed to compute the transition costs between two points in the Pareto front:

$$C_{\text{transition}}(p_i, p_{i+1}) = P_e(i) \cdot C_e(p_{i+1}) + P_w(i) \cdot C_w(p_{i+1})$$

where:

- ▶  $C_e(p_{i+1}), C_w(p_{i+1})$ : electricity and water consumption at node  $p_{i+1}$
- ▶  $P_e(i), P_w(i)$ : price coefficients for electricity and water at step  $i$ , which may be dependent on the previously selected nodes (i.e., the path so far)

Prices  $P_e(i), P_w(i)$  depend on prior path decisions, this introduces path-dependency into the cost function, and makes the problem non-trivial to solve via simple shortest path algorithms. The problem could be handled via dynamic programming, graph search (like Dijkstra or A\*), or metaheuristics such as genetic algorithms.

The subproblem is illustrated in Figure 4.7–2. Each node represents a point in the Pareto front of a step, and edges represent the transition costs between these points, that is, the cumulative cost so far ( $J_{0..i}$ ). Three paths are illustrated in Figure 4.7–2. The **dash-purple** (—) path is a path that chooses nodes with a high water use<sup>15</sup>, so in the first split it can be seen it achieves the lowest cost of operation, but also leaves the least water available for the next steps, resulting in a higher total cost of operation. On the other hand, the **green-dotted** path (.) chooses the nodes with the lowest water use, this translates in a consistently higher cost of operation and leaving some water available at the end of the horizon. Because of the formulation of the problem, this is sub-optimal since this unused water is considered lost. Finally, the **solid-orange** path (—) is a compromise between the two, it uses water more efficiently, leaving no water available at the end of the horizon and minimizing the overall cost of operation.

<sup>14</sup>: See Equations (4.1)–(4.3)

<sup>15</sup>: In Figure 4.7, nodes are ordered with increasing values of  $C_w$  from bottom to top.



# Validation in the combined cooling pilot plant

## To Do

After the chapter is complete, find and replace all mentions to RBF, ANN, RMSE and all other acronyms with the acronym with \gls.

## 5.1 Modelling

The two main components of the system (WCT and DC) are modelled with different approaches and compared in detail. Afterward, the integration of the selected modelling approach with the rest of the system components (Section 3.3) is validated in Section 5.1.5 (Complete system model validation).

### 5.1.1 Wet cooler model alternatives comparison and validation

#### Physical model

As previously mentioned<sup>1</sup>, three experimental campaigns have been performed, shown in Figure 5.1 as Exp 1, Exp 2, and Exp 3. Exp 1 corresponds to the Poppe model calibration campaign and it was designed for the calibration of the first principles model. The aims of such campaign was to fit a function (mapping) that relates the air mass flow rate at the outlet of the tower,  $\dot{m}_a$ , with the frequency of the fan,  $f_{fan}$ :

$$\dot{m}_a = -0.0014 f_{fan}^2 + 0.1743 f_{fan} - 0.7251. \quad (5.1)$$

and to calibrate a WCT performance coefficient: the Merkel number, Me. Figure 5.2 shows the variation of the Merkel number as a function of the water-to-air mass flow ratio ( $\dot{m}_w/\dot{m}_a$ ) using data from Exp1. As can be seen, the Me decreases with  $\dot{m}_w/\dot{m}_a$  values following a linear trend on log-log scale.

<b>5.1 Modelling . . . . .</b>	<b>49</b>
5.1.1 Wet cooler model alternatives comparison and validation . . . . .	49
5.1.2 Dry cooler model alternatives comparison and validation . . . . .	50
5.1.3 Main components modelling conclusions . . . . .	53
5.1.4 Condenser model validation . . . . .	55
5.1.5 Complete system model validation . . . . .	56
<b>5.2 Control and optimization results . . . . .</b>	<b>56</b>
5.2.1 Choosing an optimization algorithm . . . . .	57
5.2.2 Comparing the strategies . . . . .	58
5.2.3 Validation at pilot plant . . . . .	59

1: See Section 2.3 (Wet cooling tower)

Lidia, aquí la correlación no usa la temperatura ambiente

Make text in figure larger

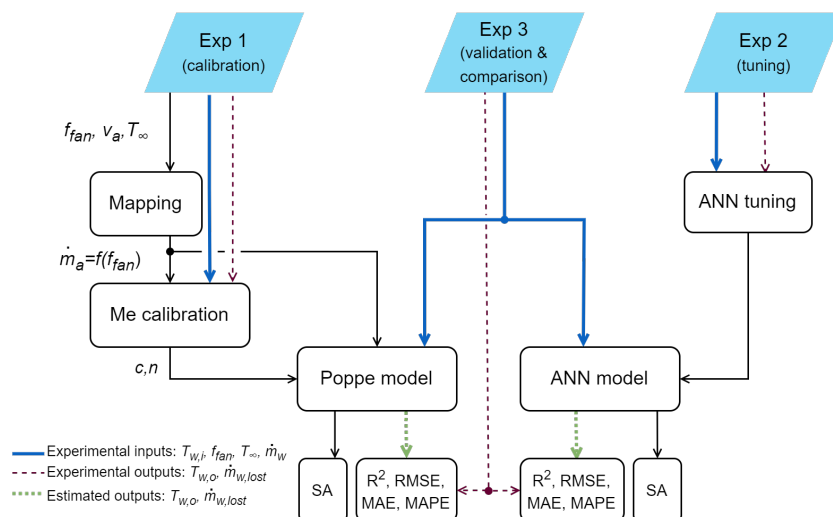


Figure 5.1: Calibration, tuning, validation and comparison procedure

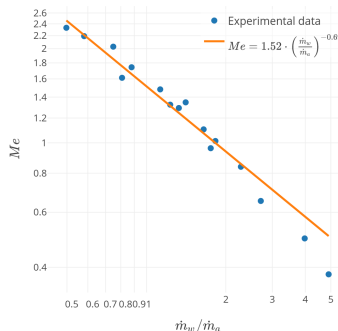


Figure 5.2: Experimental results for the Me number as a function of  $\dot{m}_w/\dot{m}_a$ .

Following the correlation for the Merkle number of a wet cooling tower described in Section 3.1.1, the parameters  $c$  and  $n$  obtained from the data fitting are 1.516 and 0.693, respectively.

### Data-driven

In order to generate the data-driven from first-principles alternative, the most relevant input variables identified in Section ?? are discretized using a fixed number of resolution steps for each variable, within ranges based on expected operating conditions, as defined in Table 5.1.

Figure 5.3 shows the generated input space distribution. The upper plot shows the frequency distribution of the samples while the lower one the actual values per input, where the x-axis represents the samples and the y-axis the values for each of the input variables.

### Prediction capabilities

Tabla tocha añadiendo casos (GPR, DD from FP, RF, GB)

The results of each modelling alternative and its comparison can be visualized in Figure ?? and Table 5.4. The results of each modelling alternative and its comparison can be visualized Figure ?? shows the results obtained with the models using Exp 3. It shows the perfect fit together with the results obtained with Poppe's model, MIMO FF, cascade CF, and MIMO RBF. In Table 5.4, the performance of the studied modelling approaches are included for the different performance metrics<sup>2</sup>. T represents the performance metric value for the training / calibration dataset (Exp 1 or Exp 2 depending on the case), and V for the validation and comparison one (Exp 3). In all cases the model representing each alternative is in the best case scenario, *i.e.* maximum number of points available. On the other hand, s.u. indicates that the units of the column are the same as from the source variable.

Comparing both modelling approaches (see Figure ??), it can be outlined that both models provide a good prediction of the output variables, falling most of the discrepancies (errors) within the uncertainty range. Poppe's model provides a better prediction of the outlet temperature, obtaining an RMSE of 0.33 °C and an  $R^2$  of 0.98. In comparison, the best ANN alternative (RBF MIMO) has a slight worse performance with an RMSE of 0.51 °C and  $R^2 = 0.95$ . In terms of water consumption, the physical model has a better prediction accuracy in terms of RMSE and  $R^2$  (8.5 l/h and 0.97) compared to 11.24 l/h and 0.95 for the best ANN model (cascade CF). It can be stated that, although the results are better for the physical model (specially in the case of the outlet temperature prediction), both approaches produce valid results with high accuracy levels.

Incluir gráfica comparativa de evolución de RMSE (incluyendo GPR) para argumentar por qué GPR es mejor no solo en términos de error, si no también en requerimiento de datos.

### 5.1.2 Dry cooler model alternatives comparison and validation

#### Physical model

#### Data-driven

In order to generate the data-driven from first-principles alternative, the most relevant input variables identified in Section 3.2.2 are discretized using a fixed number of resolution steps for each variable, within ranges based on expected operating conditions, as defined in Table 5.3. and Section ?? (??) visualizes the

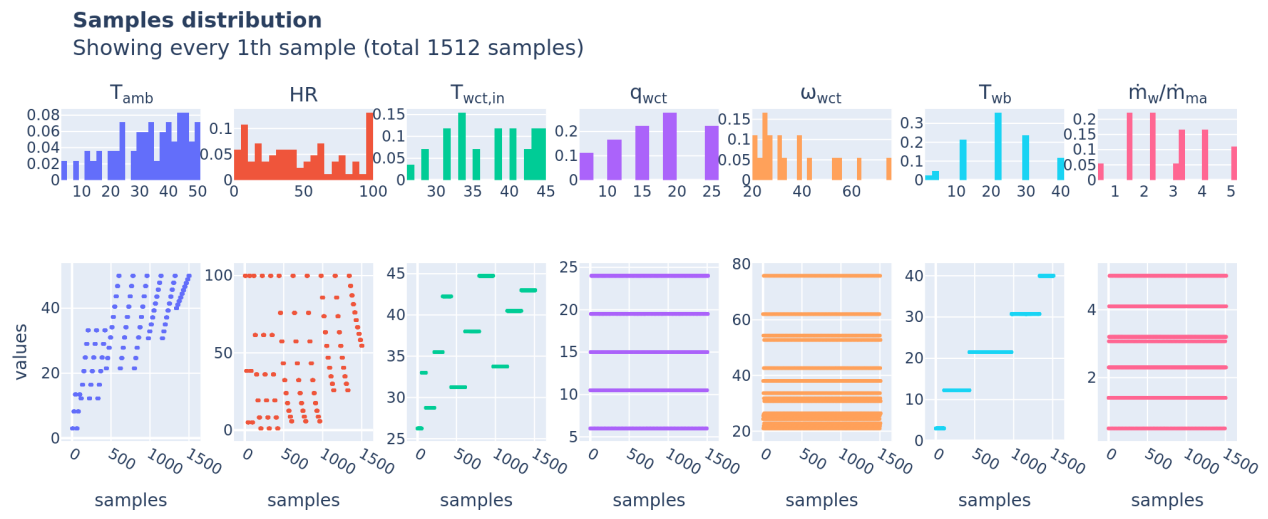
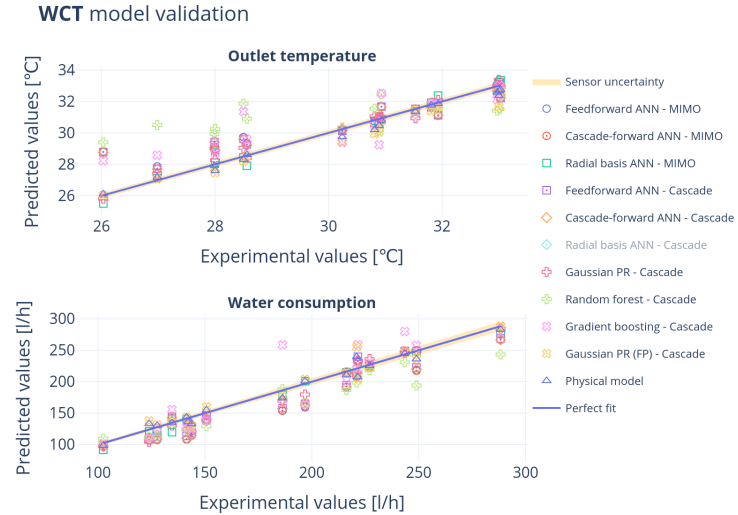


Figure 5.3: Data-driven from first-principles. Samples distribution visualization.



generated input space distribution where it can be appreciated that the samples are well distributed across the entire input space.

**Figure 5.4:** WCT models performance comparison between the different modelling approaches.



**Table 5.2:** Summary table of the prediction results obtained with the different modelling approaches studied.

Predicted variable	Modelling alternative	Model config	Topology	Performance metric								Evaluation time (s)	
				R <sup>2</sup> (-)		RMSE (s.u.)		MAE (s.u.)		MAPE (%)			
				T	V	T	V	T	V	T	V		
$T_{wet,out}$ (°C)	Physical model	-	-	-	<b>0.98</b>	-	-	-	<b>0.27</b>	-	<b>0.87</b>	6.288	
	Feedforward ANN	MIMO	20-2	0.90	0.81	0.60	0.97	0.42	0.67	1.36	2.36	0.004	
	Cascade-forward ANN	MIMO	10-10-2	0.90	0.82	0.60	0.93	0.44	0.65	1.42	2.27	0.005	
	Radial basis ANN	MIMO	34-2	0.97	0.97	0.34	0.41	0.21	0.28	0.66	0.94	0.007	
	Feedforward ANN	Cascade	20-1	0.90	0.82	0.60	0.93	0.43	0.65	1.41	2.26	0.011	
	Cascade-forward ANN	Cascade	10-10-1	0.90	0.83	0.60	0.92	0.43	0.64	1.40	2.24	0.010	
	Radial basis ANN	Cascade	92-1	0.97	-1.44	0.33	3.45	0.10	2.12	0.32	7.43	0.009	
	Gaussian PR	Cascade	N/A	0.99	<b>0.97</b>	0.20	<b>0.37</b>	0.15	<b>0.26</b>	0.47	<b>0.89</b>	0.001	
	Random forest	Cascade	N/A	0.75	0.30	0.96	1.85	0.60	1.46	2.03	5.05	0.078	
	Gradient boosting	Cascade	N/A	1.00	0.68	0.00	1.24	0.00	0.95	0.01	3.29	0.015	
$C_w$ (l/h)	Gaussian PR (FP)	Cascade	N/A	1.00	<b>0.94</b>	0.32	<b>0.54</b>	0.15	<b>0.41</b>	0.52	<b>1.32</b>	0.105	
	Physical model	-	-	-	<b>0.97</b>	-	<b>8.47</b>	-	<b>6.74</b>	-	<b>3.74</b>	6.288	
	Feedforward ANN	MIMO	20-2	0.92	0.83	14.77	21.58	11.98	18.64	9.91	10.75	0.004	
	Cascade-forward ANN	MIMO	10-10-2	0.92	0.84	15.47	20.90	12.51	17.84	10.48	10.22	0.005	
	Radial basis ANN	MIMO	34-2	0.99	0.97	5.58	9.34	3.81	7.47	3.23	4.68	0.007	
	Feedforward ANN	Cascade	20-1	0.92	0.88	15.00	18.45	11.97	15.77	10.20	8.92	0.011	
	Cascade-forward ANN	Cascade	10-10-1	0.92	0.85	15.01	20.34	12.11	17.66	10.00	10.18	0.010	
	Radial basis ANN	Cascade	33-1	0.99	0.93	4.99	14.28	3.45	10.14	2.68	6.22	0.009	
	Gaussian PR	Cascade	N/A	0.99	<b>0.95</b>	4.74	<b>12.00</b>	3.61	<b>9.96</b>	3.09	<b>6.32</b>	0.001	
	Random forest	Cascade	N/A	0.89	0.80	17.35	23.23	10.51	18.51	7.58	9.73	0.078	
	Gradient boosting	Cascade	N/A	1.00	0.77	0.24	25.07	0.07	17.21	0.05	9.55	0.015	
	Gaussian PR (FP)	Cascade	N/A	0.98	<b>0.95</b>	10.85	<b>11.63</b>	4.81	<b>8.14</b>	3.74	<b>4.52</b>	0.105	

## Prediction capabilities

Tabla tocha añadiendo casos (GPR, DD from FP, RF, GB)

## Experimental data requirements

### 5.1.3 Main components modelling conclusions

This section presents a comparison between two modelling alternatives: data-driven and first-principles. It applies to wet cooling towers and dry coolers, specifically to ACHE. The main conclusions obtained during the investigation and final recommendations can be summarized as follows:

#### Wet cooling tower

Regarding the prediction of the output variables, in the case of the outlet water temperature, both models reported good results, with low errors falling within the uncertainty range of the experimental equipment. Nonetheless, the physical model performs better than the best data-driven alternative (MIMO RBF):  $R^2 = 0.98$  and RMSE= 0.33 °C compared to  $R^2 = 0.95$  and RMSE= 0.51 °C, respectively.

For the predictions of water consumption, it was shown that the Poppe model accurately predicts this variable, with results of  $R^2 = 0.97$  and RMSE= 8.47 l/h. The best ANN alternative (cascade CF) achieves close results with an  $R^2 = 0.95$  and RMSE= 11.24 l/h.

However, the Poppe model reached such reliable prediction levels with a much lower number of tests, needing only 2. In comparison, the ANN alternatives need more data, at least 10 (with a good distribution over the operating range) for the FF and CF ANN models.

**Table 5.3:** Bounds and discretization of the model input variables.

x	Units	lb	ub	n
$T_{amb}$	°C	3	50	7
$\Delta T_{amb-dc,in}$	°C	3	30	7
$q_{dc}$	m <sup>3</sup> /h	6	24	7
$T_{dc,in}$	°C	25	45	-
$\omega_{dc}$	%	11	99.18	6

completar esta sección antes del domingo

#### Samples distribution

Showing every 1th sample (total 798 samples)

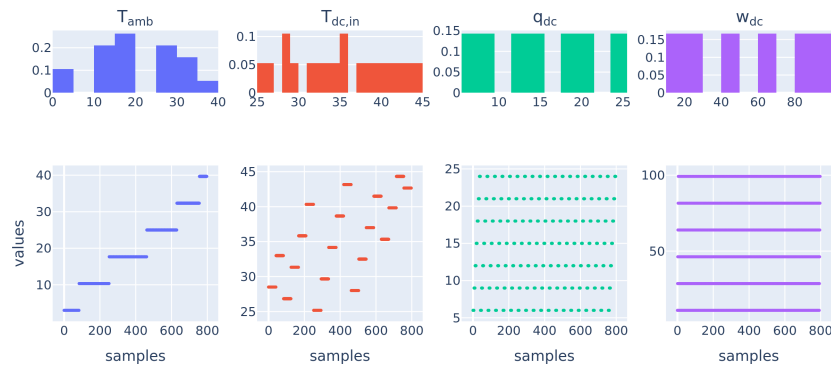


**Figure 5.5:** Data-driven from first-principles. Samples distribution visualization.



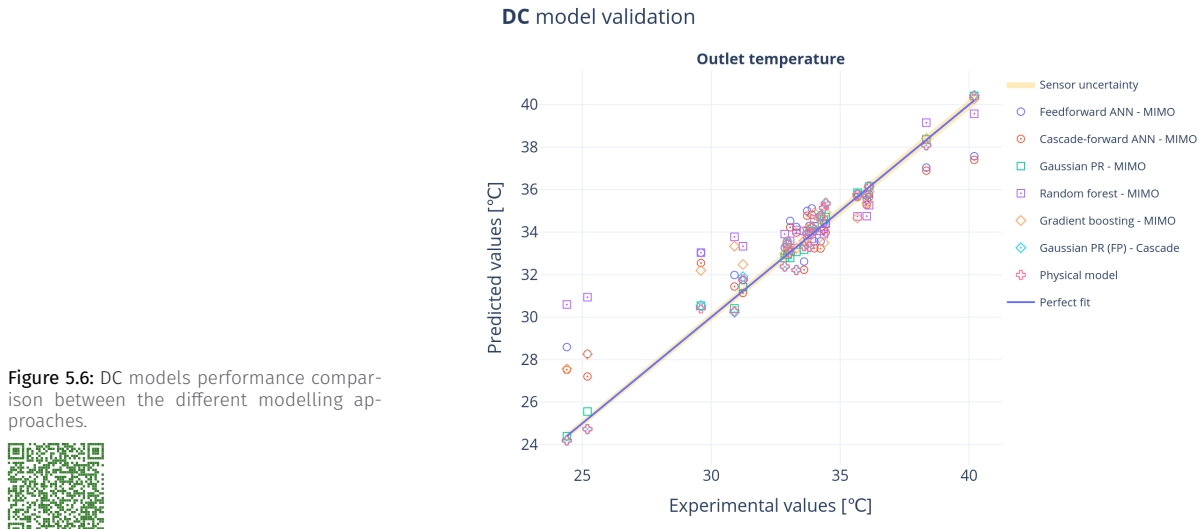


**Figure 5.6:** DC models performance comparison between the different modelling approaches.



**Table 5.4:** Summary table of the prediction results obtained with the different modelling approaches studied.

Predicted variable	Modelling alternative	Model config	Topology	Performance metric								Evaluation time (s)	
				R <sup>2</sup> (-)		RMSE (s.u.)		MAE (s.u.)		MAPE (%)			
				T	V	T	V	T	V	T	V		
T <sub>dc,out</sub> (°C)	Physical model	-	-	-	<b>0.98</b>	-	<b>0.50</b>	-	<b>0.42</b>	-	<b>1.28</b>	0.035	
	Feedforward ANN	-	20-1	0.77	0.78	1.42	1.62	1.13	1.18	3.29	3.85	0.005	
	Cascade-forward ANN	-	10-10-1	0.78	0.85	1.39	1.37	1.12	1.02	3.23	3.24	0.007	
	Gaussian PR	-	N/A	0.99	<b>0.99</b>	0.24	<b>0.32</b>	0.19	<b>0.25</b>	0.56	<b>0.77</b>	0.005	
	Random forest	-	N/A	0.84	0.61	1.19	2.17	0.72	1.36	2.05	4.69	0.022	
	Gradient boosting	-	N/A	1.00	0.86	0.00	1.31	0.00	0.86	0.00	2.92	0.035	
	Gaussian PR (FP)	-	N/A	1.00	<b>0.98</b>	0.03	<b>0.53</b>	0.02	<b>0.44</b>	0.07	<b>1.35</b>	0.002	

## Air-cooled heat exchanger

### Conclusions and recommendations

For the proposed optimization strategy in Section ?? (??), a fast, reliable model that can be scaled to different system sizes is required.

On the one hand, the first-principle models execution time is much higher than the data-driven alternatives, which is a significant drawback when it comes to the optimization strategy, where the model is evaluated many times in a short period of time. On the other hand, the data-driven counterparts are only applicable to the conditions and the particular system with which they are developed.

Conversely, one of the main strengths of both physical models presented in this chapter, is their ability to predict the operation of the coolers regardless of the conditions tested; while the data-driven execution time is faster by orders of magnitude, it can be vectorized and its execution time is more constant regardless of the input conditions.

Therefore, as combining a wet cooler and a dry cooler into a combined cooler offers potential advantages compared to the individual systems, combining both modelling approaches is the chosen solution to model the system. The best performing data-driven model, the Gaussian-Process Regression (GPR) is calibrated using data from the first-principle models, where physical models are adapted dynamically to the required scale and finally the data-driven model can be generated. This approach provides a way of having on-demand models that

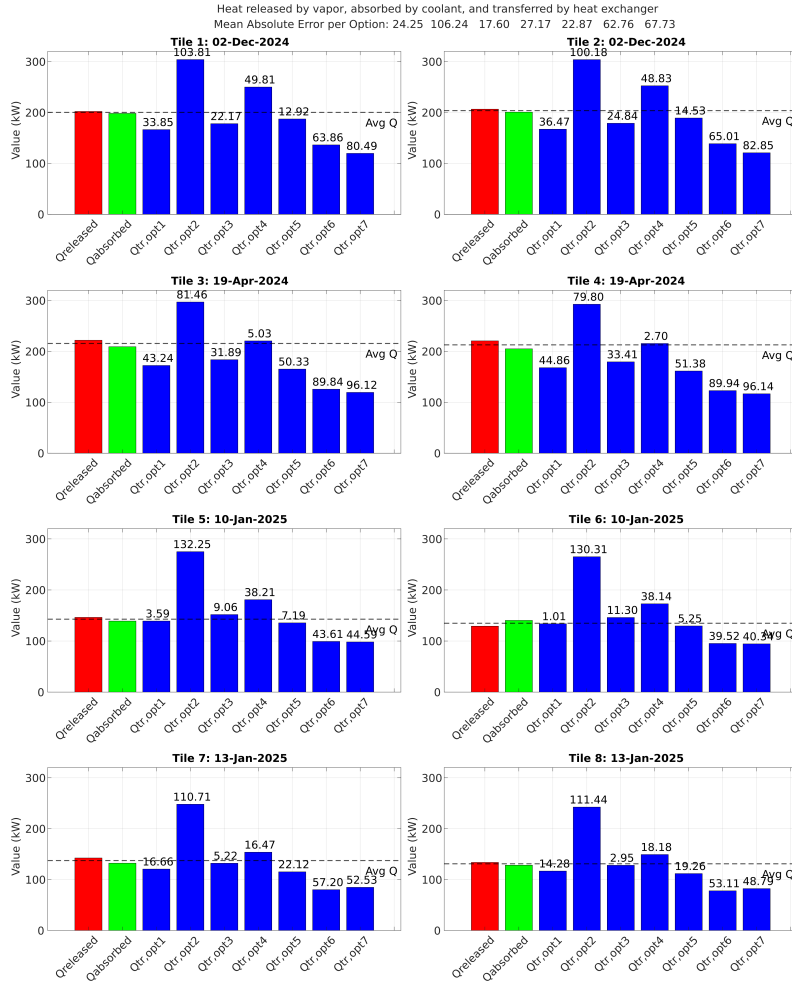


Figure 5.7: Heat transfer coefficient calibration results

can be adapted to the particular case study, while still being fast and efficient in terms of computational resources.

#### 5.1.4 Condenser model validation

For the surface condenser<sup>3</sup> a physical model is used, with the heat transfer coefficient as the only parameter to calibrate. Seven different alternative estimations of the heat transfer coefficient were calculated, using the data from the experimental campaign described in Section ?? (??). They are as follows:

1. Empirical correlation using the condenser flow rate ( $q_c$ ) and the vapor temperature ( $T_v$ ) as inputs.
2. Empirical correlation using the cooling water inlet temperature ( $T_{c,in}$ ) and  $T_v$  as inputs.
3. Empirical correlation using the flow rate per condenser tube ( $q_{c,tube} = q_c/n_{tubes} = q_c/24$ ) and the cooling water inlet temperature.
4. Nominal value from the manufacturer, which equals 1.838 W/m<sup>2</sup>°C
5. Calibra\_Uexp\_original
6. Calibra\_Uexp\_recortado

3: See Section ?? (??)

The results of the calibration are shown in Figure 5.7, where the y-axis shows the thermal power obtained and the x-axis holds different bars for the different heat transfer coefficient estimation methods, with bars also for the experimental

Estos qué son? Generar una nueva versión de la figura una vez se seleccionen los métodos finales

**Table 5.5:** Performance metrics obtained with the complete (CC) and component (Cnt) models

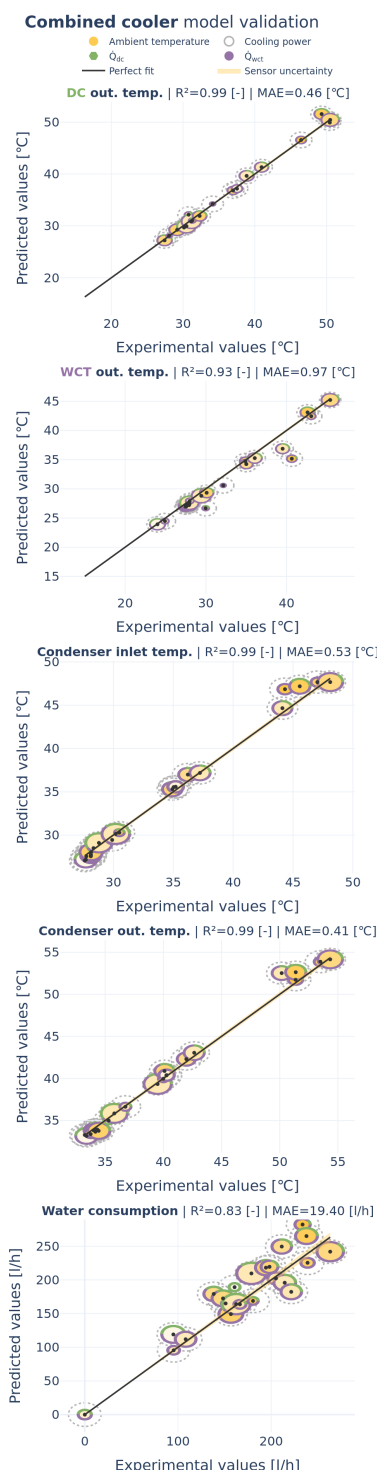


**Figure 5.8:** Complete combined cooler model validation.



Predicted variable	Performance metric					
	$R^2$ (-)		MAE (s.u.)		MAPE (%)	
	Cnt	CC	Cnt	CC	Cnt	CC
$T_{dc,out}$ (°C)	0.99	0.98	0.29	0.46	0.90	1.17
$T_{wct,out}$ (°C)	0.92	0.94	1.01	0.97	3.01	2.72
$C_w$ (l/h)	0.87	0.82	16.55	19.40	10.42	11.03
$T_{c,out}$ (°C)	0.98	0.99	0.23	0.41	1.51	1.00
$T_{c,in}$ (°C)	-	0.99	-	0.53	-	1.52

same units as the predicted variable

heat released by the vapor and absorbed by the coolant. As can be seen in the figure. The shown results are for steady-state conditions with the condenser in an equilibrium state ( $Q_{\text{released}} \approx Q_{\text{absorbed}}$ ), and with a large variation in the condenser conditions (120 to 200 kW, the whole operating range of the condenser). The results show that the heat transfer coefficient obtained with the method 3 is the one that best fits the experimental data, with a Mean Absolute Error (MAE) of 17.6 kW and a maximum error of 33.41 kW (15 %).

### 5.1.5 Complete system model validation

The complete model of the combined cooler has been validated with a different dataset composed of 24 tests. The obtained outputs regression is shown in Figure 5.8. This figure compares the experimental results with the predicted values. To visualize the operational characteristics of each test, the data points are represented with the following information:

- The dashed circle represents the nominal cooling power (200 kW<sub>th</sub>).
- The filled circle represents the cooling power measured in the test relative to the nominal value. The closer it is to the dashed circle, the closer the cooling power is to the nominal one.
- The measured cooling power is achieved using a certain percentage of DC and WCT. These contributions are distinguished by green and purple, respectively. For example, if the ring is mostly green, it reflects that the cooling contribution from DC is predominantly larger than that from WCT.
- The filling color inside the circle represents the ambient temperature. From low temperature (no filling) to high ambient temperature (dark yellow).

With this representation, it can be observed that the model provides satisfactory results over a wide range of operating and ambient conditions. The outlet temperatures show a MAE lower than 0.97 °C, with the largest error occurring in  $T_{wct,out}$ , when the cooling power was far from the nominal value. This may be due to the need to improve the relation  $\dot{m}_{air} - w_{wct}$  relationship at low flow rates. In the case of the water consumption, the tendency ( $R^2=0.82$ ) of the predicted values follows the experimental ones, being the MAE 19.4 l/h.

A summary of the models' results is shown in Table 5.5. This table includes the performance metrics of each component simulated individually (Cnt column) and those obtained with the complete model (CC column). The performance metrics obtained validate the model and provide the opportunity of using it for the analysis of the CC technology under different cases of study.

## 5.2 Control and optimization results

Once the models of the main components of the system have been validated, the next step is to validate the optimization strategy proposed in Section ?? (??). First, an optimization algorithm is chosen by comparing different alternatives in Section 5.2.1 (Choosing an optimization algorithm). Then, the two proposed

System	Algorithm	Parameters			Average fitness per obj. fun. evaluations			
		pop size	gen	wrapper algo iters	0	50	150	800
DC	IHS	50	800	N/A	1.28 ± 0.82	1.05 ± 0.29	0.80 ± 0.10	0.77 ± 0.09
		100	800	N/A	0.92 ± 0.18	0.87 ± 0.14	0.81 ± 0.11	0.77 ± 0.10
		400	800	N/A	0.81 ± 0.11	0.80 ± 0.11	0.79 ± 0.10	0.77 ± 0.10
	SEA	50	80	10	1.19 ± 0.28	0.95 ± 0.11	0.79 ± 0.10	0.77 ± 0.09
		100	80	10	0.92 ± 0.13	0.86 ± 0.10	0.80 ± 0.10	0.77 ± 0.09
		400	80	10	0.82 ± 0.10	0.80 ± 0.10	0.78 ± 0.10	0.77 ± 0.09
WCT	IHS	50	1	10	1.06 ± 0.40	0.97 ± 0.18	0.83 ± 0.10	1.04 ± 1.04
		100	0	10	0.95 ± 0.16	0.95 ± 0.16	0.95 ± 0.95	0.95 ± 0.95
		400	0	10	0.83 ± 0.10	0.83 ± 0.10	0.83 ± 0.10	0.83 ± 0.83
	SEA	50	800	N/A	0.24 ± 0.08	0.18 ± 0.04	0.10 ± 0.00	0.07 ± 0.00
		100	800	N/A	0.12 ± 0.02	0.11 ± 0.01	0.08 ± 0.00	0.07 ± 0.00
		400	800	N/A	0.07 ± 0.00	0.07 ± 0.00	0.07 ± 0.00	0.07 ± 0.00
CC	SEA	50	80	10	0.25 ± 0.04	0.16 ± 0.01	0.07 ± 0.00	0.06 ± 0.00
		100	80	10	0.17 ± 0.03	0.11 ± 0.00	0.07 ± 0.00	0.06 ± 0.00
		400	80	10	0.07 ± 0.00	0.07 ± 0.00	0.07 ± 0.00	0.06 ± 0.00
	SEA	50	1	10	0.29 ± 0.07	0.17 ± 0.02	0.09 ± 0.00	0.07 ± 0.07
		100	0	10	0.11 ± 0.00	0.11 ± 0.00	0.11 ± 0.11	0.11 ± 0.11
		400	0	10	0.07 ± 0.00	0.07 ± 0.00	0.07 ± 0.00	0.07 ± 0.07
WCT	IHS	50	1000	N/A	0.77 ± 0.12	0.80 ± 0.11	0.77 ± 0.11	0.59 ± 0.11
		100	1000	N/A	0.70 ± 0.12	0.78 ± 0.10	0.82 ± 0.15	0.61 ± 0.13
		400	1000	N/A	0.79 ± 0.19	0.82 ± 0.21	0.80 ± 0.22	0.65 ± 0.16
	SEA	50	100	10	0.92 ± 0.13	0.86 ± 0.14	0.74 ± 0.16	0.51 ± 0.10
		100	100	10	0.88 ± 0.16	0.82 ± 0.16	0.75 ± 0.21	0.62 ± 0.16
		400	100	10	0.84 ± 0.21	0.80 ± 0.18	0.74 ± 0.21	0.69 ± 0.19
CC	SEA	50	2	10	0.83 ± 0.16	0.79 ± 0.13	0.73 ± 0.14	0.56 ± 0.13
		100	1	10	0.82 ± 0.17	0.80 ± 0.13	0.77 ± 0.10	0.64 ± 0.13
		400	0	10	0.73 ± 0.16	0.73 ± 0.16	0.73 ± 0.16	0.73 ± 0.73

**Table 5.6:** Static optimization algorithm comparison results

variants for the combined cooler are compared in simulation for one operation day in the simulated pilot plant in order to see which one performs better in Section 5.2.2 (Comparing the static and horizon optimization strategies). Finally, two validation scenarios are tested in the real facility, one where a regular operation schedule is followed throughout the operation, and a second one where planned changes are introduced in the operation schedule, in order to validate how the optimization strategy adapts to changing conditions.

### 5.2.1 Choosing an optimization algorithm

#### Static problems

For every static optimization problem (referencias a problemas) three different algorithms are tested: (N+1)-ES Simple Evolutionary algorithm with self-adaptive Constraint Handling (SEA-CSTR), Improved Harmony Search algorithm (IHS) and Differential Evolution with self-adaptive Constraint Handling algorithm (DE-CSTR). For each alternative the same number of objective function evaluations are given (800) but they are distributed differently depending on the algorithm:

- ▶ SEA-CSTR and DE-CSTR make use of the Self-Adaptive Constraint handling algorithm (CSTR-SA) wrapper algorithm, which allows them to the constrained problems. 10 iterations are performed for this wrapper algorithm, leaving 80 iterations to spare for the inner algorithm.
- ▶ For all alternatives, three values are tested for the initial population size: 50, 100 and 400 individuals<sup>4</sup>.
- ▶ Depending on the algorithm only one individual is evolved ( IHS and (N+1)-ES Simple Evolutionary algorithm (SEA)) or the whole population ( Differential Evolution algorithm (DE)). This means that 800 generations are available for IHS, 80 generations for SEA-CSTR and for DE-CSTR, 1 generation is available for the population of 50 individuals, while only the initial generation is for the population of 100 and 400 individuals.

4: The initial population fitness evaluation is not counted for the budget of objective function evaluations

Table X shows the results obtained, in terms of fitness at different stages in the evolution. From the results it can be seen that for all alternatives the best performing and most consistent algorithm is ...

### Horizon optimization. Path selection

5: Only up to 50k evaluations is shown in the figure for clarity

A methodology similar to the static comparison is used. This time the algorithms evaluated are: Generalized Ant Colony Optimization algorithm (GACO), IHS, Simple Genetic Algorithm (SGA) and Particle Swarm Optimization algorithm (PSO). Three different population sizes are tested (80, 150 and 1000) if the particular algorithm evolves more than one individual; the number of generations is calculated accordingly so that all alternatives have the same budget of objective function evaluations, equal to 200k evaluations<sup>5</sup>. The results are visualized in Figure 5.9, where there are different plots for different dates, the y-axis represents the fitness and the x-axis shows the number of objective function evaluations. The results show that consistently the SGA outperforms the alternatives, and particularly, the smaller population size (80) configuration followed very closely by the 150 population size configuration.

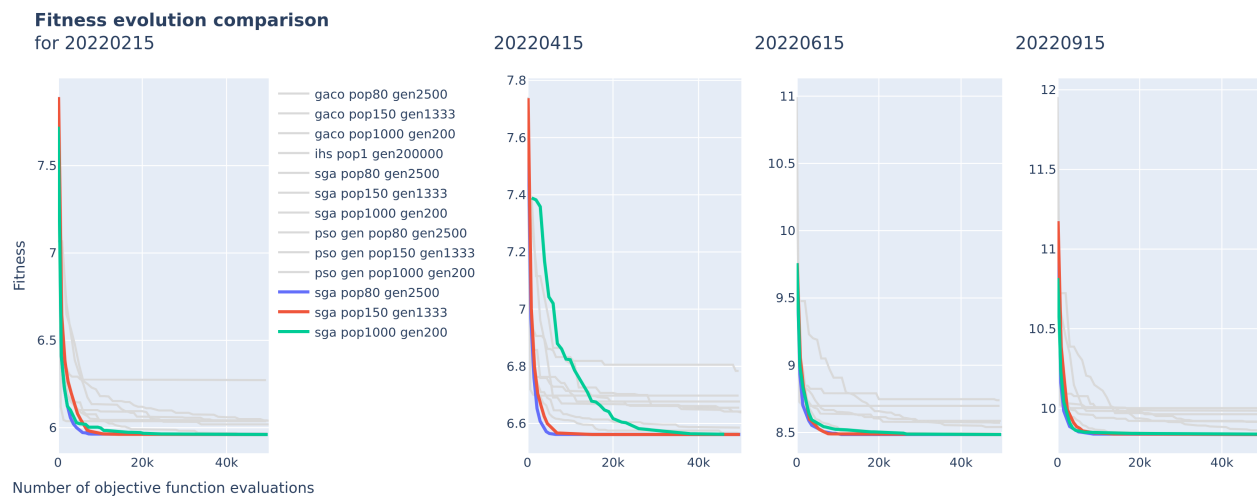


Figure 5.9: Horizon optimization – path selection subproblem. Fitness evolution comparison for different algorithms in four different dates.



#### 5.2.2 Comparing the static and horizon optimization strategies

##### TODO

Poner la figura de resultados del horizonte para SOLO un día detallado aquí (más días hace que no se distingan bien las barras, tampoco se puede poner el pareto). Debe incluir la distribución hidráulica en barras comparando estático con horizonte, el frente de pareto del horizonte, y la comparativa de coste acumulado.

La figura es provisional. Actualizar la figura con cambios mencionados

Comentar la figura, sobre el frente de pareto que se muestra, cómo la estática al principio abusa del agua y para el final del día aumenta muchos sus costes, etc.

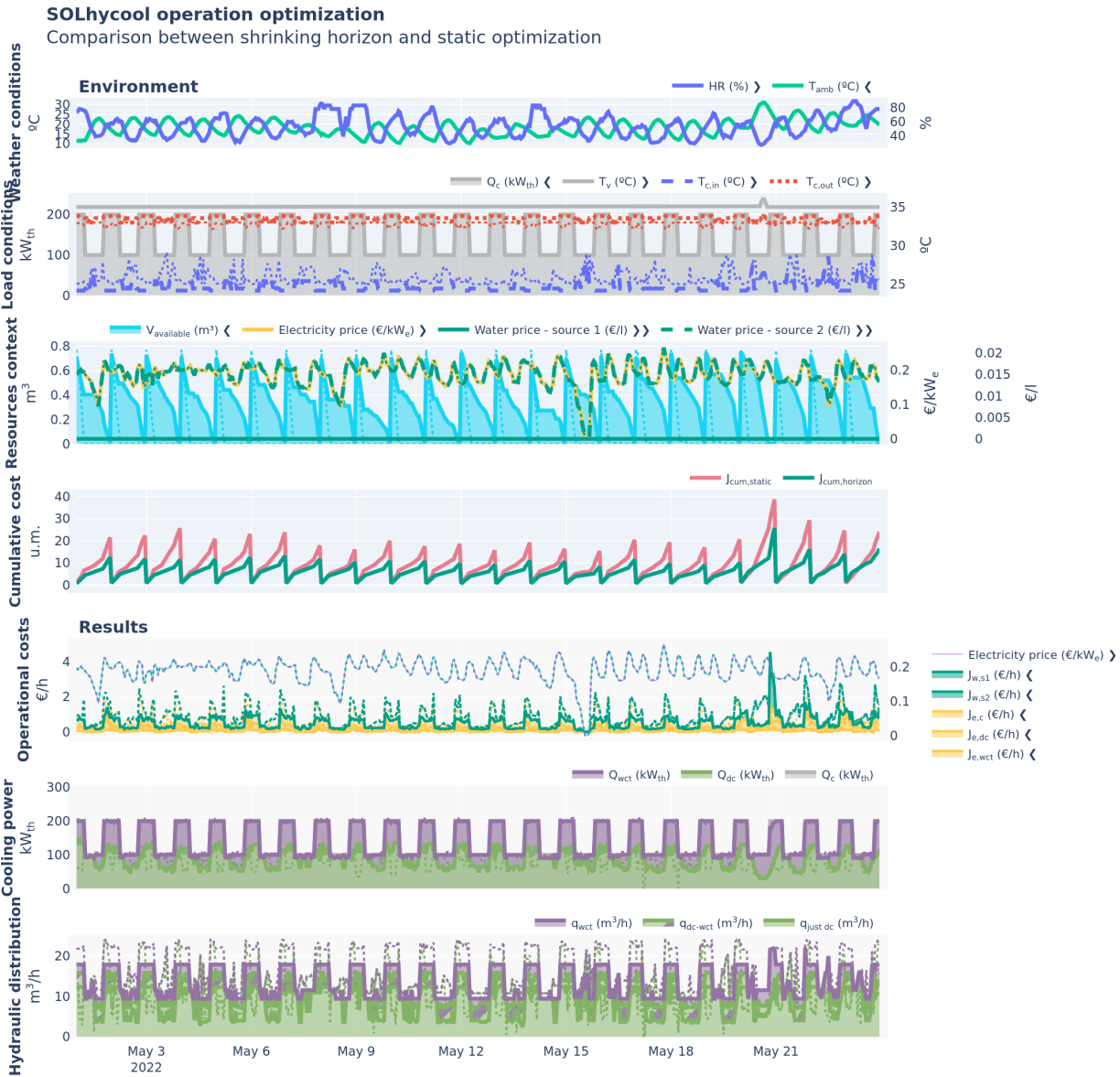


Figure 5.10: Detailed simulation results for the horizon optimization compared to the static alternative.



### 5.2.3 Validation at pilot plant

A hierarchical control strategy has been implemented in order to validate the optimization strategy in the real facility. Figure ?? shows a diagram of the methodology, where the left side represents the upper layer with the proposed shrinking horizon optimization<sup>6</sup> and the right side shows the low-level regulatory control layer, which directly interfaces with the actuators and sensors of the facility.

6: See Section ?? (??)

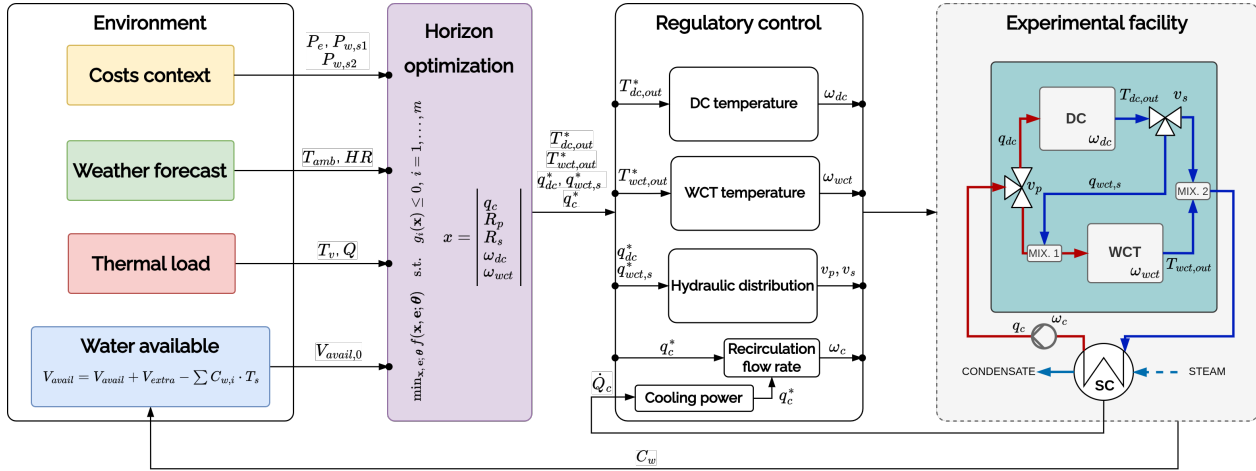


**Table 5.7:** Box-bounds for the decision variables.

**Figure 5.11:** Implementation of the optimization strategy in the real facility. Hierarchical control

x	Units	lb	ub
$q_c$	$\text{m}^3/\text{h}$	5.22	24.15
$R_p$	-	0.00	1.00
$R_s$	-	0.00	1.00
openweather %	%	11.00	99.18
$\omega_{wct}$ %	%	21.00	93.42

**Environment.** To generate the environment for the optimization, weather forecasts using the OpenWeather API [openweater\_api] were used, for the electricity costs data from the 2022 Spanish grid was used, updating the year to the one in which the experiment was performed, and the water cost was set to  $C_{w,s1} = X$  and  $C_{w,s2} = Y$ . For the thermal load a profile was generated by setting a constant vapor temperature of  $T_v = 45^\circ\text{C}$  while an arbitrary cooling power was generated considering the heat availability from the flat-plate collector field, which is the heat source of the system, for the particular day. Finally, an initial value for the water availability was set to  $V_{avail,0} = 0.5 \text{ m}^3$ , and from there it is updated by reading the actual system consumption online.

**Optimization layer.** The optimization algorithm is run every 30 minutes, and generates a new set of results for the remaining operation time. The results of the optimization are then passed to the regulatory control layer by setting them as setpoints for the low-level control. The box-bounds for the decision variables are shown in Table 5.7.

**Control layer.** Four controllers are implemented in this layer...

In order to validate the optimization strategy, several tests were performed over different days. In particular Figure ?? visualizes one test carried out in the 1st August to analyze in this section. The objective of the test was twofold. For the first part of the test a set operation plan was established:

- ▶  $\dot{Q}$  = Ramp up from 150 to 200 kW from 08:40 until 10:00, and hold the 200 kW value until the end of the test (13:00).
- ▶  $T_v = 45^\circ\text{C}$ . Held constant throughout the experiment (08:40 – 13:00)

The objective was to validate that the optimized operation based on the provided predictions was effectively able to correctly manage resources and cool the thermal load with the predicted associated consumptions. During operation of a CSP plant changes to the operation plan can arise in response to changes in electricity market dynamics, or other unforeseen environment circumstances. At 10:20 a change is introduced in the operation plan to simulate this behavior, the thermal load was ramped down with a similar (inverse) profile to the initial one. This allows to verify the adaptability of the proposed strategy to changing conditions and is the second objective of the test.

The operation strategy was as follows:

aiuda Lidia!

- ▶ Before the test and while the system starts up by generating vacuum in the surface condenser, the optimization layer was evaluated to have an initial perspective on the day operation and expected consumptions. If the operator was satisfied the provided values were used as reference and manually set to bring the system into stable operation after gradually increasing the thermal load.
- ▶ The optimization sample time was 20 minutes, it takes around that time to compute and is evaluated every 40 minutes.
- ▶ The thermal load was designed to change every 40 minutes, this means that for each optimization evaluation, two setpoint changes are provided to the regulatory control layer per optimization evaluation and thus predictions must be valid for those at least 40 minutes.
- ▶ For every optimization layer evaluation, first the environment is updated and then is provided as input to the optimization evaluation (see Figure 5.11).
- ▶ The low-level control layer has available the operation strategy for the whole horizon provided by the upper layer and following its schedule updates its setpoints.

Figure ?? is divided in several sections. In general solid lines represent measured (experimental) values, while the thin-dashed equivalent (same color) is the predicted value by the upper-optimization layer. This predicted value is provided by the latest evaluated optimization. The upper section of the figure displays the environment evolution (weather conditions, load conditions and resources context). They are followed by a comparison between predicted and actual results for: (a) distribution between cooling systems, in terms of flows (*hydraulic distribution*) and in terms of the assigned cooling power (*cooling power distribution*) and (b) individual cooler outputs in terms of temperature profile and water consumption in the wet cooler case. Finally, the bottom of the plot shows the low-level control layer performance for each control loop: coolers outlet temperature and flows.

In Figure ?? – *Hydraulic Distribution*, several sequentially added bars are shown. The first bar corresponds to the experimental value, while the remaining bars represent the predicted hydraulic distributions from successive optimization evaluations: the second bar comes from the first evaluation, the third from the second, and so on.

From the results, a few observations can be made:

- ▶ Overall a very good agreement between the optimization layer predicted operation and the experimental values can be observed. It can be seen that as long as the environment, specifically the thermal load, does not change, the generated operation strategy is valid for hours. Particularly, the initial evaluation at XX:XX. In another test (not shown) where the thermal load does not change throughout the day the initial optimization held valid until the end of operation.
- ▶ The dry system is very sensitive to the ambient temperature when operating in its limits. Less than half-degree prediction error in the ambient temperature (0.4 °C between 09:04 and 09:17) translates in a 15% difference between the expected and the actual fan speed.
- ▶ When both systems are operating, if the dry cooler falls short in its cooling allocation, the wet cooler can compensate for the dry cooler shortcoming on its cooling allocation. However, as can be seen at the beginning of the test (09:04 – 09:17), when only the dry cooler is used and does so in its limits (Figure ?? - DC outlet temperature loop - Control signal) it can happen that the load is undercooled resulting in a higher condenser pressure (in terms of temperature, +1-2 °C can be observed, which would translate in a penalty in the power produced by the turbine). A low-level supervisory controller should be set in place to prevent this.

- ▶ To avoid using the alternative more expensive alternative water source, the optimization prioritized the use of the dry cooling (as far as being dry-only as long as the ambient temperature and demanded thermal load allowed it 09:20) to conserve water until the end of operation. After the operation plan change, the lower expected load gives more room for adjustment and the optimization increases the load through the wet system from 0-40% to about 50% (Figure ?? - Hydraulic distribution and Cooling power distribution).
- ▶ The restricted availability of the water resource, means that the optimizations strategy always prioritizes water savings either by dry-only operation, or combined operation using a series configuration, at no point the parallel configuration is used despite progressively increased electricity cost (*Resources context –  $P_e$* ).
- ▶ The good agreement between upper and lower layer, means that the upper layer predicted controlled variables values could be used by the low-level control, for example, in a static feed-forward action.
- ▶ From the initial optimization evaluation, the low-level control layer has available an operation strategy for the whole horizon. This makes the strategy robust in the case the optimization is not evaluated again, or not evaluated on time.

# Annual analysis: ANDASOL-II CSP plant

## TL;DR

This chapter presents the annual simulation results for different cooling systems: a WCT, a DC and the presented CC optimized with static optimization and with horizon optimization. They provide cooling to the power block of the XX hours storage–CSP plant ANDASOL-II with an off-peak operation strategy. Results for the case study report a specific cooling cost of XX, XX and XX for the WCT, DC and CC, respectively, compared to the 5 L/kWh figure provided by the developer.

6.1 Environment definition . . . . .	63
6.1.1 Water context . . . . .	63
6.1.2 Thermal load . . . . .	64
6.1.3 Costs context . . . . .	65
6.2 Results . . . . .	65
6.3 Cooling alternatives comparison	67

## Introduction

A modeling framework has been developed to simulate and optimize the operation of various cooling systems, with a particular focus on the proposed combined cooling system. This methodology has been validated using data from a pilot plant. In this chapter, the objective is to apply the framework to a specific case study: a commercial 50 MW<sub>e</sub> CSP plant.

As previously mentioned, CSP plants are among the most water-intensive power generation technologies [22], a concern that is especially relevant in the arid regions where they are typically located. To assess the performance-water use and operational costs- of different cooling systems, the proposed methodology is applied to a real-world case study through an annual simulation. The case study examined is the Andasol-II CSP plant.

In the south-east of Spain, near Guadix and next to the Sierra Nevada mountain range (see Figure 6.1), thanks to the region high altitude (1100 m) and the semi-arid climate, the site has exceptionally high annual direct insolation (2260 W/m<sup>2</sup>) and thus is ideal for solar projects. This is why the first parabolic trough power plant in Europe, Andasol-I, was built there in 2008. One year later Andasol-II followed, located in the immediate neighbourhood and with almost identical construction. It has a rated output of 50 MW with 7.5 hours<sup>1</sup> of thermal storage, providing electricity for up to 200,000 people. More specifications are available in Table 6.1.

According to the developer, Andasol-II vaporizes 870 000 m<sup>3</sup>/year, or in specific units 5 l/kWh.

## 6.1 Environment definition

### 6.1.1 Water context

Obtaining accurate water availability data is challenging. Unlike resources such as electricity—where demand, supply, and prices are readily available—water availability data is often lacking. Water prices are not standardized; they vary from region to region, and even within the same region, depending on the source and the specific agreements in place.

For the simulation scenario, two sources of water are considered<sup>2</sup>. The first source is rainwater or water from a dam, which is assumed to be available at a constant price of XX [[empty citation](#)]. To create a representative dataset,



[22]: Meldrum et al. (2013), "Life Cycle Water Footprint of Concentrated Solar Power Plants," *Journal of Industrial Ecology*, 17(2), 2013, pp. 201–215.

Figure 6.1: Andasol-II and III aerial view. Andasol-II is the one at .

Source: [https://en.wikipedia.org/wiki/File:Andasol\\_5.jpg](https://en.wikipedia.org/wiki/File:Andasol_5.jpg)

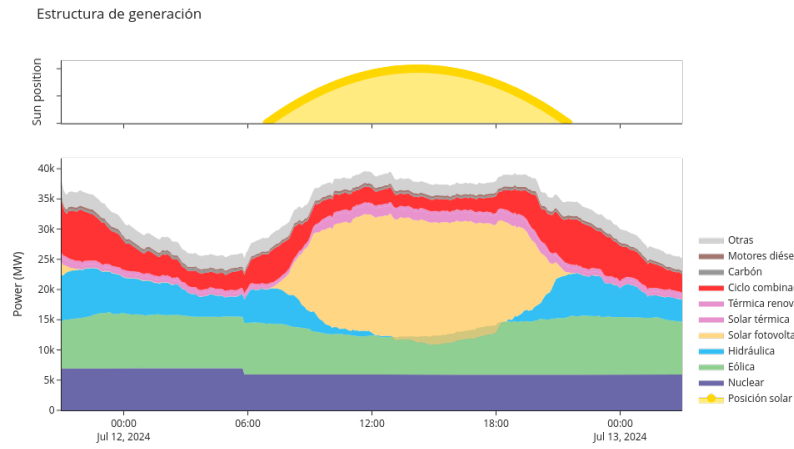
1: This means that if fully charged, it can produce the nominal rated power of the turbine for that duration

Table 6.1: ANDASOL-II plant main characteristics

Technology	Parabolic Trough
Solar Resource	2260 W/m <sup>2</sup>
Nominal Capacity	50 MW
Status	Operational
Start Year	2009
Expected Generation	158 GWh/year
Total Land Area	2 km <sup>2</sup>
LCOE (2020)	0.27 €/kWh
TF Inlet Temperature	293°C
TF Outlet Temperature	393°C
Power Cycle	Steam Rankine
Turbine Efficiency	38.1%
Cooling Type	Wet
Storage Type	Molten salts
Storage Capacity	7.5 Hours – 1 GWh

Source: Institute for Advanced Sustainability Studies (IASS) and others, 2022; data by Lillestam@IASS, Thonig@IASS, Zang@CAS, Gilmanova@CAS and other Sections under a Creative Commons Attribution 4.0 International License.

<a href="#">empty citation



**Figure 6.2:** Spanish electricity mix on July 12, 2024. The peak in photovoltaic generation is clearly visible at midday, while thermosolar generation is more evenly distributed throughout the day. Peak production is majorly from CSP plants with no storage.

Data source: Figure elaborated using data extracted from <https://www.ree.es/es/datos>

[68]: AG (), Meteonorm V8.2.0.24079

3: This is not an exogenous idea; the Villena CSP plant, for example, uses wastewater from a nearby prison to partially meet its water needs [empty citation]

[9]: Lilliestam et al. (2021), “The Near- to Mid-Term Outlook for Concentrating Solar Power: Mostly Cloudy, Chance of Sun”

[26]: Thonig et al. (2023), CSP.Guru 2023-07-01

[27]: Bonilla et al. (2024), “CSP Data: A Data Discovery Web Application of Commercial CSP Plants”

4: The storage is primarily used to extend generation past sunset.

5: This trend is already observable in Spain during the summer months; see Figure 6.2

<empty citation>

water availability is modeled as a function of precipitation data, which can be obtained from hourly Typical Meteorological Year (TPY) data [68]. A linear model is fitted to relate maximum precipitation to maximum available water, and when there is no precipitation, water availability is set to zero. The data is then resampled every 15 days, and the daily volume of available water is calculated by dividing the resampled fortnightly volume by 15. This approach accounts for the presence of water reservoirs and some degree of management capacity.

The alternative source is regenerated water<sup>3</sup> is not limited in volume.

### 6.1.2 Thermal load

Traditionally, thermal power plants were designed and operated to generate electricity only when solar energy was available. This approach remained common until the rapid rise in competitiveness of PV plants, which offer significantly lower generation costs. In response, concentrated solar power plants began integrating thermal energy storage systems to enable dispatchable power generation. Today, 21 out of 51 CSP plants in Spain—approximately 42%—have thermal storage capacities exceeding two hours [9, 26, 27]. This enables them to produce electricity even when solar input is unavailable.

However, many of these plants still follow traditional operating patterns, generating most of their electricity during peak solar hours<sup>4</sup>. This strategy is increasingly seen as suboptimal and is likely to be phased out as the electric grid becomes saturated with PV generation<sup>5</sup>.

In this work, a different operational strategy is adopted: the plant is configured to generate electricity during off-peak solar hours, typically in the evening when electricity demand is at its highest. This is achieved by shifting the plant’s production to align with these peak demand periods.

A model of the Andasol-II plant, developed by Bartolomé et al. [empty citation], was configured to follow this production strategy and simulated over an entire year. The resulting thermal load profile represents the demand to be met by the cooling system. The simulation used the same weather dataset as that employed for modeling the cooling system.

### 6.1.3 Costs context

**Electricity.** The spanish grid operator Red Eléctrica de España (REE) provides an API<sup>6</sup> to access the electricity market prices. A python script was developed to systematically download monthly data<sup>7</sup> for each month in the desired year. The data is fetched in hourly intervals and saved in JSON format, then every file is read and joined into a single dataset resulting in prices for the whole year.

**Water.** Rainwater has a constant lower price of XX. This price was obtained considering that the plan has access to the same water than the irrigation community of the area[<empty citation>]. The alternative source, *i.e.* regenerated water, is considerably more expensive, and its price is linked to the electricity price, specifically by a factor of XX<sup>8</sup>.

#### Simulation data and parameters information

- ▶ **Weather data.** Hourly weather data from TPY of Guadix (Spain) for the year. Data from [68].
- ▶ **Thermal load.** Hourly thermal load data from the power block of Andasol-II CSP plant from a simulation model [ortegadelgado\_theoretical\_2016].
- ▶ **Electricity price.** Spanish electricity market from 2022.
- ▶ **Maximum available water.** The maximum available water for ...
- ▶ **Alternative water source factor ...**

The full environment dataset is available at



6:

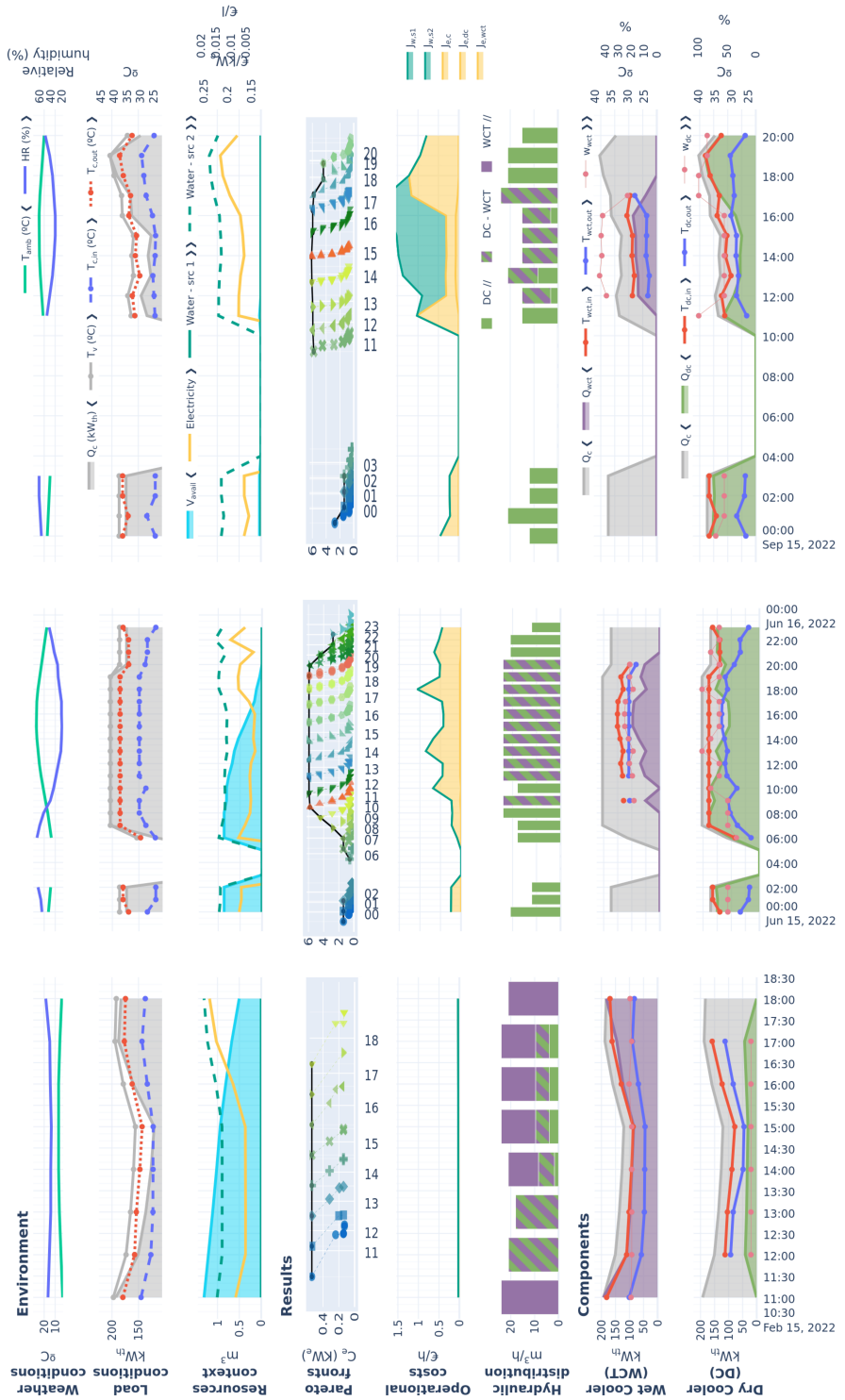
<https://api.esios.ree.es>

7: Longer periods would result in silent errors in the API

<empty citation>

8: This value includes a scaling factor to normalize the values

## 6.2 Implementation results



## 6.3 Cooling alternatives comparison

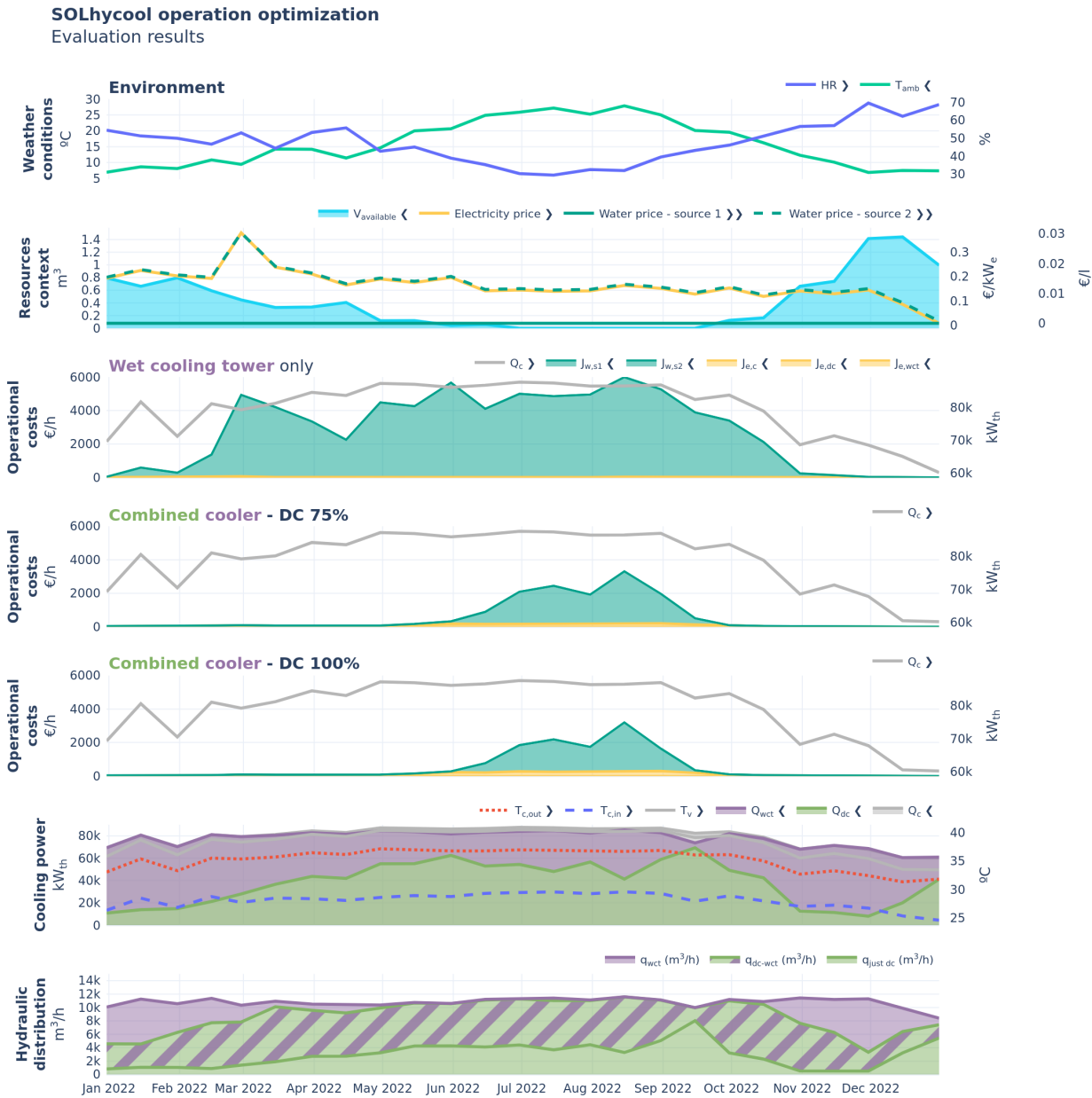


**Figure 6.4:** Annual simulation results for the different studied alternatives optimized with the proposed horizon optimization. Results are resampled every 15 days using their mean values.



One caveat that no optimization strategy will ever be able to overcome is that in most locations, ambient temperatures are lowest (favoring the dry system) at times with the most annual water availability (favoring the wet one). The inverse is true in the hot-dry summer season where water will inherently be a scarce

resource. Still as shown, there is a lot of margin for improved water management via system optimization with integrated dry and wet systems. Additionally, CSP systems should consider not operating in the hottest hours of the summer days - when water is scarce and enough power generation from other renewables is available - and produce during off-peak hours when the cooling is more efficient and other renewables are not producing.

From the results it is clear than water is the main cost driver, and thus the most limiting resource depending on the location and chosen cooling solution. For the analyzed case study, this is the case even when considering a conservative alternative water source price of 0.03 €/m<sup>3</sup>. From conversations with the Villena CSP plant O&M team, a figure of above 1 €/m<sup>3</sup> for this alternative source can be expected.

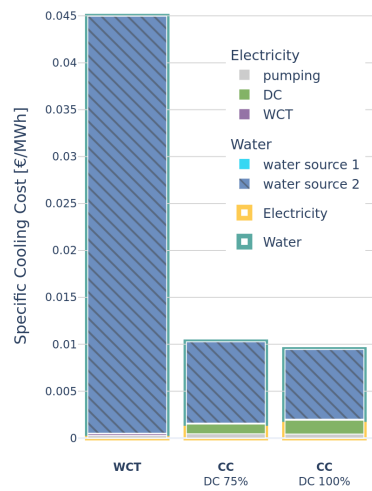


**Figure 6.5:** Composite specific cooling costs comparison.



## **CONCLUSIONS AND OUTLOOK**



## Conclusions

### Outlook and future work

#### Optimal water and electricity management in a combined cooling system

**Improved Pareto front computation.** In the current optimization implementation, the Pareto front for each step in the optimization horizon is constructed using a grid search over the decision space. This approach can become computationally expensive, especially as the grid resolution increases. Additionally, the Pareto front must be recalculated from scratch at every step, even though the sequential steps are often very similar—cost parameters remain constant, and only the thermal load and weather conditions change, typically with small variations. A more efficient solution would be to use a multi-objective optimization algorithm such as NSGA-II [[<empty citation>](#)], which can transfer evolved populations between successive evaluations, significantly reducing redundant computations.

<empty citation>

**Better water management** In the current implementation, the primary water source is distributed evenly each day, so the optimization process uses up the entire supply daily. However, a more intelligent daily distribution—essentially, a new optimization problem—could improve water management by allocating different amounts on different days, based on expected weather conditions and predicted generation. This approach would likely be incorporated as a new upper layer in the hierarchical control structure.<sup>9</sup> At the higher level a simpler and more abstract model would be considered to predict the long term behavior of the system and to optimize it over a long time horizon, probably considering the availability and capacity of a water reservoir.

9: The resulting structure would be: 1. Water allocation, 2. CCS operation optimization, 3. CC regulatory control.

**Analyze different combined coolers configurations and within each configuration, different component sizes.** The cooler analyzed has a combined dry and wet coolers which can either satisfy the nominal cooling load. Different ratios could be analyzed and one would probably be a better fit for the particular case study. Furthermore, the ACHE is used for the DC, but other options could be considered and added to the comparison, such as an ACC in parallel with a surface condenser together with a WCT or a deluged condenser.

This in itself is a design optimization problem that is not addressed in this thesis. However, it is important to integrate a method like the proposed optimization and include it in the design process to evaluate the performance of different configurations and sizes. In the end the decision of cooling system configuration and size will be informed by a techno-economic analysis.

**Techno-economic analysis.** The presented cooling alternatives comparative in this thesis focus on the operation cost of the system, but to get a better picture of the alternatives performance, a techno-economic analysis that includes the capital cost of the system and the expected lifetime of the components should be performed *i.e.* considering all costs associated with the system the plant's lifetime. This is currently being worked on as part of [SOLHycool], where the methodology presented here in terms of operation costs will be integrated in a techno-economic analysis for different case studies.

#### Energy management in MED processes driven by variable energy sources

**Alternative configurations for an MED brine concentrator.** Configuraciones alternativas para procesos MED para aplicaciones de concentración de salmueras:

geometría variable de efectos, fuentes externas en efectos distintos al primero, acoplamiento con MSF para efectos posteriores.

**Alternative configurations for solar-driven MED.** Configuraciones alternativas para el proceso solar MED (almacenamiento con distintos puntos de carga y descarga, MED con distintos puntos de fuente externa, etc. Incluir diagrama de draw.io con las distintas configuraciones)

The layout configuration of the facility focused on realibility and simplifying operation and maintenance, not strictly on thermodynamic efficiency. The efficiency of the system could be improved:

1. if direct coupling between solar field and thermal storage was used, avoiding the heat exchanger energy transfer associated losses
2. thermal storage allowed charge and discharge from different levels, in order to take advantage of the temperature stratification and avoid fluid mixing
- 3.
- 4.

These decisions were made to, on the one hand allow to separate the solar field and thermal storage into two distinct decoupled circuits, providing flexibility, reducing the volume of additives required (only added to the solar field circuit), and operational flexibility (other external loads can be connected to the solar field when the MED is not being operated).

In conclusion this system, although improvable, allows to validate the feasibility of the proposed approach by means of the implementation of a suitable control system, in such a way, that the ideas and techniques presented in this work, could be directly extrapolated to a commercial system just by modifying some of the decision variables to suit the particular implementation.

## Derived scientific contributions

1. Publicaciones en revista
2. Contribuciones a congreso
3. Coloquios doctorales
4. Colaboraciones en proyectos de investigación
5. Estancias de investigación
6. Repositorios de código
7. Repositorios de datos
8. Herramientas interactivas
9. Contribuciones a librerías de código abierto?

## Bibliography

Here are the references in citation order.

- [1] Shahab Rohani et al. "Optimization of Water Management Plans for CSP Plants through Simulation of Water Consumption and Cost of Treatment Based on Operational Data." In: *Solar Energy* 223 (July 15, 2021), pp. 278–292. doi: [10.1016/j.solener.2021.05.044](https://doi.org/10.1016/j.solener.2021.05.044). (Visited on 06/17/2025) (cited on pages 11, 14, 17, 19, 20, 37).
- [2] Carrie Schoeneberger et al. "Solar for Industrial Process Heat: A Review of Technologies, Analysis Approaches, and Potential Applications in the United States." In: *Energy* 206 (2020), p. 118083. doi: [10.1016/j.energy.2020.118083](https://doi.org/10.1016/j.energy.2020.118083). (Visited on 08/07/2025) (cited on page 12).
- [3] IEA SHC. *Solar Heat Worldwide 2025*. 2025 (cited on page 12).
- [4] Richard Thonig and Johan Lilliestam. "Concentrating Solar Technology Policy Should Encourage High Temperatures and Modularity to Enable Spillovers." In: *AIP Conference Proceedings* 2815.1 (Oct. 6, 2023), p. 050005. doi: [10.1063/5.0149423](https://doi.org/10.1063/5.0149423). (Visited on 06/13/2025) (cited on page 12).
- [5] Mark Mehos et al. "Concentrating Solar Power Best Practices Study." In: (2020). (Visited on 08/05/2025) (cited on page 12).
- [6] Mark Mehos et al. "Concentrating Solar Power Gen3 Demonstration Roadmap." In: (2017). doi: [10.2172/1338899](https://doi.org/10.2172/1338899). (Visited on 08/02/2025) (cited on page 12).
- [7] Stefan Pfenninger et al. "Potential for Concentrating Solar Power to Provide Baseload and Dispatchable Power." In: *Nature Climate Change* 4.8 (Aug. 2014), pp. 689–692. doi: [10.1038/nclimate2276](https://doi.org/10.1038/nclimate2276). (Visited on 08/08/2025) (cited on page 12).
- [8] Christian Binz et al. "Toward Technology-Sensitive Catching-Up Policies: Insights from Renewable Energy in China." In: *World Development* 96 (Aug. 1, 2017), pp. 418–437. doi: [10.1016/j.worlddev.2017.03.027](https://doi.org/10.1016/j.worlddev.2017.03.027). (Visited on 08/08/2025) (cited on page 12).
- [9] Johan Lilliestam et al. "The Near- to Mid-Term Outlook for Concentrating Solar Power: Mostly Cloudy, Chance of Sun." In: *Energy Sources, Part B: Economics, Planning, and Policy* 16.1 (2021), pp. 23–41. doi: [10.1080/15567249.2020.1773580](https://doi.org/10.1080/15567249.2020.1773580) (cited on pages 12, 13, 64).
- [10] Nuno Bento and Charlie Wilson. "Measuring the Duration of Formative Phases for Energy Technologies." In: *Environmental Innovation and Societal Transitions* 21 (Dec. 1, 2016), pp. 95–112. doi: [10.1016/j.eist.2016.04.004](https://doi.org/10.1016/j.eist.2016.04.004). (Visited on 08/08/2025) (cited on page 12).
- [11] Pere Mir Artigues, Pablo del Río González, and Nàtalia Caldés. *The Economics and Policy of Concentrating Solar Power Generation*. Springer Nature, 2019. (Visited on 08/08/2025) (cited on page 12).
- [12] Thomas M. Schmitt. "(Why) Did Desertec Fail? An Interim Analysis of a Large-Scale Renewable Energy Infrastructure Project from a Social Studies of Technology Perspective." In: *Local Environment* 23.7 (July 3, 2018), pp. 747–776. doi: [10.1080/13549839.2018.1469119](https://doi.org/10.1080/13549839.2018.1469119). (Visited on 08/08/2025) (cited on page 13).
- [13] IRENA. *Renewable Power Generation Costs in 2024*. 978-92-9260-669-5. Abu Dhabi, July 22, 2025. (Visited on 08/02/2025) (cited on pages 13, 14).
- [14] Franziska Schöniger et al. "The Need for Dispatchable RES: A Closer Look at the Future Role of CSP in Europe." In: *Renewable Energy Based Solutions*. Ed. by Tanay Sıdkı Uyar and Nader Javani. Cham: Springer International Publishing, 2022, pp. 219–239. doi: [10.1007/978-3-031-05125-8\\_8](https://doi.org/10.1007/978-3-031-05125-8_8). (Visited on 06/13/2025) (cited on page 13).
- [15] Javier Bonilla et al. "Feasibility and Practical Limits of Full Decarbonization of the Electricity Market with Renewable Energy: Application to the Spanish Power Sector." In: *Energy* 239 (Jan. 15, 2022), p. 122437. doi: [10.1016/j.energy.2021.122437](https://doi.org/10.1016/j.energy.2021.122437). (Visited on 08/09/2025) (cited on page 13).
- [16] IEA. "Net Zero by 2050 - A Roadmap for the Global Energy Sector." In: (2021) (cited on page 14).
- [17] IRENA. "World Energy Transitions Outlook 2024: 1.5°C Pathway." In: (2024) (cited on page 14).
- [18] Johan Lilliestam et al. "Scaling up CSP: How Long Will It Take?" In: *AIP Conference Proceedings* 2815.1 (Oct. 6, 2023), p. 050003. doi: [10.1063/5.0148709](https://doi.org/10.1063/5.0148709). (Visited on 06/13/2025) (cited on page 14).
- [19] China Solar Thermal Alliance. *Blue Book of China's Concentrating Solar Power Industry 2024*. 2024 (cited on pages 14, 18).

- [20] Samantha Kuzma et al. "Aqueduct 4.0: Updated Decision-Relevant Global Water Risk Indicators." In: (Aug. 16, 2023). (Visited on 08/09/2025) (cited on page 15).
- [21] Tarun Kumar Aseri, Chandan Sharma, and Tara C. Kandpal. "Condenser Cooling Technologies for Concentrating Solar Power Plants: A Review." In: *Environment, Development and Sustainability* 24.4 (Apr. 2022), pp. 4511–4565. doi: [10.1007/s10668-021-01678-5](https://doi.org/10.1007/s10668-021-01678-5). (Visited on 06/15/2025) (cited on pages 15, 18, 21).
- [22] J Meldrum et al. "Life Cycle Water Use for Electricity Generation: A Review and Harmonization of Literature Estimates." In: *Environmental Research Letters* 8.1 (Mar. 2013), p. 015031. doi: [10.1088/1748-9326/8/1/015031](https://doi.org/10.1088/1748-9326/8/1/015031). (Visited on 06/13/2025) (cited on pages 16, 63).
- [23] Antonio Colmenar-Santos et al. "Water Consumption in Solar Parabolic Trough Plants: Review and Analysis of the Southern Spain Case." In: *Renewable and Sustainable Energy Reviews* 34 (June 1, 2014), pp. 565–577. doi: [10.1016/j.rser.2014.03.042](https://doi.org/10.1016/j.rser.2014.03.042). (Visited on 06/02/2023) (cited on page 16).
- [24] Philipp Habl, Ana Blanco-Marigorta, and Berit Erlach. "Exergoeconomic Comparison of Wet and Dry Cooling Technologies for the Rankine Cycle of a Solar Thermal Power Plant." In: () (cited on page 16).
- [25] Lidia Martín and Mariano Martín. "Optimal Year-Round Operation of a Concentrated Solar Energy Plant in the South of Europe." In: *Applied Thermal Engineering* 59.1 (Sept. 25, 2013), pp. 627–633. doi: [10.1016/j.applthermaleng.2013.06.031](https://doi.org/10.1016/j.applthermaleng.2013.06.031). (Visited on 06/13/2025) (cited on pages 16, 37).
- [26] Richard Thonig, Alina Gilmanova, and Johan Lilliestam. *CSP.Guru* 2023-07-01. Zenodo, July 1, 2023. (Visited on 05/31/2025) (cited on pages 17, 18, 22, 64).
- [27] Javier Bonilla et al. "CSP Data: A Data Discovery Web Application of Commercial CSP Plants." In: (July 2024) (cited on pages 17, 18, 64).
- [28] C. Turchi. *Parabolic Trough Reference Plant for Cost Modeling with the Solar Advisor Model (SAM)*. NREL/TP-550-47605, 983729. July 1, 2010, NREL/TP-550-47605, 983729. doi: [10.2172/983729](https://doi.org/10.2172/983729). (Visited on 08/09/2025) (cited on page 17).
- [29] J Maulbetsch. *Comparison of Alternate Cooling Technologies for U.S. Power Plants: Economic, Environmental, and Other Tradeoffs*. 1005358. Palo Alto, CA: EPRI, Aug. 2004 (cited on pages 17, 18, 21, 22).
- [30] J Maulbetsch. *Economic Evaluation of Alternative Cooling Technologies*. 1024805. Palo Alto, CA: Electric Power Research Institute (EPRI), Jan. 2012. (Visited on 08/09/2025) (cited on pages 17–19, 21, 38).
- [31] T Jászay. "Indudustrial Review-Aus Der Industrie. The Air-Cooled Condensing Equipment" System Heller" a Comprehensive Survey." In: *Periodica Polytechnica Mechanical Engineering* 2.4 (1958), pp. 389–402 (cited on page 17).
- [32] A. Balogh and J. Budik. "Heller's Indirect Approach Widens Applicability of Dry Cooling." In: *Modern Power Systems* 26.7 (July 2006), ?? (Cited on page 17).
- [33] O. O. Mil'man and P. A. Anan'ev. "Air-Cooled Condensing Units in Thermal Engineering (Review)." In: *Thermal Engineering* 67:12 (Dec. 1, 2020), pp. 872–891. doi: [10.1134/S0040601520120058](https://doi.org/10.1134/S0040601520120058). (Visited on 08/11/2025) (cited on page 17).
- [34] Nalagh Andras and Szabo Aoltan. "Advanced Heller System Technical Characteristics." 2005 (cited on page 17).
- [35] Mariano Martín. "Optimal Annual Operation of the Dry Cooling System of a Concentrated Solar Energy Plant in the South of Spain." In: *Energy* 84 (May 1, 2015), pp. 774–782. doi: [10.1016/j.energy.2015.03.041](https://doi.org/10.1016/j.energy.2015.03.041). (Visited on 06/12/2025) (cited on pages 18, 37).
- [36] Kelly Birkinshaw, Marwan Masri, and Robert L Therkelsen. "Comparison of Alternate Cooling Technologies for California Power Plants Economic, Environmental and Other Tradeoffs." In: (Feb. 2002) (cited on page 18).
- [37] M. C. Hu. *Engineering and Economic Evaluation of Wet/Dry Cooling Towers for Water Conservation*. COO-2442-1. United Engineers and Constructors, Inc., Philadelphia, PA (USA), Oct. 31, 1976. doi: [10.2172/7101949](https://doi.org/10.2172/7101949). (Visited on 08/09/2025) (cited on page 18).
- [38] F. R. Zaloudek et al. *Study of the Comparative Costs of Five Wet/Dry Cooling Tower Concepts*. BNWL-2122. Battelle Pacific Northwest Labs., Richland, WA (USA), Sept. 1, 1976. doi: [10.2172/7101320](https://doi.org/10.2172/7101320). (Visited on 08/09/2025) (cited on pages 18, 19).
- [39] W. V. Loscutoff. *Preliminary Evaluation of Wet/Dry Cooling Concepts for Power Plants*. BNWL-1969. Battelle Pacific Northwest Labs., Richland, Wash. (USA), Dec. 31, 1975. doi: [10.2172/7341661](https://doi.org/10.2172/7341661). (Visited on 08/09/2025) (cited on pages 18, 19).
- [40] L. E. Wiles et al. *Description and Cost Analysis of a Deluge Dry/Wet Cooling System*. PNL-2498. Battelle Pacific Northwest Labs., Richland, WA (USA), June 1, 1978. doi: [10.2172/6700397](https://doi.org/10.2172/6700397). (Visited on 08/10/2025) (cited on pages 18, 19).

- [41] Babak Golkar et al. "Determination of Optimum Hybrid Cooling Wet/Dry Parameters and Control System in off Design Condition: Case Study." In: *Applied Thermal Engineering* 149 (Feb. 25, 2019), pp. 132–150. doi: [10.1016/j.applthermaleng.2018.12.017](https://doi.org/10.1016/j.applthermaleng.2018.12.017). (Visited on 06/21/2025) (cited on pages 19, 37).
- [42] G. Barigozzi, A. Perdichizzi, and S. Ravelli. "Wet and Dry Cooling Systems Optimization Applied to a Modern Waste-to-Energy Cogeneration Heat and Power Plant." In: *Applied Energy* 88.4 (Apr. 1, 2011), pp. 1366–1376. doi: [10.1016/j.apenergy.2010.09.023](https://doi.org/10.1016/j.apenergy.2010.09.023). (Visited on 03/10/2023) (cited on page 19).
- [43] G. Barigozzi, A. Perdichizzi, and S. Ravelli. "Performance Prediction and Optimization of a Waste-to-Energy Cogeneration Plant with Combined Wet and Dry Cooling System." In: *Applied Energy* 115 (Feb. 15, 2014), pp. 65–74. doi: [10.1016/j.apenergy.2013.11.024](https://doi.org/10.1016/j.apenergy.2013.11.024). (Visited on 03/10/2023) (cited on pages 19, 37).
- [44] Patricia Palenzuela et al. "Experimental Assessment of a Pilot Scale Hybrid Cooling System for Water Consumption Reduction in CSP Plants." In: *Energy* 242 (Mar. 1, 2022), p. 122948. doi: [10.1016/j.energy.2021.122948](https://doi.org/10.1016/j.energy.2021.122948). (Visited on 03/10/2023) (cited on page 20).
- [45] Wanchai Asvapoositkul and Mantheerapol Kuansathan. "Comparative Evaluation of Hybrid (Dry/Wet) Cooling Tower Performance." In: *Applied Thermal Engineering* 71.1 (Oct. 5, 2014), pp. 83–93. doi: [10.1016/j.applthermaleng.2014.06.023](https://doi.org/10.1016/j.applthermaleng.2014.06.023). (Visited on 03/10/2023) (cited on pages 20, 37).
- [46] Hemin Hu et al. "Thermodynamic Characteristics of Thermal Power Plant with Hybrid (Dry/Wet) Cooling System." In: *Energy* 147 (Mar. 15, 2018), pp. 729–741. doi: [10.1016/j.energy.2018.01.074](https://doi.org/10.1016/j.energy.2018.01.074). (Visited on 03/10/2023) (cited on pages 20, 37).
- [47] SPX. SPX Awarded Contract to Supply Parallel Condensing System For Crescent Dunes Solar Energy Project near Tonopah, Nevada. Mar. 24, 2012. URL: <https://www.powersystemsdesign.com/articles/spx-awarded-contract-to-supply-parallel-condensing-system-for-crescent-dunes-solar-energy-project-near-tonopah-nevada/8/3720> (visited on 08/12/2025) (cited on pages 21, 22).
- [48] Steinbeis 2i GmbH. Blog #29 – Full Scale Testing in Stellenbosch, South Africa | MinwaterCSP. Jan. 27, 2020. URL: <https://www.minwatercsp.eu/blog-29-full-scale-testing-in-stellenbosch-south-africa/> (visited on 08/02/2025) (cited on page 22).
- [49] UNE. *Thermal Performance Acceptance Testing of Mechanical Draught Series Wet Cooling Towers*. manual. UNE. 2004 (cited on page 25).
- [50] CTI. *Code Tower, Standard Specifications. Acceptance Test Code for Water Cooling Towers*. manual. Cooling Technology Institute. 2000 (cited on page 25).
- [51] Patricia Palenzuela et al. *Steady-State Operation Dataset of an Experimental Wet Cooling Tower Pilot Plant Located at Plataforma Solar de Almería*. Zenodo, June 21, 2024. (Visited on 08/31/2025) (cited on page 25).
- [52] Juan Miguel Serrano et al. "Wet Cooling Tower Performance Prediction in CSP Plants: A Comparison between Artificial Neural Networks and Poppe's Model." In: *Energy* (May 29, 2024), p. 131844. doi: [10.1016/j.energy.2024.131844](https://doi.org/10.1016/j.energy.2024.131844). (Visited on 05/30/2024) (cited on page 25).
- [53] Ashrae. "HVAC Systems and Equipment." In: *Chapter 36 Cooling Towers*. 2004 (cited on page 32).
- [54] M. Hosoz, H. M. Ertunc, and H. Bulgurcu. "Performance Prediction of a Cooling Tower Using Artificial Neural Network." In: *Energy Conversion and Management* 48.4 (Apr. 1, 2007), pp. 1349–1359. doi: [10.1016/j.enconman.2006.06.024](https://doi.org/10.1016/j.enconman.2006.06.024). (Visited on 03/08/2023) (cited on pages 26, 30).
- [55] F. Merkel. "Verdunstungskühlung." In: *VDI Zeitschrift Deutscher Ingenieure, Berlin, Alemania* (1925), pp. 123–128 (cited on pages 29, 31).
- [56] C Bourillot. "Hypotheses of Calculation of the Water Flow Rate Evaporated in a Wet Cooling Tower." In: (Aug. 1983) (cited on page 29).
- [57] H. Jaber and R. L. Webb. "Design of Cooling Towers by the Effectiveness-NTU Method." In: *Journal of Heat Transfer* 111.4 (Nov. 1989), pp. 837–843. doi: [10.1115/1.3250794](https://doi.org/10.1115/1.3250794) (cited on page 29).
- [58] M. Poppe and H. Rögner. "Berechnung von Rückkühlwerken." In: *VDI wärmeatlas* (1991), p. Mi 1 (cited on pages 30, 31).
- [59] J.C. Kloppers and D.G. Kröger. "A Critical Investigation into the Heat and Mass Transfer Analysis of Counterflow Wet-Cooling Towers." In: *International Journal of Heat and Mass Transfer* 48.3 (2005), pp. 765–777 (cited on page 30).
- [60] C. G. Cutillas et al. "Energetic, Exergetic and Environmental (3E) Analyses of Different Cooling Technologies (Wet, Dry and Hybrid) in a CSP Thermal Power Plant." In: *Case Studies in Thermal Engineering* 28 (Dec. 1, 2021), p. 101545. doi: [10.1016/j.csite.2021.101545](https://doi.org/10.1016/j.csite.2021.101545). (Visited on 03/27/2024) (cited on page 30).

- [61] Ming Gao et al. "Artificial Neural Network Model Research on Effects of Cross-Wind to Performance Parameters of Wet Cooling Tower Based on Level Froude Number." In: *Applied Thermal Engineering* 51.1 (Mar. 1, 2013), pp. 1226–1234. doi: [10.1016/j.applthermaleng.2012.06.053](https://doi.org/10.1016/j.applthermaleng.2012.06.053). (Visited on 03/08/2023) (cited on page 30).
- [62] Jialiang Song et al. "A Novel Approach for Energy Efficiency Prediction of Various Natural Draft Wet Cooling Towers Using ANN." In: *Journal of Thermal Science* 30.3 (May 2021), pp. 859–868. doi: [10.1007/s11630-020-1296-0](https://doi.org/10.1007/s11630-020-1296-0). (Visited on 03/04/2023) (cited on page 30).
- [63] P. Navarro et al. "Critical Evaluation of the Thermal Performance Analysis of a New Cooling Tower Prototype." In: *Applied Thermal Engineering* 213 (2022), p. 118719. doi: [10.1016/j.applthermaleng.2022.118719](https://doi.org/10.1016/j.applthermaleng.2022.118719) (cited on pages 30–32).
- [64] Faisal Asfand et al. "Thermodynamic Performance and Water Consumption of Hybrid Cooling System Configurations for Concentrated Solar Power Plants." In: *Sustainability* 12.11 (2020). doi: [10.3390/su12114739](https://doi.org/10.3390/su12114739) (cited on page 37).
- [65] Ayman Mdallal et al. "Modelling and Optimization of Concentrated Solar Power Using Response Surface Methodology: A Comparative Study of Air, Water, and Hybrid Cooling Techniques." In: *Energy Conversion and Management* 319 (Nov. 1, 2024), p. 118915. doi: [10.1016/j.enconman.2024.118915](https://doi.org/10.1016/j.enconman.2024.118915). (Visited on 06/17/2025) (cited on page 37).
- [66] Tao Tang et al. "Study on Operating Characteristics of Power Plant with Dry and Wet Cooling Systems." In: *Energy and Power Engineering* 5.4 (4 June 30, 2013), pp. 651–656. doi: [10.4236/epe.2013.54B126](https://doi.org/10.4236/epe.2013.54B126). (Visited on 06/13/2025) (cited on page 37).
- [67] David Wales and Jonathan Doye. "Global Optimization by Basin-Hopping and the Lowest Energy Structures of Lennard-Jones Clusters Containing up to 110 Atoms." In: *The Journal of Physical Chemistry A* 101.28 (July 1, 1997), pp. 5111–5116. doi: [10.1021/jp970984n](https://doi.org/10.1021/jp970984n). (Visited on 06/11/2025) (cited on page 45).
- [68] Meteotest AG. *Meteonorm V8.2.0.24079*. URL: <https://meteonorm.com/climate/> (visited on 06/09/2025) (cited on pages 64, 65).

## Alphabetical Index

preface, vii